INL/EXT-12-27189
Revision 1

Pre-Irradiation Testing and Analysis to Support the LWRS Hybrid SiC-CMC-Zircaloy-4 Unfueled Rodlet Irradiation

Isabella J. van Rooyen

January 2013

The INL is a U.S. Department of Energy National Laboratory
operated by Battelle Energy Alliance

INL/EXT-12-27189
Revision 1

Pre-Irradiation Testing and Analysis to Support the LWRS Hybrid SiC-CMC-Zircaloy-4 Unfueled Rodlet Irradiation

Isabella J. van Rooyen

January 2013

Idaho National Laboratory
Idaho Falls, Idaho 83415

http://www.inl.gov

Prepared for the
U.S. Department of Energy
Office of Nuclear Energy
Under DOE Idaho Operations Office
Contract DE-AC07-05ID14517

EXECUTIVE SUMMARY

The purpose of this report is to provide the details of selected cold characterization tests conducted at the Idaho National Laboratory (INL). The specific set of characterization tests included those identified for prototype testing to ascertain neutron irradiation readiness. These tests support rodlet design activities and validate methods for examining chemical, mechanical and physical properties of the mock-up hybrid fuel rodlet design and component materials. The hybrid fuel rodlet design is being investigated under the Light Water Reactor Sustainability (LWRS) program for further development and testing of a possible advanced LWR nuclear fuel cladding design.

Two sets of samples are investigated as part of this method development experiment: "Mock-up hybrid samples" and "SiC-CMC sleeve samples". Due to the limited Zircaloy-4 (Zr-4) tube material available for the LWRS Advanced LWR Fuel Development pathway, only four Zr-4 tubes were made available for these initial tests. Hence no verification hybrid mock-up tests could be done at this stage. The motivation for selection of the SiC ceramic matrix composites (SiC-CMC) sleeves, was based on two main processing parameters, namely the number of PIP processing cycles and the number of braided CMC plies. Comparative information on the behavior between a 1 and 2 ply braided SiC-CMC sleeve will provide valuable design development information. The hybrid mock-up samples incorporate SiC-CMC sleeves fabricated with 7 polymer infiltration pyrolysis (PIP) cycles, which was found to provide the desired matrix density. As important design decisions are based on the economics of processes, the comparative properties between the SiC-CMC sleeves fabricated with 5 and 7 PIP cycles is useful to design optimization and was also included in the SiC-CMC sleeve sample set. In addition to the four mini-rodlet tube hybrid mock-up samples, two bare Zr-4 mini rodlet mock-up samples were also made for use as a standard for comparison.

Baseline studies revealed that no significant density differences were observed between the 5 and 7 PIP processed cycles or the 1 and 2 ply braided SiC-CMC sleeves. These characterization data revealed a specific subsample, LWRS-1-6-A-1-5, to have the highest density which could not be attributed to the number of PIP cycles. Thus, another SiC-CMC sleeve fabrication parameter plays a role in the higher density value and it is recommended that this trend be further investigated. A suggestion is that the PIP polymer properties, like the polymer composition, temperature of pyrolysis heat treatment or the time of pyrolysis, be investigated to determine the cause of this higher density value. Metallurgical examination showed that the SiC-CMC sleeves fabricated with only 5 PIP cycles exhibit open fibers and larger cracked flakes (approximately 30 μm) of SiC matrix material to the more compact and smaller flakes (approximately 5 μm) SiC matrix material of the 7 PIP cycle sleeves. It was further found that the 1 ply SiC-CMC sleeves revealed a higher amount of open and broken CMC fibers. The effect of the difference in microstructure becomes very apparent during the bend test results and subsequent crack evaluations.

The bend test method development for both the hybrid SiC-CMC-Zr-4 mock-up and SiC-CMC sleeve samples, were successfully completed as a comparative method to asses performance of cladding design options. The 2 ply sleeve samples show a higher bend momentum compared to those of the 1 ply sleeve samples. This is applicable to both the hybrid mock-up and SiC-CMC sleeve samples. Comparatively, both the 1- and 2 ply hybrid mock-up samples showed a higher bend momentum if compared with the standard Zr-4 mock-up sample. The characterization of the hybrid mock-up samples after bend testing showed that the 1 ply SiC-CMC sleeve matrix shows signs of distress and preliminary signs of defraying at the protective Zr-4 sleeve areas. In addition, the microstructure of the 1 ply SiC-matrix at the crack location show significant cracking and flaking after the bend test. The 2 ply SiC-CMC sleeve samples showed, however, a more well bonded cohesive SiC matrix structure. The cracking and fraying introduce potential concerns for increased fretting during the actual use of the cladding tubes.

It should be noted that at this stage only preliminary conclusions can be given on the samples exposed to hot water corrosion flow (HWCF) tests. Although the current HWFC system could not provide stable conditions to conduct the tests under ATR representative conditions, much valuable information was

obtained during the method development tests. The in-line measurements were validated by “tap” measurements taken periodically though the HWCF tests. It is, however, found that the time delay between off- line verification measurements caused differences in the water properties and is currently under investigation. Possible causes are the precipitation of certain chemical/substances, and the change in oxygen potential due to the pressure differences.

During periodic inspections during the HWCF tests, precipitates were observed underneath the Zr-4 protective sleeve at the flow-end side of the mock-up samples. This is typically expected due to the flow direction of the water. This observation shows that this potentially can happen as well during ATR irradiation and future application of this design in the LWR. It is therefore recommended that the design of this protective sleeve needs to be modified to avoid build-up of solids.

Material removal patterns (or flow patterns) were observed in the SiC-CMC microstructures of both the hybrid mock-up samples at the end of the 10 day corrosion test. This is most probably an indication of the water flow pattern at that specific area. Images from the SiC-4 (2 ply) mock-up sample surfaces is smoother when compared to the SiC-3(1 ply) sample. It may be argued that it is due to higher water flow compared to SiC-3, but this cannot be conclusively stated. Evidence is provided during the metallurgical examination that SiC-CMC sleeve material was removed during the tests. The presence of Cl and Si in the corrosion products filtered from the system water, also suggest this observation.

A white layer covered most of the SiC-CMC surface of both the SiC-3 and SiC-4 samples at the end of the 10 day test. Based on the SEM-EDS results, Al, O, Cu, Si, Cl were the main elements of this layer. The Cl content was determined for water taken periodically from the HWFC tests as well. Although duplicate measurements (for validation) are in process, preliminary observation is noted that the Cl content decreased as the 10 day corrosion test progressed. An explanation of this is still under investigation.

No dimensional differences due to the HWCF tests were observed. Although detailed measurement analysis was conducted and the null hypotheses was not rejected, meaning that no differences were observed, final conclusions cannot be reached as the current sample size is insufficient. In addition, it may be that the measurement technique applied for these measurements is not sensitive enough to identify possible differences. It is recommended that more investigation needs to be performed on the measurement technique; however, the inclusion of surface roughness measurements, using atomic force microscope (AFM) analysis, is to be considered as it will provide information on the surface roughness, showing micro-level changes. This may be particular useful for further corrosion or chemical interaction studies.

The value of this report is measured and summarized against the objectives of these mock-up sample tests as follows:

- Method development or method/test confirmation, as many of these methods are first of a kind and uniquely designed for this type of cladding design.
    a. Bend test method development was successful and test plans can be updated for standard prototype tests.
    b. HWCF test method development is not yet in the final stages as many unknown operational issues were identified during the test method development.
- Comparative results on two different preliminary SiC-CMC sleeve designs based on PIP processing techniques.
    a. Supportive evidence is provided in this study that the 1 ply braided material exhibits reduced performance.
    b. Data indicate that density cannot be used as the only acceptance criteria for the fabricated SiC-CMC material.

c. Results further showed that 5 PIP cycled material has more grainy and loose structure, but due to the small quantities of samples investigated, it is recommended that the development work on all the effects of other fabrication process parameters be identified.

- Analytical results from these tests as an *early* indication of ATR insertion readiness

  a. The entrapment of the precipitates during the HWCF test showed on a possible design change for the protective Zr-4 sleeve. This was an early indication that this typically will enhance fretting and degradation of the SiC-CMC sleeve in that area.

  b. The gamma irradiation test, although not conclusively, showed that the specific bonding technique will not withstand neutron irradiation. Alternate bonding techniques should be investigated.

  c. The bend test, although not a direct measurement of irradiation behavior, provide information that the 2 ply SiC-CMC sleeves are more stable at the protective Zr-4 sleeve ends compared to the 1 ply. This may be an early indication that 2 ply SIC-CMC sleeves will withstand more vibration (decreased fretting) in the reactor appreciation. This needs to be confirmed with actual vibration studies to be fully conclusive.

It is recommended that the full interpretation and reporting of the HWFC test be completed to enhance the current data provided. A full gap analysis of the actual system capabilities needs to be conducted. This will enable the development team to set the parameter limits for representative comparison of any reactor conditions. Additionally, the actual flow characteristics of the HWCF system need to be finalized and understood.

It is further recommended that the bend test tomography analysis be expanded for incorporation of this information in the development of cladding model. This will benefit decisions on process design changes as well as fuel performance modeling.

The finalization of the electron back scatter diffraction (EBSD) technique for hydrogen embrittlement identification is also strongly recommended. This necessitates the controlled hydrogen gas embrittlement studies with EBSD analyses to set a standard.

It is also recommended that prototype test (quality level 2) to be completed after all the actions are finalized.

ACKNOWLEDGEMENTS

Acknowledgements are given to the following persons:

- Characterization:
  - Amber Miller for dimensional measurements, visual inspections, photography, assistance with the water analysis, compilation of characterization server and the preparation and monitoring of the corrosion flow testing.
  - Amber Miller for the compiling of Section 3.4.3.1 on dimensional measurements for the bend test and corrosion flow samples
  - Tammy Trowbridge for leach testing, bend test and SEM, SEM-EDS and visual examinations
  - Karen Wendt for the X-ray examination
  - Byron White for the chemical analysis of the water of the corrosion flow experiments
  - Arnold Erikson for XRD and density measurements
  - Todd Morris for microscopic sample preparation
  - Steve Reese for the preliminary Raman results of the corrosion flow SiC-CMC samples.
- Mock –up sample fabrication:
  - Michael Teague and Kristine Barrett for the fabrication of the mock-up samples.
- Hot water flow corrosion system:
  - John Garnier, Kevin McHugh, Matt Weseman and Tristan Griffith for the design, manufacture and operation of the corrosion flow equipment
  - Michael Teague, Kristine Barrett and Jesse Johns for design inputs to the corrosion flow equipment
  - Amber Miller for the compilation of the HWCF graphs, assistance with Section 3.4.2.
- Bend test:
  - Randy Lloyd for the design input on bend test, modifications on sample holders and execution of bend tests
  - Tammy Trowbridge for assistance during the design and execution of the bend test method
  - Steve Novascone for the preliminary simulations of the bend tests.
- Shannon Bragg-Sitton and Kristine Barrett for the review of this report.

CONTENTS

FIGURES

TABLES

ACRONYMS

AFM	Atomic force microscope
ASTM	American Society for Testing and Materials
ATR	Advanced Test Reactor (ATR)
DOE	U.S. Department of Energy
EDMS	Engineering Document management System
EDS	energy dispersive spectroscopy
EPMA	Electron probe micro-analysis
FTIR	Fourier transform infrared spectrometry
GTAW	Gas tungsten arc welding
HWCF	Hot Water Corrosion Flow
INL	Idaho National Laboratory
LWR	Light Water Reactor
LWRS	Light water reactor sustainability
MOOSE	Multiphysics Object-Oriented Simulation Environment
N/A	Not applicable
PB	Parallel beam
PI	Principal Investigator
PIP	Polymer infiltration pyrolysis
QADP	Quality Assurance Program Document
SEM	Scanning electron microscopy
SiC-CMC	SiC ceramic matrix composites
SIMS	Secondary ion mass spectrometry
Stdev	standard deviation
TEM	Transmission Electron Microscope
WDS	Wave length dispersive spectrometry
XRD	X-ray diffraction
Zr-4	Zircaloy-4

Pre-Irradiation Testing and Analysis to Support the LWRS Hybrid SiC-CMC-Zircaloy-4 Unfueled Rodlet Irradiation

1. INTRODUCTION

Nuclear fuel performance is a significant driver of nuclear power plant operational performance, safety, economics and waste disposal requirements. The Advanced Light Water Reactor (LWR) Nuclear Fuel Development Pathway focuses on improving the scientific knowledge basis to enable the development of high-performance, high burn-up fuels with improved safety and cladding integrity and improved nuclear fuel cycle economics. To achieve significant improvements, fundamental changes are required in the areas of nuclear fuel composition, cladding integrity, and fuel/cladding interaction.

1.1 Background

Selection of alternate cladding and structural materials must first take into account physical (geometric) and chemical compatibility with currently operating LWR designs. Cladding options under consideration have focused on the use of silicon carbide (SiC). Both monolithic SiC and SiC composite have been studied by a variety of international research programs, resulting in a substantial body of data available to guide the current LWRS effort. Early research in the LWRS Fuels Pathway has focused on developing a better understanding of SiC ceramic matrix composites (SiC-CMC). Various candidate materials and designs are investigated of which a fully ceramic or a “hybrid” design, which would incorporate SiC as a structural material supplementing an inner metal tube (possibly Zircaloy-4), are specific examples.

The Light Water Reactor Sustainability (LWRS) program Advance fuel cladding development plan[1] focuses on addressing critical-path items in fielding of advanced clad technology. In addition to an appropriate level of mechanistic and systems-level modeling, significant out-of-pile testing is anticipated to fully characterize mechanical, physical and chemical properties of candidate materials and designs and to demonstrate performance under nominal operating conditions and postulated accident conditions. Nonnuclear tests will provide a basis for initial down selection of candidate advanced cladding designs.

Advanced cladding materials must provide substantial benefit over the current zirconium-based cladding (e.g., Zircaloy-4, Zircaloy-2, ZIRLO and other). The planned tests are intended to either produce quantitative data or to demonstrate the properties required to achieve initial performance conditions relative to standard Zr-4 cladding:

1. Decreased hydrogen uptake (corrosion).
2. Decreased fretting of the cladding tube under normal operating and postulated accident conditions.
3. Increased coping time under postulated accident conditions (i.e. loss of coolant accident).
4. Reduced exothermic reaction rate with steam under postulated accident conditions (reduced hydrogen generation).
5. Possibility for power uprates and operation to higher burnup.

A series of out-of-pile tests will be performed to fully characterize candidate materials. An example of the characterization plan for the hybrid cladding system is shown in Figure 1 (acronyms are described on page xv). Cold characterization testing will establish baseline properties in advance of any future irradiation testing. These data will be compared to the current zirconium-based cladding in operating LWRs to inform the down selection process for an advanced clad system. Full characterization of cladding materials and designs will require a variety of test equipment and will encompass both

non-destructive and destructive testing. The hybrid fuel rodlet design is being investigated under the LWRS program for further development and testing of advanced LWR cladding designs.

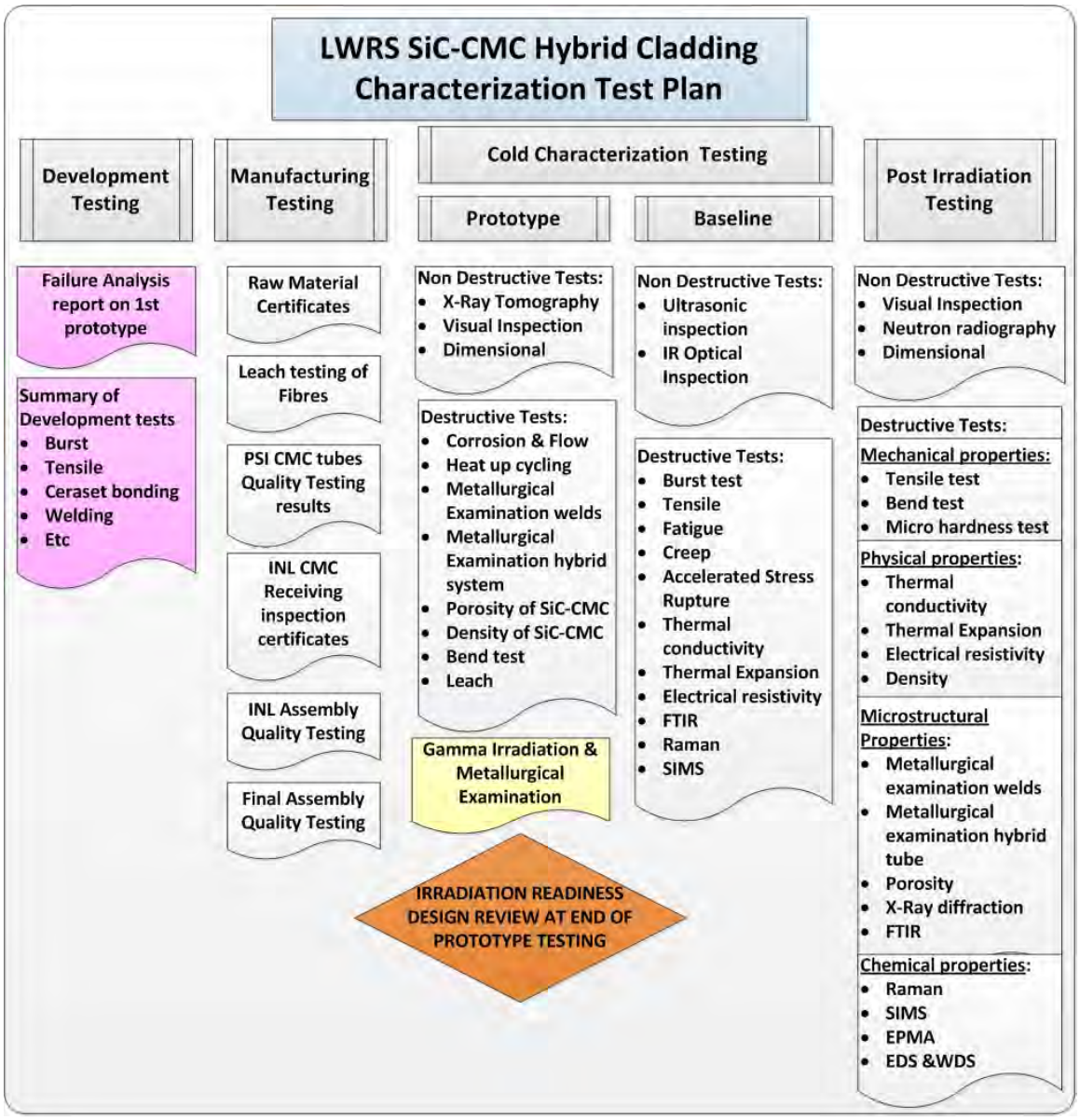

Figure 1. Figure showing the LWRS SiC-CMC hybrid cladding characterization test plan.[2]

1.2 Scope

The purpose of this report is to provide the details of selected cold characterization tests conducted at the Idaho National Laboratory (INL) and identified for prototype testing to ascertain neutron irradiation readiness. These tests support rodlet design changes and validate methods for examining chemical, mechanical and physical properties of the a mock-up hybrid fuel rodlet design and materials in a simulated pressurized water reactor (PWR) water environment in the case of some characterization tests.

These characterization tests were performed in preparation for neutron irradiation tests planned for a silicon carbide (SiC) ceramic matrix composite (CMC) zircaloy-4 (Zr-4) hybrid fuel rodlet that may be tested in the INL Advanced Test Reactor (ATR) if the design is selected for further development and testing. Figure 2 shows the geometry of the LWRS capsule assembly design for the SiC-CMC hybrid Zr-4 cladding rodlet.[3]

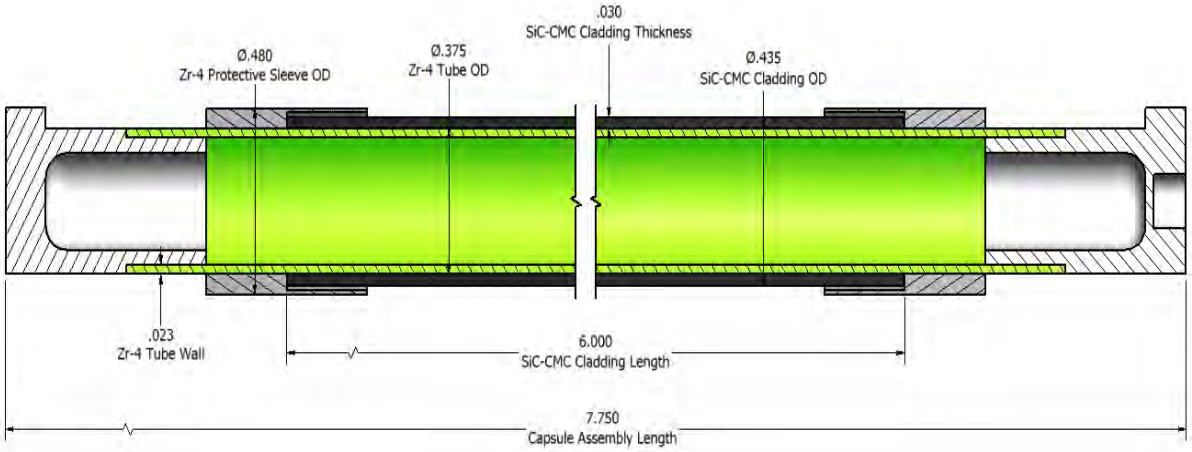

Figure 2. Geometry of the LWRS capsule assembly design for the Si-CMC hybrid Zr-4 cladding rodlet.[3]

Completion of the suite of tests identified in Figure 1 will provide full prototype rodlet characterization for irradiation readiness reviews. Due to a change in program direction in mid-FY-12, only a subset characterization tests were conducted for the current set of cladding samples. These tests are bend, hot water corrosion flow (HWCF) and leach tests. Discretionary baseline tests were included to aid adequate and effective comparative results for conclusions to be reached. Baseline test included density, X-ray diffraction (XRD), tomography and scanning electron microscopy (SEM) metallurgical examination. The two gamma irradiation tests reported previously by Van Rooyen,[4] form also part of the prototype testing classification performed in the earlier stages of the financial year with only a summarized abstract provided in this report.

It needs to be clearly noted that this report and data collected are not to be used for ATR readiness review as the samples used for these characterization test reporting here, are mock-up samples only and not prototypes. The objectives of these mock-up sample tests are summarized as follows:

1. Method development or method/test confirmation as many of these methods are first of the kind and uniquely designed for this type of cladding design.
2. Comparative results on two different preliminary SiC-CMC sleeve designs based on PIP processing techniques
3. Analytical results from these test as an *early* indication of ATR insertion readiness

As the bend test and hot water corrosion flow tests are uniquely designed for this configuration of samples and application, mock-up samples were fabricated for method development purpose prior to prototype testing. In this report the reporting of the materials, methods used and all the results with conclusions reached, are described in this report. This report describes materials, methods, results and conclusions for the tests conducted. The full scope of the work is discussed in Section 2.1. The specific SiC-CMC sleeve and mock-up sample fabrication details are not described (see Reference 9 for further fabrication details); a summary of the fabrication is provided in Section 2.1.2 as a basis for presenting characterization results.

1.3 Quality Requirements

The quality requirements are provided in the LWRS Quality Assurance Program Document (QADP).[5] Work was performed under controlled conditions using test plans to perform characterization. As some tests were first of the kind and no prior test methods were available, the opportunity was taken during this execution of the tests, to update/redlining the draft test plans for improvement and future repeatability. Work directions were given during a weekly briefing meeting, as well as ad hoc meetings as necessary. Specific pre-job briefings were given in accordance with LWP-9201[6] prior the start-up of the bend test and hot water corrosion flow tests and are recorded in the laboratory note books in accordance with MCP-2875.[7] Mock-up samples and SiC-CMC sleeve samples were received from the LWRS storage cabinet located in INL EROB building accompanied by the "Activity sheet" and relevant quality labeling (e.g., green tag or white tag) (see Appendix A). The samples were registered in the lab C17a register and stored in the locked storage cabinet until use. All samples are well numbered and labeled at all times. Characterization routing cards were compiled by the characterization PI which accompanied the samples to the various characterization activities. (At the moment this is handwritten to determine the usefulness of it, but in future for the actual prototypes it can be recorded in an official document: See Appendix A for a typical example). Results, sketches and notes are recorded in dedicated LWRS characterization laboratory note books. Specific characterization results are also recorded in the specific qualified researcher's note book. A list of the relevant note books is shown in Appendix C. The interpretation and conclusions of all characterization data are reported in technical reports.
Inspection/measuring/characterization is performed by qualified researchers and calibrated equipments or standards are used. Characterization plans and test plans for LWRS experiments will be placed under configuration control in the INL Engineering Document management System (EDMS) in accordance with LWP-1201 upon updating and approval.[8] The characterization tests and the work performed in this report is quality level 3.

2. MATERIALS AND METHODS

2.1 Materials

Two sets of samples are investigated as part of this method development experiment and are referred to as "Mock-up hybrid samples" and "SiC-CMC sleeve samples." Due to the limited Zr-4 tube material available for the LWRS fuel program, only 4 Zr-4 tubes were made available for these tests and therefore no verification hybrid mock-up tests could be done at this stage.

2.1.1 Sample Set Description

The decision making motivation for choosing the type of SiC-CMC sleeves, were based on two main processing parameters, namely the number of PIP processing cycles and the number of braided CMC plies as shown in Table 1. Comparative information on the behavior between a 1 and 2 ply braided SiC-CMC sleeve will provide valuable design development information. The hybrid mock-up samples incorporated SiC CMC sleeves fabricated with 7 PIP cycles, which was found to provide the desired matrix density. As important design decisions are based on the economics of processes, the comparative properties between the SiC-CMC sleeves fabricated with 5 and 7 PIP cycles will be useful and was also included in the SiC-CMC sleeve sample set. In addition, prior characterization work was already done on SiC-CMC sleeve samples fabricated with 5 PIP cycles as reported in a previous report by Van Rooyen [4]. This will therefore provide the opportunity to include some of the baseline characterization as comparisons in this study. In addition to the four mini-rodlet tube hybrid mock-up samples, two bare Zr-4 mini rodlet mock-up samples were also made to be used as a standard for comparison.

Various smaller samples of the SiC-CMC sleeves only were also identified for tests. Please note that the mock-up hybrid samples are described by a new unique number namely SiC-1 to SiC-4 and the rest of the samples are SiC-CMC sleeves only. Mock-up samples SiC-5 and SiC-6 were Zr-4 only which is used as a standard for comparison, as no specification/requirement exist at present as the bend test and corrosion flow test on these hybrid samples are newly developed. The SiC-CMC sleeve samples are identified by their original fabrication number with an added digit for further sub-sample sets. The specific sub-samples used for this study are described in Table 2 Subsection 2.2.1. Comparative studies are based on analysis of 1- and 2-ply braided CMC plies fabricated with 7 PIP cycles and 2-ply CMCs fabricated with 5 PIP cycles as shown in Table 1.

Table 1. Braided SiC-CMC sleeve sample history.

Number of PIP process cycles		Number of braided CMC plies
5	7	
	X	1
X	X	2

2.1.2 Mock-up Sample Fabrication

As mentioned in Section 1.2, no detailed description and discussion will be given on the fabrication method of the hybrid mock-up samples and SiC-CMC sleeves and only a short summary will be provided in this report. More detail on mock-up sample fabrication are provided by Barrett.[9] The mock-up hybrid samples were fabricated at INL where the SiC-CMC tubes were slid over a Zircaloy-4 (Zr-4) tube and Zr-4 end caps were welded to produce the mini tube mock-up. An autogenous orbital weld called gas tungsten arc welding (GTAW) technique was used to connect the Zr-4 tube to the endcaps. The weld was performed using argon as a shielding gas but was not performed in a completely inert environment (i.e., in a glove box filled with argon). A second weld was performed using an autogenous laser weld with argon as a shielding gas to attach protective Zr-4 sleeves to the Zr-4 inner tube. The purpose of the Zr-4 protective sleeves is to prevent the ends of the SiC-CMC braided sleeves from damage during high water flow past the rodlet while in the ATR.

2.2 Characterization Methods

2.2.1 Sample Description and Characterization Tests Planned

Detail of the samples and the designated characterization tests are indicated in Table 2. For additional detail, see the cold characterization test plan PLN-3927.[2] The samples described in Table 2, are organized by the main characterization test method with the results reported as such in Section 3.

Table 2. Sample description and characterization tests planned for this experiment.

Original Sample Description	SiC-CMC Fabrication	QA labels & Numbers	Pre-test Characterization		Post-test Characterization			
			Visual & Dimension	X-ray	Visual & Dimension	X-ray	SEM	Other
BEND TEST (results reported in Subsection 3.3)								
LWRS-1-6-A-2-3	5 cycles, 2 ply	Sleeve only	X	X	X	X	X	N/A
LWRS-1-6-A-3-4	5 cycles, 1 ply	Sleeve only	X	X	X	X	X	N/A
LWRS-1-6-A-6	5 cycles, 1 ply	Sleeve only	X	X	X	X	X	N/A
LWRS-1-6-A-9	7 cycles, 2 ply	SiC-1	X	X	X	X	X	N/A
LWRS-5-6-B-1	7 cycles, 1 ply	SiC-2	X	X	X	X	X	N/A
Zr-4 assembled	N/A	SiC-6	X	X	X	X	X	N/A
HOT WATER CORROSION FLOW TEST (results reported in Subsection 3.4)								
LWRS-1-6-A-7	7 cycles, 2 ply	Cracked	Visual & SEM only		N/A	N/A	N/A	N/A
LWRS-1-6-A-8	7 cycles, 2 ply	SiC-4	X	X	X	X	X	Water analysis
LWRS-5-6-B-2	7 cycles, 1 ply	SiC-3	X	X	X	X	X	Raman
Zr-4 assembled	N/A	SiC-5	X	X	X	X	X	TEM* EBSD*
BASELINE TESTS ON REPRESENTATIVE SAMPLES (results reported in Subsection 3.1)								
Original sample description	SiC-CMC fabrication	Characterization tests						
LWRS-1-6-A-7-1-2	7 cycles, 2 ply							
LWRS-1-6-A-9-1-2	7 cycles, 2 ply							
LWRS-1-6-B-2-1-2	7 cycles, 1 ply							
LWRS-1-6-A-2-2	5 cycles, 2 ply	Density						
LWRS-1-6-A-7-1-1	7 cycles, 2 ply							
LWRS-1-6-A-9-1-1	7 cycles, 2 ply	XRD						
LWRS-1-6-B-2-1-1	7 cycles, 1 ply	SEM						
LWRS-1-6-A-2-1	5 cycles, 2 ply	Leach & Chemical Analysis						

*Planned for future work but not included in this report

2.2.2 Bend Test

2.2.2.1 Summarized motivation. This method covers the determination of a flexural strength test of the fully assembled hybrid tube at ambient temperature. Although the ASTM standard C1161-02c[10] is used as the basis for this four-point bend test, this test will be conducted on the actual experiment assembly and not rectangular standard test pieces. It is decided to use the actual experiment assembly as the sleeve-end cap fixture design is of interest in the success of this design. The bend test may show possible weaknesses in that area due to the pulling out of the fibers as the sleeve end cap side. Furthermore, it is known that surface condition influences the flexural strength as well as the corrosion properties of the material. Using the actual experiment assembly will ensure that the surface finish is fully representative of the as-fabricated condition. As it is not a standardized test, results will be done in comparison with the Zr-4 standard tube with end caps. Results of this four-point bend test will not be used for acceptance of irradiation readiness review but will be used for information on the robustness of the hybrid design. Bend tests are however one of the proposed mechanical tests needed to support structural analysis of the Si- CMC Zr-4 hybrid design fueled capsules to meet the intent of ASME Section III, Class 1 code, and therefore bend test method development was needed. Detail of this examination is described in Reference 11. Further inspection may be performed as determined by the Characterization PI.

2.2.2.2 Equipment and calibration. As mentioned, this is not a standardized method to do bend test on tubular samples and therefore test method development is reported in Subsection 3.3. The universal Instron load cell (5 kN) was INL calibrated in accordance with ASTM E4-10.[12]

2.2.3 Hot Water Corrosion Flow Tests

2.2.3.1 Summarized motivation. The LWRS Program has set up a hot water corrosion flow (HWCF) test system at INL to characterize the thermal, chemical, and structural properties of candidate advanced fuel cladding materials and designs under a variety of simulated flow and internal heating conditions to mimic operational reactor conditions. It is expected that the data from the HWCF tests will support down selection of advanced cladding material and design and will provide baseline data for future evaluation of clad performance under irradiation. This test is uniquely designed for this project to measure the following characteristics under accelerated conditions (i.e., high water flow and elevated temperatures similar to ATR irradiation conditions):

- Deterioration of SiC/CMC tube due to water flow
- Corrosion properties of the hybrid SiC/CMC/Zr-4 tube.

The results of this test are important to determine irradiation readiness, as it will provide a simulated effect that water flow and temperature will have on the hybrid cladding tube under controlled conditions. Acceptance standards and decision on visual deterioration to SiC-CMC tube, brittle phase changes in the Zr-4 tube and pitting corrosion under SiC/CMC tube (i.e., interface) will be based on the characterization PI's expert judgment. As a baseline, a Zr-4 standard tube will be used as a comparative standard. Detail of the Flow/corrosion testing along with acceptance criteria is described in Reference 13.

2.2.3.2 Equipment and calibration. The HWCF is designed to expose cladding materials to heated, pre-conditioned water ranging from 40 to 180°F (278 to 355 K), less than 25 psig (0.17 MPa), and water flow rates ranging from 0.01 to 40 ft/second (0.003 to 12 m/s). High-purity water introduced in the closed-loop system will range from a pH of approximately 5 to 8, depending on the specific test requirements. Water conditions are set to be representative of reactor primary coolant chemistry and fluid flow. For this experiment however, method development to simulate the ATR conditions was undertaken. The water conditions are representative of the ATR primary coolant fluid flow and chemistry conditions. The flow rate, chemical composition, pH, oxygen content, pressure and temperature are measured continuously during testing. Water chemistry, pH and oxygen content are measured periodically via analysis of water samples taken from the test loop to validate the in-line measurements.

Initially for the method developmental and mock-up testing, constant conditions will be applied for a 1-day (called dry-run), 3-day and 10-day test. Basic flow and heat-up profiles were performed to test the integrity of the piping system, components and safety features and reported by Garnier *et al.*[14] Only a brief system description will be given here as background with a diagram of the HWCF system provided in Figure 3. Although the HWCF system is designed for two modes of operation, the results reported in Subsection 3.4 are of the corrosion/flow operational mode only. The thermal stress operation mode tests will be conducted at a later stage once the method and system is proven to be responsive to the specified conditions set and the method fully developed. Operator pre-set alarms and safety interlocks are used to activate water pump and heater shutdown should an off-normal event occur, such as a power outage or water leakage. Set-points are established for water level, temperature, pressure, and flow rate.

The results of this test cannot be compared directly with tests conducted in accordance with the ASTM Standard G 2/G 2M, as the maximum temperature of the HWCF system can reach is only 180°F if compared to the 680°F of this standard.[15] "Standard Test Method for Corrosion Testing of Products of Zirconium, Hafnium, and Their Alloys in Water at 680°F [360°C] or in Steam at 750°F [400°C]."

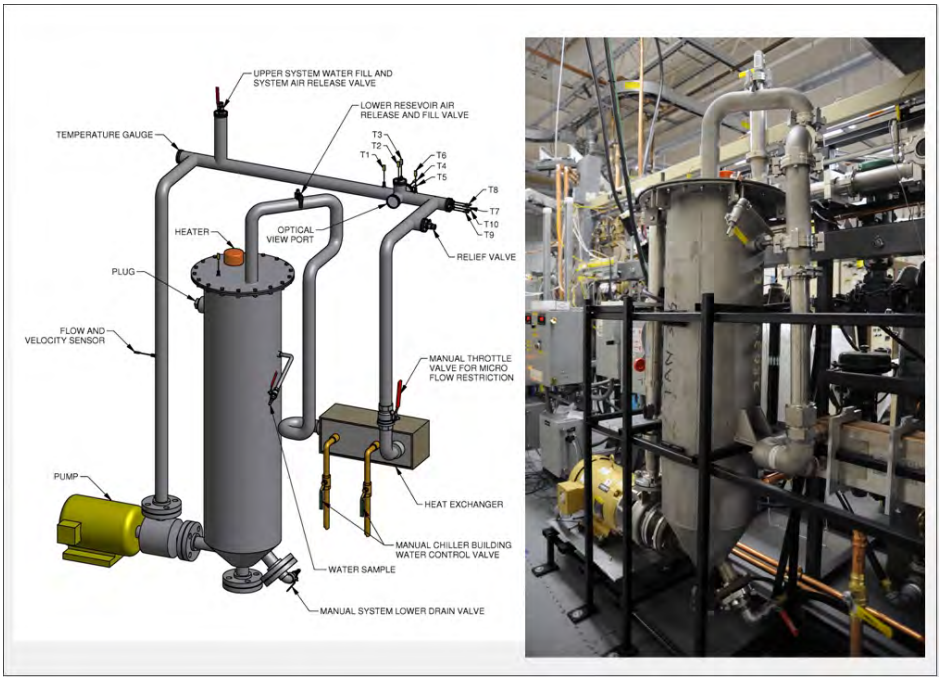

Figure 3. Diagram of the hot water corrosion flow test system and the assembled test equipment at INL; test samples are installed in the top leg of the flow loop at the optical view port position.

2.2.4 Leach Test and HWCF Water Analysis

2.2.4.1 Summarized motivation. Selected water chemical analysis is done to measure changes due to chemical reaction during irradiation. These results may also give an indication of any leachable chemicals which may enter the ATR coolant water. The leach test[16] is used for assessment of whether or not ATR restricted chemicals[17] will leach into the test water from the specimen at greater than allowable concentrations. Leach tests shall be conducted per SP-10.3.1.13[18] guidance on materials that will be exposed to the reactor coolant which contain compounds of halides or halogens such as chlorine/chlorides or sulfates in concentrations of individual halide/halogen or sulfate constituents exceeding 250 ppm.[17] As the fabrication method includes a polymer infiltration and pyrolysis (PIP) process where chlorinated raw materials are used, the leach test will be conducted on test pieces of the final fabricated and assembled hybrid tube.

2.2.4.2 Equipment and calibration. Chemical analysis was conducted via a Dionex ICS-3000 Ion Chromatograph with an Auto-sample. The analyzed for were fluoride, chloride and bromide. Fluoride, chloride, and bromide could instigate corrosion and also have neutron absorption cross sections that are significant; therefore they are undesirable in the specimen water in the setting of nuclear reactor. Chloride is especially undesirable and therefore is limited to a concentration of less than 0.1 parts per million in the primary coolant system chemistry. Example of the calibration standard and measurement on sample 2W is attached in Appendix B.

2.2.5 Three-Dimensional Tomography

2.2.5.1 Summarized motivation. 2D X-ray technique is used to show bonding or surface properties and interaction between the two interfaces. This may be beneficial to show any possible fretting, defraying or corrosion activities on the interface. Although 3D Tomography is more ideal, it was not available at INL at the initial stages of this work and only introduced for the radiographic examination of some of the latter post test characterization.

2.2.5.2 Equipment and calibration. 2D Radiographic inspection was completed on the samples in accordance with PLN-3950[19] using a Kevex model KM16010E-A serial #29761 source with a Varian PaxScan 2520 detector.

The 3D Computed Tomography X-ray imaging system at the INL Research Center was designed by North Star Imaging of Rogers, MN. Possibly the most important components of the system are the extremely powerful graphical processing unit housed in the image reconstruction computer and the proprietary image processing software. Additional system components consist of a Hamamatsu 130 kVp microfocus x-ray unit capable of producing approximately 10 μm resolution images, a Varian PaxScan flat panel digital x-ray detector, and a rotational stage.

2.2.6 Density/Porosity of SiC-CMC

2.2.6.1 Summarized motivation. The density and porosity measurements of the SiC-CMC material are of importance as it gives an indication of water permeability during irradiation. It is also expected that the density of the CMC may change slightly due to the irradiation. As it is not yet quantified, this measurement is necessary as part of the test battery to be integrated with the rest of the results. Density measurements are a relative easy method to do for an ongoing production environment, and it will be very useful if this method is investigated in these early stages of the project. Density values will also provide a metric for changes in porosity which may be later correlated to chemical reactivity and hydrogen embrittlement.

2.2.6.2 Equipment and calibration65-23. Measurements will be performed by immersion density or micro-pycnometry. The immersion density measurement uncertainty is less than ±2%. Density measurements are described in PLN-3957[20] and are based on an ASTM (Standard Test Methods of Powder Metallurgy (PM) Materials Containing Less than Two Percent Posity-ASTM B 311-08) method[21] that doesn't require a calibration. A Mettler Toledo AG204 DeltaRange balance (INL Dwg. 715461) with a valid calibration at time of relevant measurements, was used. The measurements were completed at room temperature and weighing was executed with a balance with a sensitivity of 0.0001 g and density values are rounded off to the nearest 0.01g/cm^3. Results are recorded in Arnold Erickson's log book No. 6, pages 79-77 and 79.

2.2.7 Visual Examination and Dimensional Measurements

2.2.7.1 Summarized motivation. Visual examination will show possible fraying or defects or discoloration which may give an indication of any chemical reactions with the water during irradiation. CMC sleeve and Zr4 tube may expand differently during irradiation due to irradiation structural changes and temperature effects. Dimensional information can be used for stress calculations and possible predictions of fretting behavior.

2.2.7.2 Equipment and calibration. The dimensional inspection was completed in accordance with PLN-3961[22] and it focused on two parts namely the SiC/CMC tube and the Zr- 4 tube. All measurements were completed with equipment in known calibration status. Dimensional analyses were performed according to the following figure using a Mitutoyo series 500 calibrated caliper (see Figure 4). Samples were handled with gloves and all measurements were performed in triplicate. A Nikon 6C-2 profile project equipped with a calibrated Mitutoyo dimensional analysis instrument and a 20 × magnifying lens was used to measure the 'depth' of the CMC weave (Lab B-11). The depth was calculated as the difference between the "mountain" and "valley" measurements taken at triplicate locations at three points along the length of the SiC sleeve.

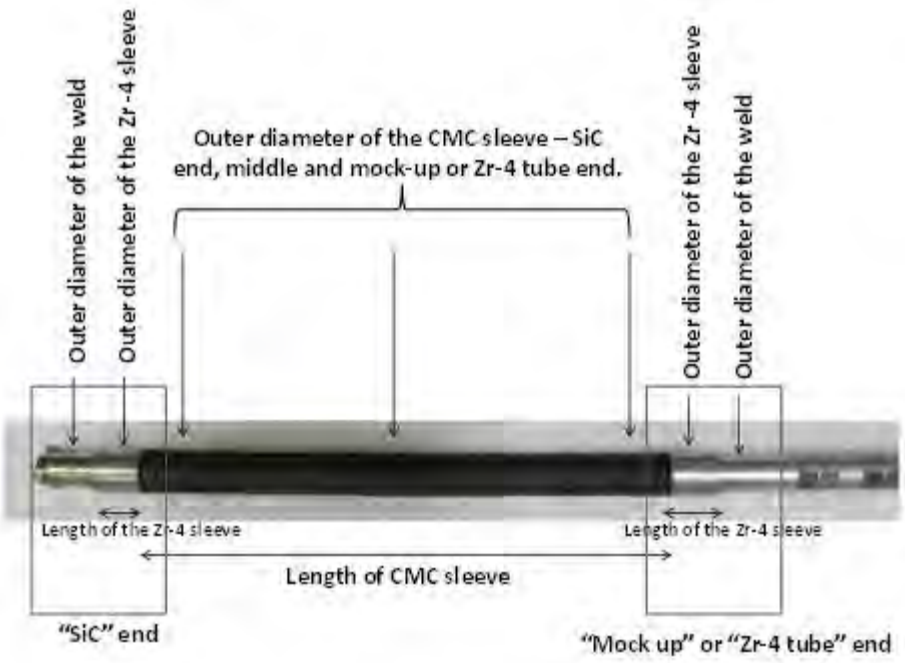

Figure 4. Diagram showing the position and labels of dimensional analysis of SiC sleeves on Zircalloy tubes.

2.2.8 Metallurgical Examination (SEM, SEM-EDS)

2.2.8.1 Summarized motivation. Metallurgical Examination is necessary to examine the interface properties and again may suggest the initiation of hydrogen embrittlement or any other corrosion and/or abrasive activity. Possible surface metallurgical changes may also be observed due to irradiation and temperature interactions. Hydrogen content will be determined after neutron irradiation.

2.2.8.2 Equipment and calibration. Electron microscopic examination is described in PLN-3964 [14] and is executed using a Quanta 650 FEG SEM with the EDAX Triton package. The calibration is performed by the service engineer with a SIRA S170 Certified Test Specimen. This is a magnification standard that is copied from a NIST standard. Ten cubes on this test specimen is equivalent to ~4.63 microns. An archived image from the last calibration from this specimen is available. An old NBS standard is then used for an image and is measured against the known values and is also archived in the SEM laboratory. Measurements are well within specification for the instrument which is ±3%. The NBS standard number is JY-55-VO.

2.2.9 XRD

2.2.9.1 Summarized motivation. XRD is completed to determine the actual SiC phase(s) and possible changes due to irradiation.

2.2.9.2 Equipment and calibration. X-ray diffraction patterns were measured using a Bruker-AXS D8-A25 in parallel beam mode at 40 kV and 40 mA. Parallel beam (PB) mode is created by a "Gobel Mirror" in the incident beam and removes sample displacement error that would be very apparent in the traditional Bragg/Brentanno mode because of the round sample. In PB mode the incident copper k alpha 1 and 2 hits the center of the sample in a narrow band about 13 mm long. The samples were set in some glazier putty diagonally to expose as much of the surface area. The information collected was matched with Bruker-AXS EVA software version 14.0 with a 2008 ICDD PDF-2 data base. Detection limit for a phase (element or compound) is greater than 5 w%.

Phase identification (search and match on Bruker's "EVA" software) uses Powder Diffraction Files (PDF) purchased from The International Centre for Diffraction Data or ICDD. These files normally report powder samples that contain very little texture also known as preferred orientation. Solid materials often have texture and do not follow the peak height or more recently peak area as reported by the PDF. The peaks themselves occur when diffraction occurs along a crystallographic plane.

A NIST alumina standard 1976 using the Al_2O_3 104 peak the tolerances below in 2Theta need to be met namely

- 2theta for Bragg Brentano (BB) =35.149 ±0.02
- 2theta for Parallel Beam (PB) =35.138 ±0.02.

2.2.10 Raman

2.2.10.1 Summarized motivation. Raman measurements may be useful to identify oxidation levels and oxidation products on the SiC-CMC sleeves of the HWCF mock-up samples. Preliminary work is done in this study to establish the usefulness of this technique to determine the corrosion levels.

2.2.10.2 Equipment and calibration. The system used is a Jobin Yvon Horiba LabRAM system, driven by a 532 nm Coherent Verdi laser. Measurements were taken at 50x magnification. The LabRAM system offers 10x and 100x objectives as well. During these preliminary exploratory measurements, the system was not calibrated prior to making these measurements. However, calibration was conducted prior the second set of measurements and the silicon standard provided on a microscope slide by the Raman instrument suppliers was used. The silicon calibration standard produces a peak at 520.7 cm-1. Prior to calibration, the standard peak was shown at 519.1 cm-1 and after calibration, the standard peak is shown at 520.8 cm-1. Results presented in this report are not cleaned up to remove the noise and results are reported in the raw format (the narrow, sharp spikes in the data are noise).

3. RESULTS AND DISCUSSION

3.1 Baseline Characterization

3.1.1 Density

The density was measured on four subsamples representing the range of samples tested in the bend and HWCF tests. Two additional sub sample results are available as it was measured as part of the gamma irradiation tests.[4] The detail of the sub-samples and measured density values are provided in Table 3 with detail of measurements in Appendix D. No significant differences are observed between the 5 and 7 PIP processed cycles (Figure 5) or the 1 and 2 ply braided (Figure 6) SiC-CMC sleeves when comparing these density values. The density value of subsample LWRS-1-6-A-1-5 is the highest. When comparing only LWRS-1-6-A-1 and LWRS-1-6-A-9, the suggestion is that the higher density value of LWRS-1-6-A-1-5 is due to the number of PIP cycles, but the general trend in the first graph makes this preliminary suggestion void. Thus another SiC-CMC sleeve fabrication parameter plays a role in the higher density value of LWRS-1-6-A-1-5. It is recommended that this trend is further investigated. A suggestion is that the PIP polymer properties, like the polymer composition, temperature of pyrolysis heat treatment or the time of pyrolysis, being investigated for this higher value.

Table 3. Density measurements of representative SiC-CMC sleeve sub-samples as fabricated.

Sample Number	SiC-CMC Processing Parameters	Density as received (g/cm^3)	STD
LWRS-1-6-A-1-5*	5 cycles, 2 ply	2.66	0.003
LWRS-1-6-A-3-3*	5 cycles, 1 ply	2.60	0.003
LWRS-1-6-A-2-2	5 cycles, 2 ply	2.58	0.011
LWRS-1-6-A-7-1-2	7 cycles, 2 ply	2.58	0.002
LWRS-1-6-A-9-1-2	7 cycles, 2 ply	2.55	0.011
LWRS-5-6-B-2-1-2	7 cycles, 1 ply	2.59	0.032

*Measurements reported in Gamma Irradiation report and were not exposed to gamma irradiation [4].

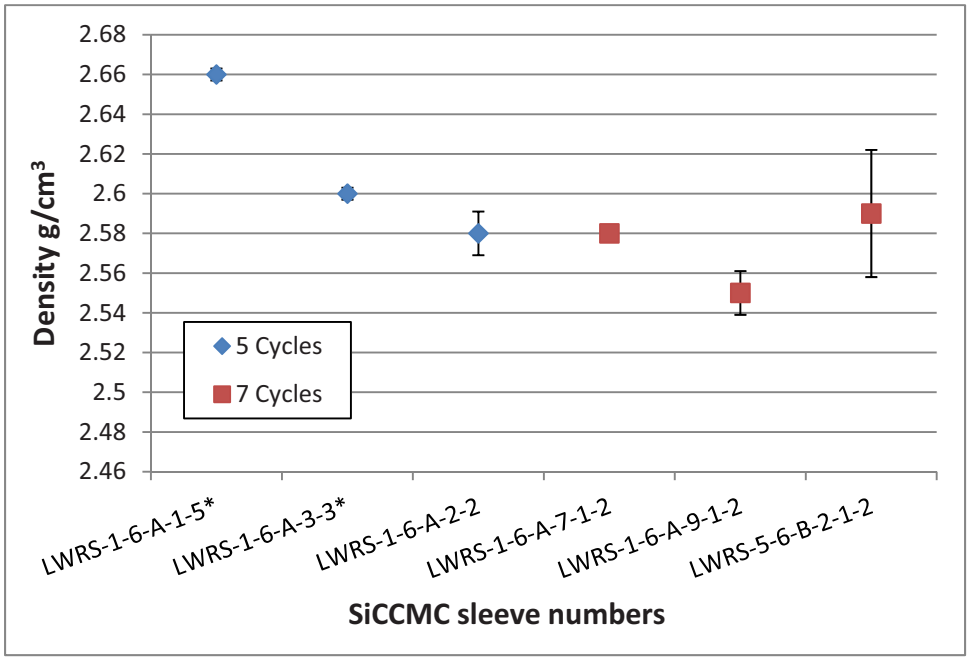

Figure 5. Density values of representative SiC-CMC sleeve samples presenting to show no significant difference between the 5 and 7 processed PIP cycles.

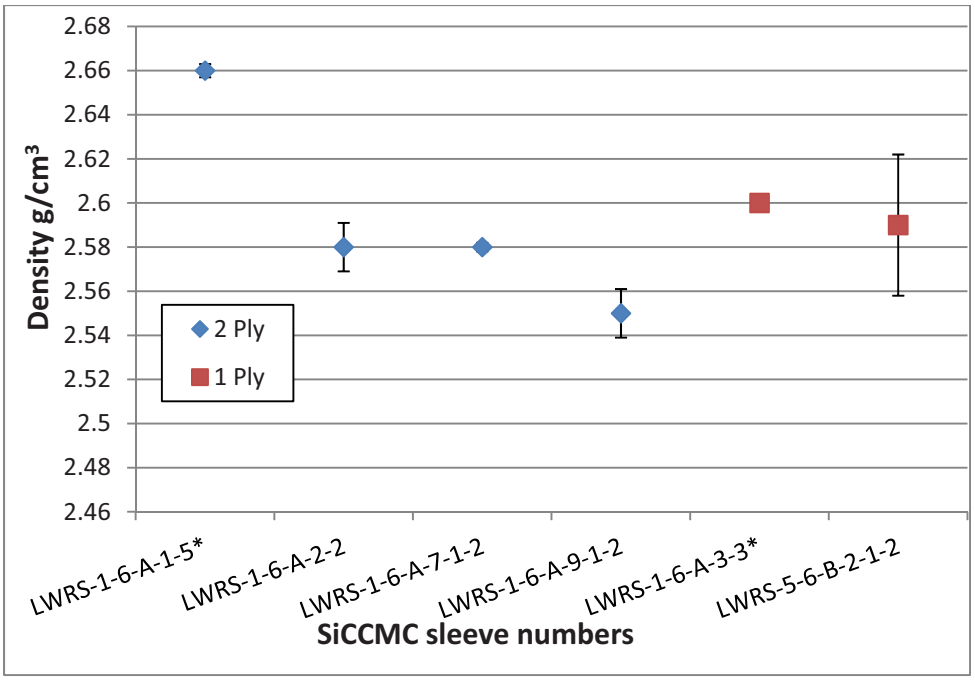

Figure 6. Density values of representative SiC-CMC sleeve samples presenting to show no significant difference between the 1 and 2 ply braided SiC-CMC tubes.

3.1.2 X-ray Diffraction

Figure 7 shows the comparative XRD patterns of the representative SiC-CMC sleeves processed with 7 PIP cycles (LWRS-1-6-A-7-1-1, LWRS-1-6-A-9-1-1 and LWRS-B-2-1-1) with a 5 cycle PIP processed sleeve (LWRS-1-6-A-2-1). The XRD patterns of the three samples fabricated with 7 PIP cycles showed similar patterns irrespective of number of braids. Mainly 3C-SiC are noted as indicated by the black arrows, however small indications of 6H SiC are also noted as shown in Figure 7 as shown by the grey arrows. However, the XRD pattern of the sleeve fabricated by 5 cycles only is slightly different by showing an additional peak at 47.596 of an unknown substance. Further work is required in consultation with the vendor to be able to identify this substance and the origin of it.

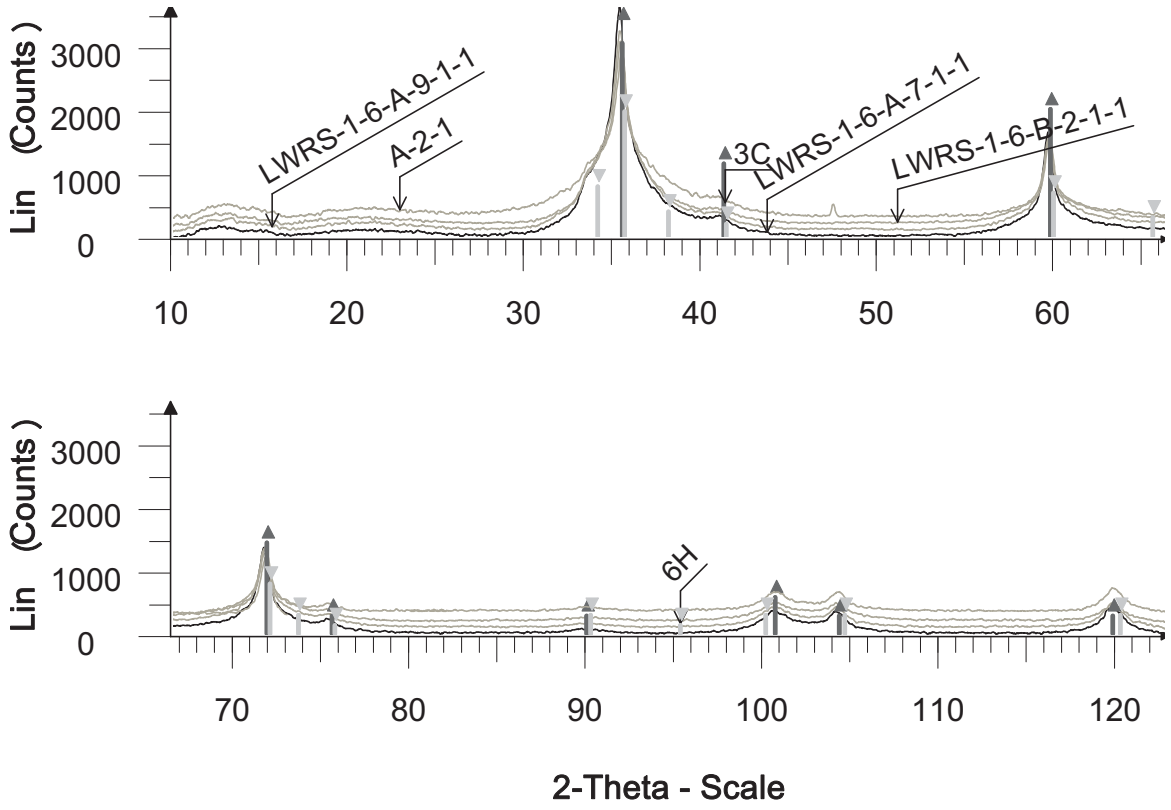

Figure 7. Comparative XRD patterns of the representative SiC-CMC sleeves processed with 7 PIP cycles (LWRS-1-6-A-7-1-1, LWRS-1-6-A-9-1-1 and LWRS-B-2-1-1) with a 5 cycle PIP processed sleeve (LWRS-1-6-A-2-1). Mainly 3C SiC with small indications of 6H SiC is observed in all samples.

3.1.3 Scanning Electron Microscopy

The micrographs in Figures 8 and 9 show the microstructure of the representative 2- and 1 ply SiC-CMC sleeve subsamples. The microstructures exhibit the same features namely open CMC fibers within a cracked SiC matrix with porosity visible. An increase in size and amount of visible flakes are observed comparing the microstructure of the 5 PIP processed to the 7 PIP cycle SiC matrix material. Additionally, the microstructure of the 1 ply braided SiC-CMC sleeve showed multiple exposed and broken CMC fibers as well as cracked SiC matrix with porosity. From these microstructures, it is expected that the bend momentum and corrosion behavior between the 1 and 2 ply SiC-CMC sleeves will show a difference.

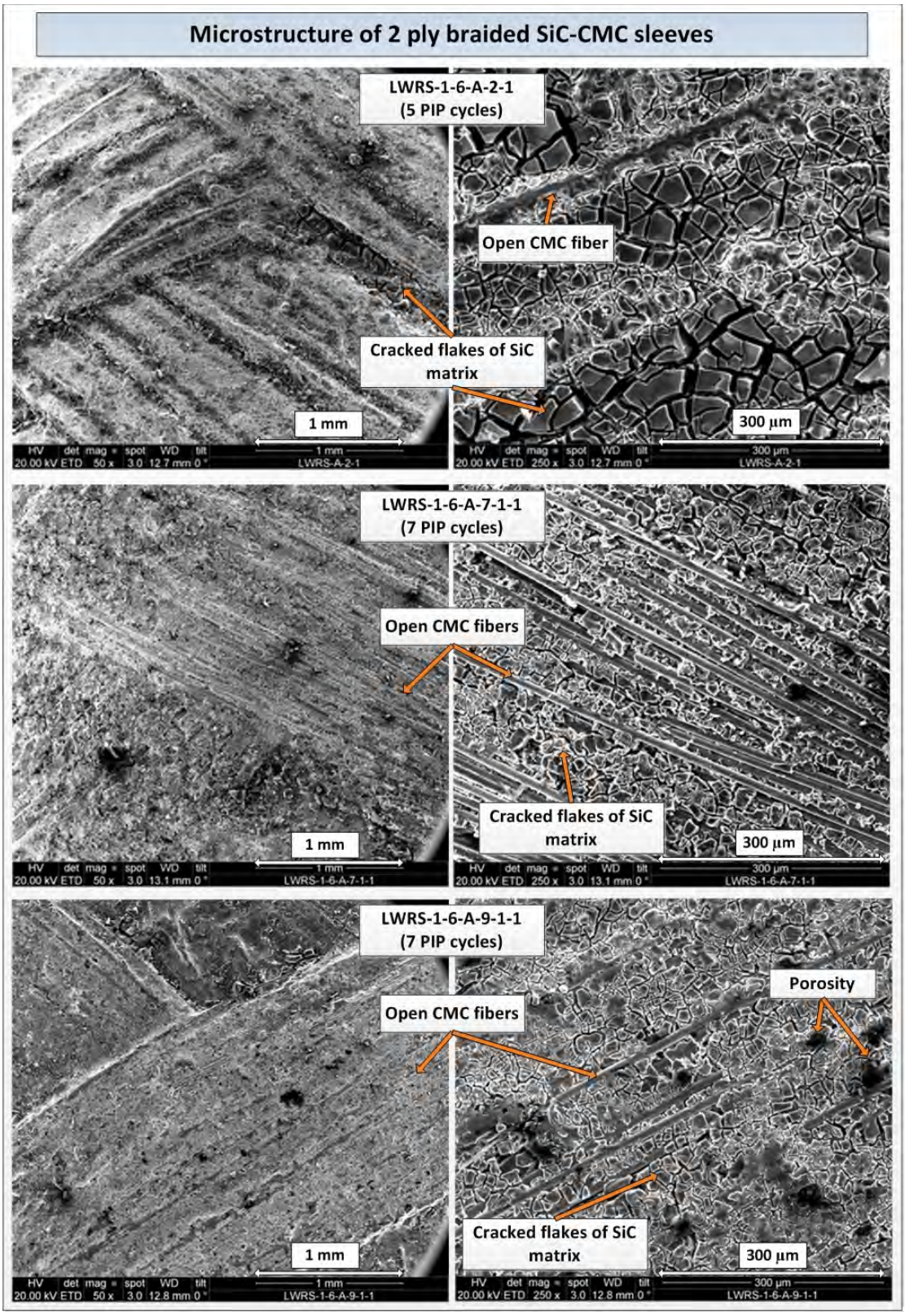

Figure 8. Micrographs showing the microstructure of the representative SiC-CMC sleeve subsamples of the 2 ply braided SiC-CMC tubes.

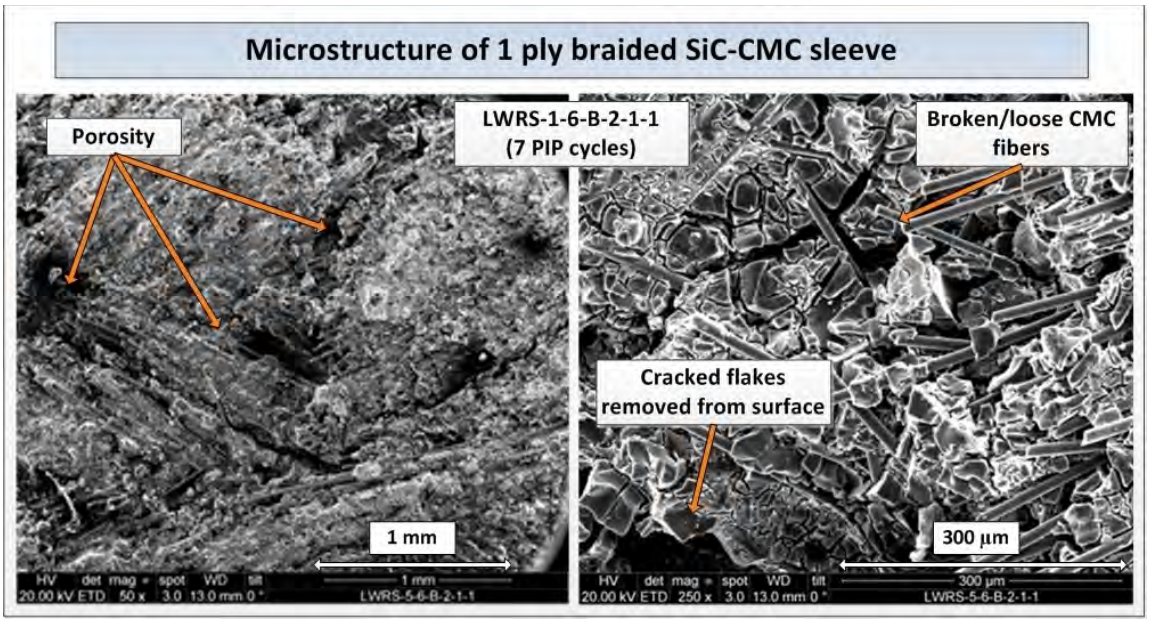

Figure 9. Micrographs showing the microstructure of the representative SiC-CMC sleeve subsamples of the one ply SiC-CMC tubes.

3.1.4 Qualitative Chemical Analysis

The Zircaloy-4 tubes were received with certification from the vendor. As part of the non-disclosure agreement, no third party chemical analysis was allowed. As part of the metallurgical examination of the gamma irradiation parts[4], representative unirradiated Zr-4 samples were examined as a baseline to determine the surface condition and the main chemical elements using SEM-EDS. The primary elements were identified as Zr, Sn, C, O and N as shown in Figure 10. This analysis cannot be used as a quantitative measure, but it confirms only that this material is not a Zircodyne alloy as no Nb and Hf was identified. However, due to the unintentional use of Zircodyne (Hf containing Zr-alloy) during the fabrication of the second gamma irradiation test, SEM-EDS analysis were completed on all the Zr-4 tubes of the mock-up samples. All these analyses confirm Zr-4 as the material used for the bend test and HWCF mock-up samples. The specific SEM–EDS analysis will be shown in Subsections 3.3.1 and 1.1.1 as part of the SEM metallurgical examination.

Additionally, SEM-EDS analysis was also completed on the SiC-CMC sleeves although secondary ion mass spectrometry (SIMS) analysis is recommended for the receiving inspection stages for a detail quantitative analysis. The EDS analysis showed the presence of the main elements, due to the detection limit, trace-elements will not be detected. The XRD and Raman examinations maybe used with further work to identify the presence of additional elements; however, this needs to be explored further as characterization techniques.

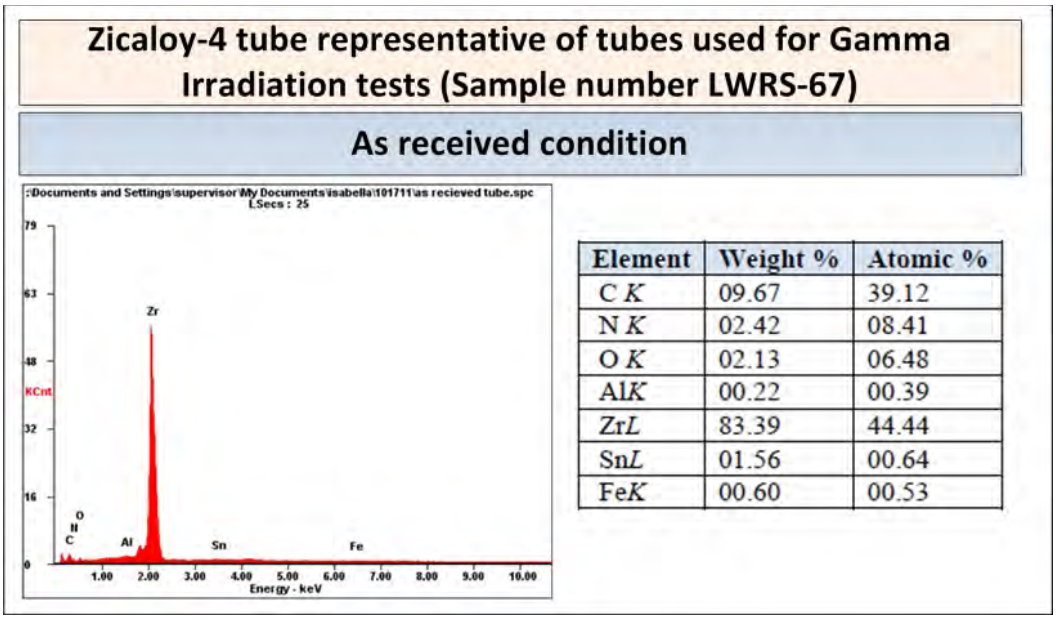

Element	Weight %	Atomic %
C *K*	09.67	39.12
N *K*	02.42	08.41
O *K*	02.13	06.48
Al*K*	00.22	00.39
Zr*L*	83.39	44.44
Sn*L*	01.56	00.64
Fe*K*	00.60	00.53

Figure 10. SEM-EDS analysis of the Zr-4 tube used for the gamma irradiation tests (sample number LWRS-67).

3.2 Leach Testing

3.2.1 Leach Testing on CMC Fibers

The bare Hi-Nicalon Type S SiC fibers were tested to ensure lot compliance before the SiC tubes were braided. Each lot of SiC fiber was qualified as compliant with the ATR water specifications as shown in Table 4. The specifications are given in SP-10.3.1.13 (referencing SAR-153)[12] as being below 250 ppm individually, or combined 500 ppm of ions.

Table 4. Bare Hi-Nicalon Type S SiC Fiber Sample Results for Ion Chromatography (1 µg/mL is equivalent to 1 ppm.)

Sample	µg F \ mL	µg Cl \ mL	µg Br \ mL
57A	<0.393	10.538	<0.024
57B	<0.393	5.559	<0.024
58A	<0.393	8.136	<0.024
58B	<0.393	4.510	<0.024
59A	<0.393	1.516	<0.024
59B	<0.393	1.161	<0.024
60A	<0.393	0.730	<0.024
60B	<0.393	<0.073	<0.024
61A	<0.393	0.146	<0.024
61B	<0.393	<0.073	<0.024
62A	<0.393	<0.073	<0.024
62B	<0.393	<0.073	<0.024
63A	<0.393	<0.073	<0.024
63B	<0.393	<0.073	<0.024

3.2.1.1 Leach testing on SiC-CMC braided sleeves. Although the chloride concentration increased from 0.228 ppm to 20 ppm for the LWRS-1-6-A-1-4 sample, it is still within the specification of <250 ppm (Table 5). It is also interesting that samples LWRS 1-6 A 3-2 and LWRS 1-6- A-2-1 showed a detectable quantity when compared to the rest of the samples. These results showed no specific trend for differences observed to differentiate between the number of braided plies and the number of PIP processing cycles. However, this needs to be verified with a larger number of samples for a better statistical soundness.

Table 5. Leach test water analysis on representative SiC-CMC samples.

Sample Number	F	Cl	Br	Al dissolved	Fe dissolved (ppb)	Cu dissolved (ppb)	Si
	(ppm)			(ppb)			(ppm)
LWRS 1-6- A-1-4* (5 cycles, 2 ply)	ND	20.008	ND	<0.158	NM	NM	77.100
LWRS 1-6-A-3-2* (5 cycles, 1 ply)	ND	1.213	0.455	<0.158	NM	NM	46.950
Water Control - 8/15/12	<0.544	<0.066	<0.116	Results not available at time of report writing			
LWRS 1-6- A-2-1** (5 cycles, 2 ply)	<0.544	3.713	0.291				
LWRS 1-6- A-7-1-1** (7 cycles, 2 ply)	<0.544	0.661	<0.116				
LWRS 1-6-A-9-1-1** (7 cycles, 2 ply)	<0.544	0.627	<0.116				
LWRS 5-6-B-2-1-1** (7 cycles, 1 ply)	<0.544	1.564	<0.116				

ST = Specify total only

NS = Not specified

NM = Not measured

ND = Not determined

*Representative samples used in gamma irradiation tests 2.[4]

** Representative samples used in this study

3.3 Bend Test

3.3.1 Method Development and Simulation

The results of 4-point bending tests performed on fully assembled hybrid cladding tube mock-ups, an assembled Zr-4 cladding tube mock-up as a standard and initial testing results on the bare SiC-CMC sleeves to assist in design parameters are reported in this section. Although the tests and results described in this section are on tubular samples, the ASTM standard C1161-02c[10] was used for guidance. Four point bend tests are the ASTM preferred method. Flexural strength of ceramic material is strongly dependent on both its inherent resistance to fracture and the severity of flaws. Therefore it was also important for this program that the actual surface finish of the SiC-CMC sleeve is used during this test and no sample preparation is used to obtain a smooth defect free surface. Typically for four point bend tests, a span width ratio of either 3:1 or 4: 1 can be used. This span width ratio is shown schematically in Figure 11.

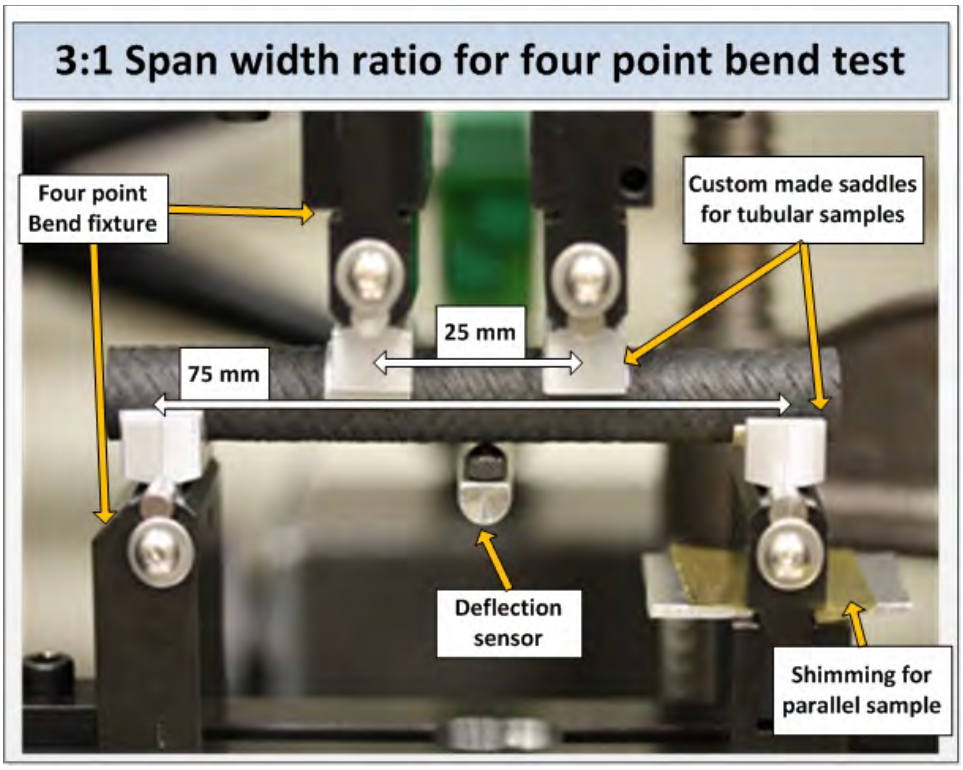

Figure 11. Micrograph demonstrating the span width ratio determination and bend test parts.

A next-generation nuclear fuel performance code called BISON[23] was used for simulating the 4-point bend tests. BISON is built using the INL Multiphysics Object-Oriented Simulation Environment (MOOSE),[24] which is a massively parallel, finite element-based framework to solve systems of coupled non-linear partial differential equations using the Jacobian-Free Newton Krylov method. Only initial finite element analysis of a plain Zr-4 tube in the elastic region is simulated. Results showing the stress distribution for varying lengths between loading points (span width). Figures 12 and 13 show the difference in stress distribution for a four point bend test on Zr-4 with span width 3:1 and 4:1, respectively. No significant differences were observed during this simulation. It was decided to proceed with the initial method development using a 3:1 span width ratio for the four point bend tests.

The initial method development started with the calibration of the deflect meter and programming of the Universal Instron main frame (load cell) Instron 5869 (Figure 14). To ensure adequate and even stress distribution when loading the tubular sample, custom made “saddles” were fabricated by INL as shown in Figure 15. In addition to these saddles, additional supportive rollers were design for the sleeve-only tests to prevent the SiC-CMC sleeve from being crushed on applying the load.

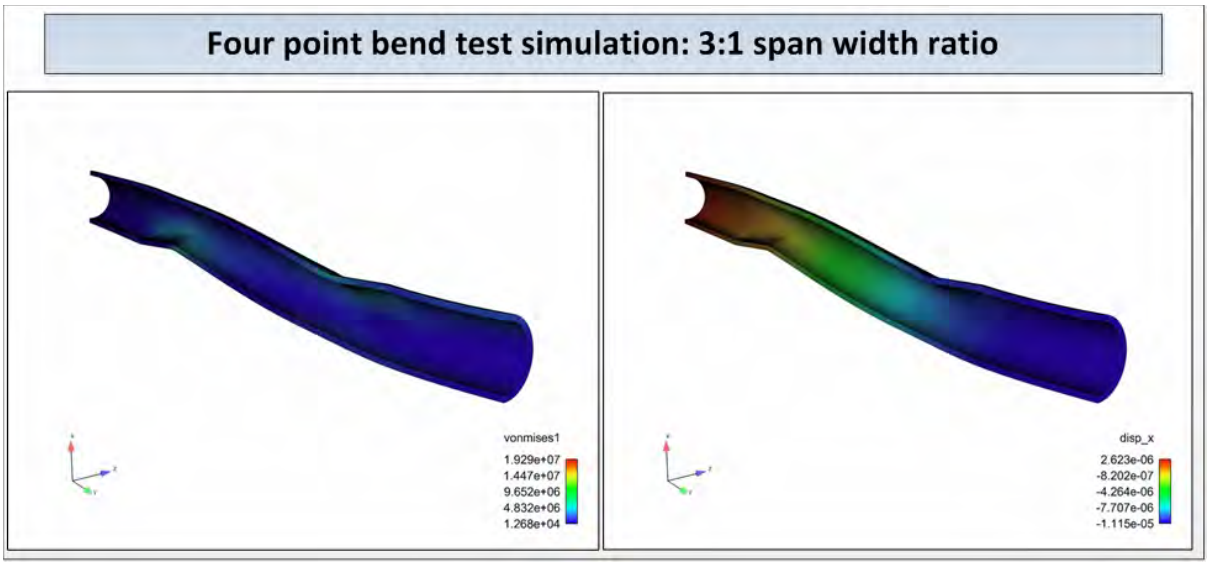

Figure 12. Initial simulation results presenting the elastic case during a four point bend test with a 3:1 load span width on Zr-4. The simulation was completed on half of the sample length.

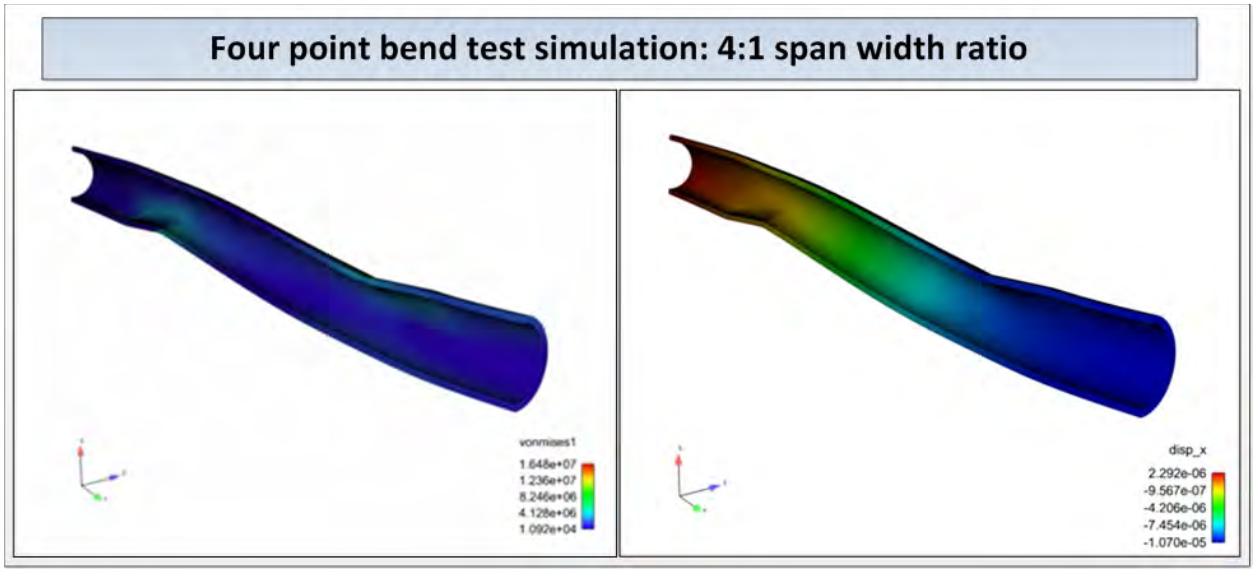

Figure 13. Initial simulation results presenting the elastic case during a four point bend test with a 4:1 load span width on Zr-4. The simulation was completed on half of the sample length.

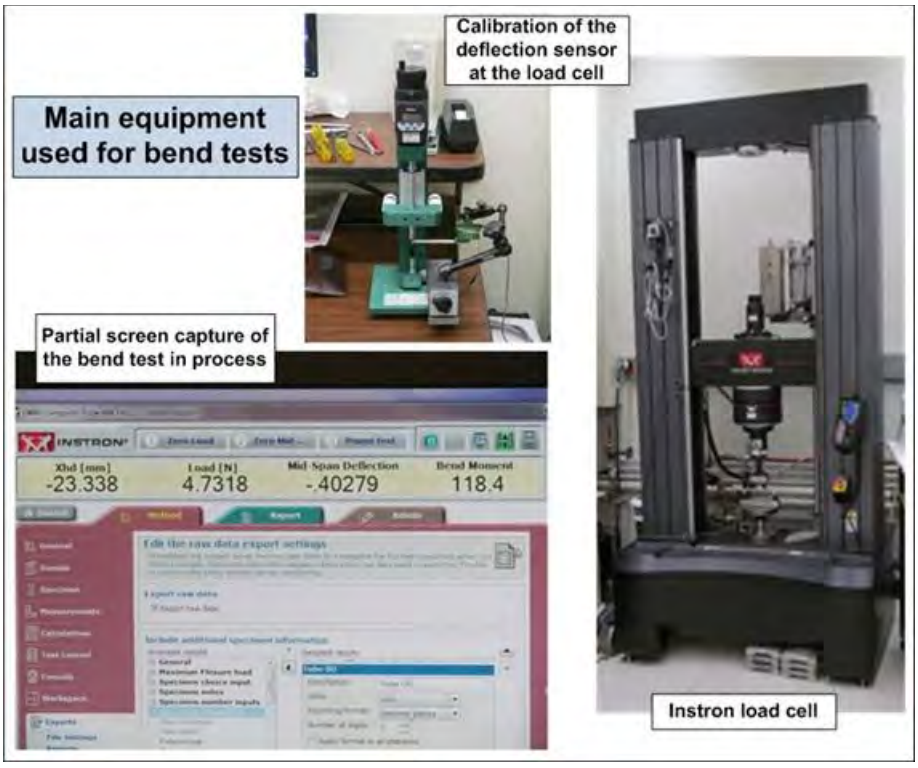

Figure 14. Main components used for the bend tests of the LWRS mock-up and SiC-CMC sleeve samples.

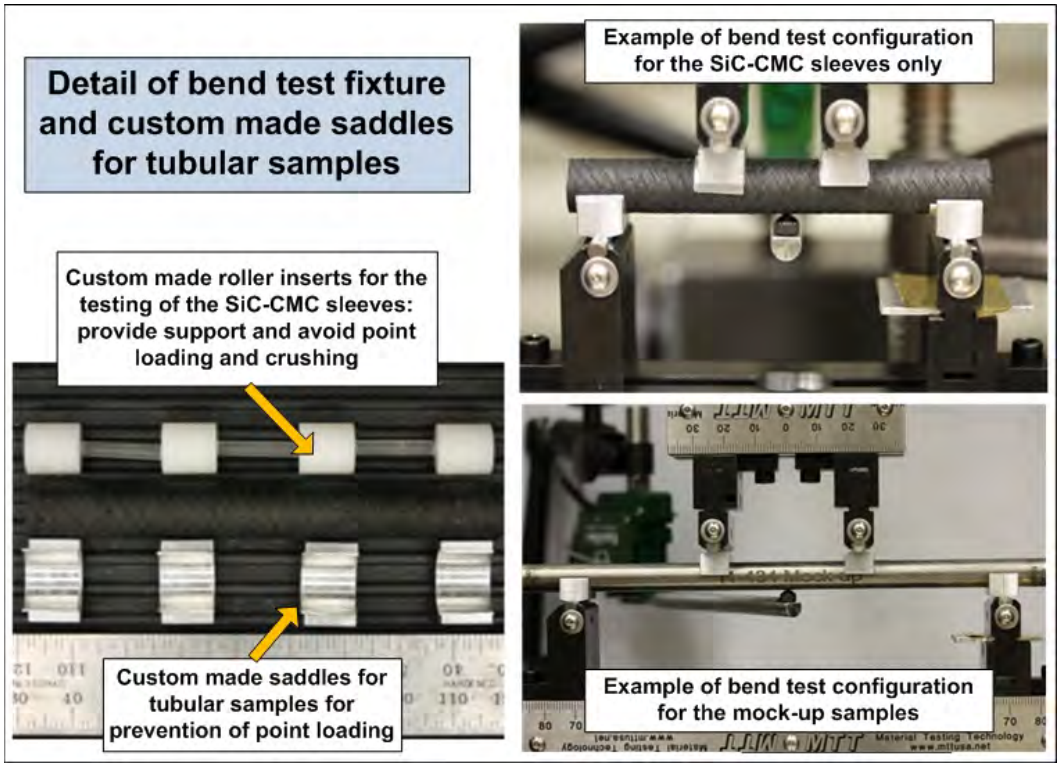

Figure 15. Bend test fixture and saddle design for the mock-up samples and SiC-CMC sleeves.

The program used for executing this bend tests, is recorded with Bluehill 3 software version 3.13.1260. As part of the input requirements for the bend moment calculations during the programming stages, accurate outer dimensions were needed. As these hybrid mock-up samples were delivered as development samples (quality level 3) actual as-built measurements were taken by the characterization team. The first question for the bend test was whether there was a difference in the outer diameter of the 1-ply vs. the 2-ply hybrid mock-up samples. All the measurements were averaged along the length of the samples and compared the sample means and their associated variability in a t-test (Table 6). The test was two-tailed with a α of 0.025 in each tail. The conclusion is that there is not a difference in the outer diameter of the SiC-1 and SiC-2 tubes and therefore the same program could be used for testing both hybrid mock-up samples.

Table 6. Comparison of outer dimension of SiC-1 and SiC-2.

Sample ID	Weave ply	Outer Diameter		Test Statistic	t-value (df =17, α = 0.025)	Conclusion
		Average (mm)	stdev			
SiC-1	2-ply	11.08	0.083886	2.7×10^{-22}	1.960	Do not reject null hypothesis
SiC-2	1-ply	11.25	0.080687			

3.3.2 Bend Test Results

Initial testing started with the Zr-4 mock-up tube (SiC-6) to verify that the saddles and program was sufficient. As strain rate is an important factor, a standard 1.0 mm/min were initially used for the Zr-4 mock-up sample. The strain rate was decreased to 0.5 mm/min for the hybrid mock-up samples as it was unknown at that stage how soon changes will be noted. The strain rate was further decreased during the bend test method development for the SiC-CMC sleeves as discussed in Subsection 3.3.2.2. As the strain rates were chosen to be typically in the order of 0.1 to 0.25% /min which are regular tensile test strain rates, it is expected that there should be no rate effects of consequence at these low rates.

A summary of the bend test process parameters is provided in Table 7.

Table 7. Bend test process parameters for all samples tested during method development.

Sample Number	Sample Description	Bend Test Rate (mm/min)	Actual Span Width (mm)	Span Width Ratio
LWRS-1-6-A-2-3	5 cycles, 2 ply Sleeve only	0.15	75/25	3:1
LWRS-1-6-A-3-4	5 cycles, 1 ply Sleeve only	0.25*	75/25	3:1
LWRS-1-6-A-6	5 cycles, 1 ply Sleeve only	0.15	75/25	3:1
LWRS-1-6-A-9	7 cycles, 2 ply SiC-1	0.5	120/40	3:1
LWRS-5-6-B-1	7 cycles, 1 ply SiC-2	0.5	120/40	3:1
Zr-4 assembled	N/A SiC-6	1.0	140/46.7	3:1

*First bend test on SiC-CMC sleeves. The strain rate was found to be too fast and was decreased for the next two tests.

3.3.2.1 Mock-up hybrid samples. The first test on the Zr-4 mockup tube showed a shortfall in the initial test, as a maximum deflection value of 10% prohibited the test to continue to a maximum load condition for Zr-4 as shown in Figure 16. This was corrected when the hybrid mock-up samples were conducted. The deflectometer used in the test, shown in Figure 17, was used to do a more accurate measurement of the deflection up to 2% changes, as it was important to detect early material changes. Additionally, this also aids as verification for the built-in deflection measurement system of the Instron load cell. No differences between these two measurements were found for all three mock-up samples. (Graphs in Figure 16 show only the Instron measurements.) Figures 17 to 18 show the bend test at the start and completion of all three mock-up samples. Slippage of the saddles was observed at the end of the testing of the hybrid mock up samples SiC-1 and SiC-2. This is not considered to have an influence on the final results as the comparative nature of the test showed still sufficient differences between the bending momentums of the three samples. It is seen from Figure 16, that the 2 ply SiC-CMC hybrid mock-up sample exhibited the highest bending moment with the Zr-4 mock-up sample exhibiting the lowest. Cracks and bundling of the SiC-CMC fibers were observed for the 2 ply braided sleeve hybrid mock-up sample (SiC-1) in the mid section of maximum deflection, while no bundling or cracking was observed for the 1 ply braided hybrid mock-up sample (SiC-2). The metallurgical examination and discussion of these maximum bending sections is shown in Subsection 3.3.3.

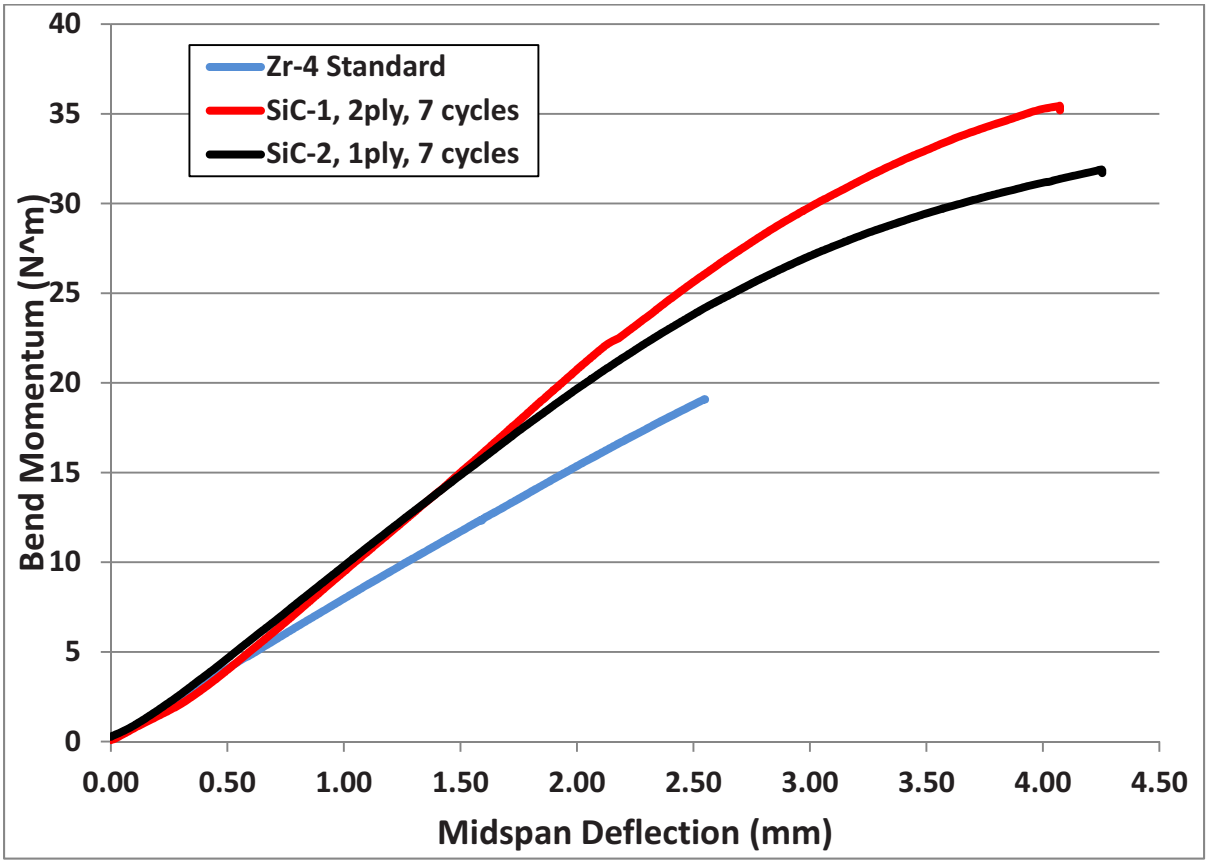

Figure 16. Bend test results of the mock-up samples showing bending momentum vs. mid-span deflection. The 2 ply SiC-CMC hybrid mock-up sample exhibits the highest bend momentum.

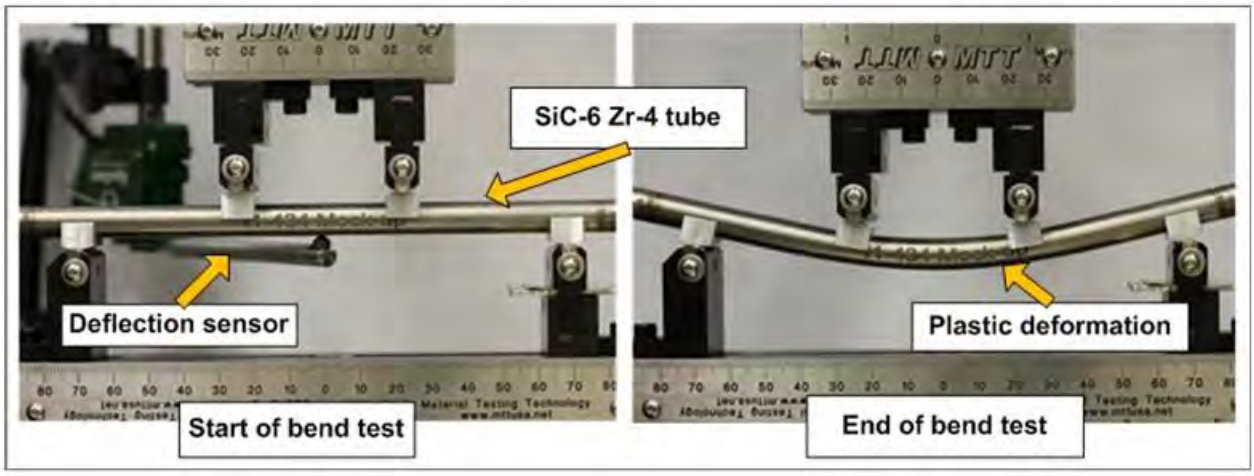

Figure 17. Bend test results of the Zr-4 mock-up sample (SiC-6) at start and end of bend test, showing plastic deformation.

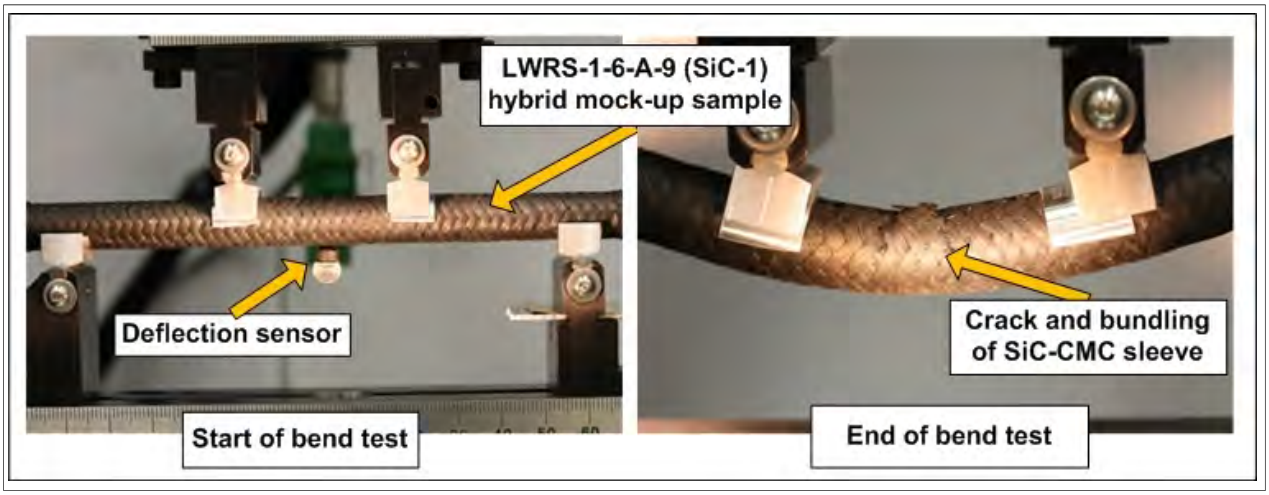

Figure 18. Bend test results of the 7 cycles, 2 ply LWRS-1-6-A-9 mock-up sample (SiC-1) at start and end of bend test, showing cracking and bundling of the SiC-CMC sleeve.

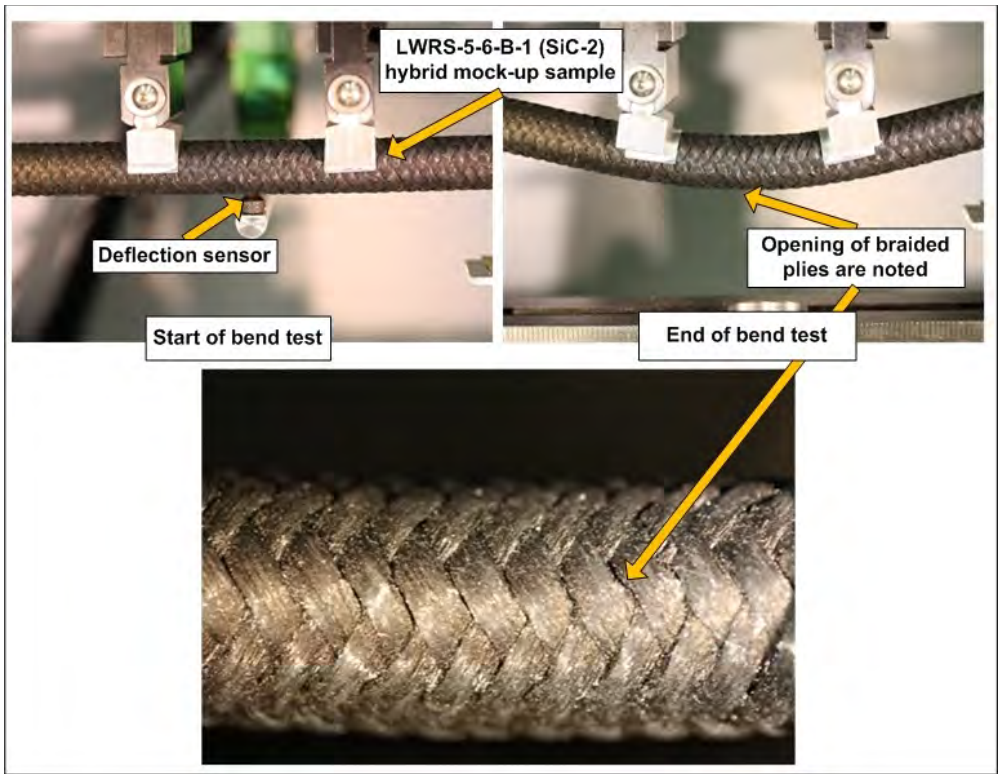

Figure 19. Bend test results of the 7 cycles, 1 ply LWRS-5-6-B-1mock-up sample (SiC-2) at start and end of bend test, showing the opening of the braided plies.

3.3.2.2 SiC-CMC sleeve samples. As mentioned previously, special roller inserts were manufactured for the bend test of the SiC-CMC sleeves alone. Only sleeves fabricated with 5 PIP cycles were available for these tests, although differentiation could be made between the numbers of braided plies. A one ply sleeve, LWRS-1-6-A-3-4, were tested first using half of the strain rate used for the mock-up samples. This was decided upon due to the expected brittle nature of the SiC-CMC sleeve without the ductile Zr-4 tube as inner tube. For the validation test on a 1 ply braided sleeve fabricated identical, the strain rate was decreased even further to 0.15 mm/min. Bend test results of the 5 cycles, 1 ply (LWRS-1-6-A-3-4 and LWRS-1-6-A-6) in comparison with the 5 cycles, 2 ply (LWRS-1-6-A-2-3) SiC-CMC sleeves, showing the higher bending moment of the 2 ply SiC-CMC (Figure 20). Figures 21 to 23 show the bend test at the start and completion of all three mock-up samples. Cracks in the SiC-CMC sleeves are observed for two sleeves namely the 1 ply (LWRS-1-6-A-6) and the 2 ply (LWRS-1-6-A-2-3). No cracking was visually noted on the 1 ply LWRS-1-6-A-3-4 sleeve although loosening of the braided weaves was noted. However, the 3 D x- ray tomography inspection also showed cracking in this sample as shown in Subsection 3.3.3.1. The metallurgical examination and discussion of these maximum bending sections is shown in Subsection 3.3.3.2.

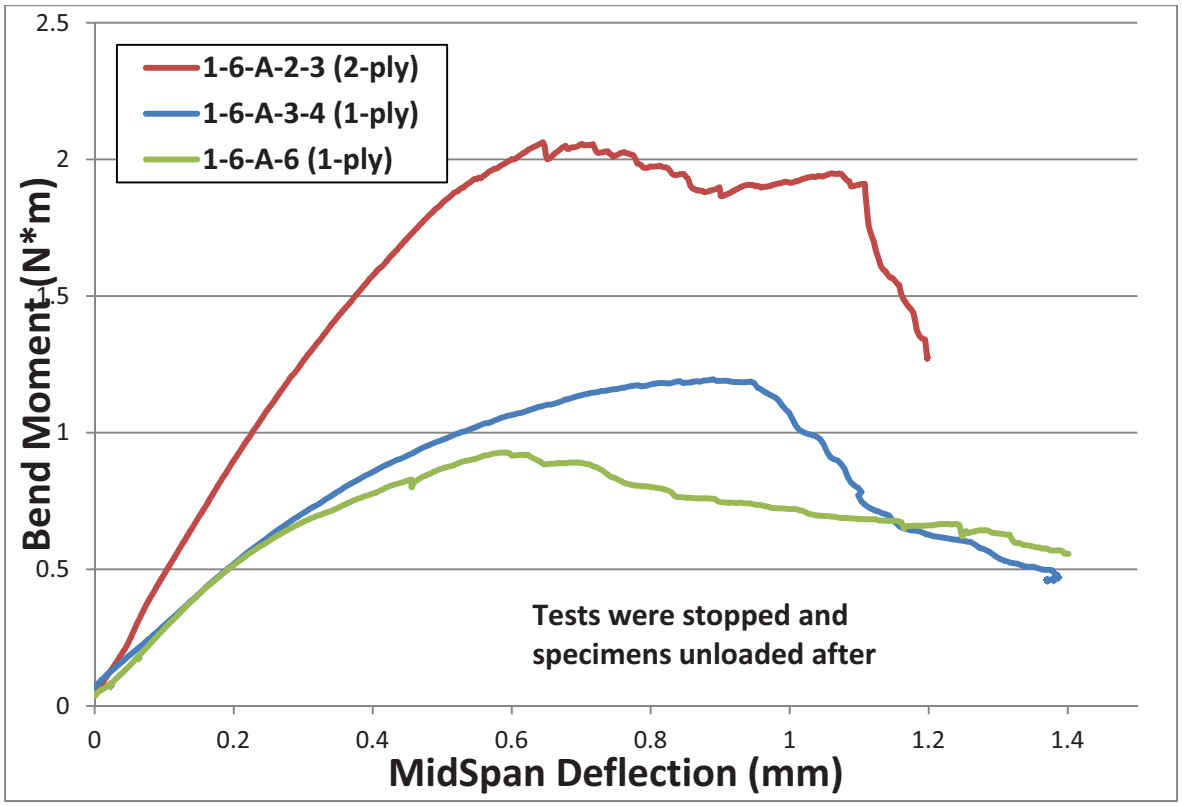

Figure 20. Bend test results of the two identical fabricated 5 cycles, 1 ply (LWRS-1-6-A-3-4 and LWRS-1-6-A-6) in comparison with the 5 cycles, 2 ply (LWRS-1-6-A-2-3) SiC-CMC sleeves, showing the higher bend moment of the 2 ply SiC-CMC.

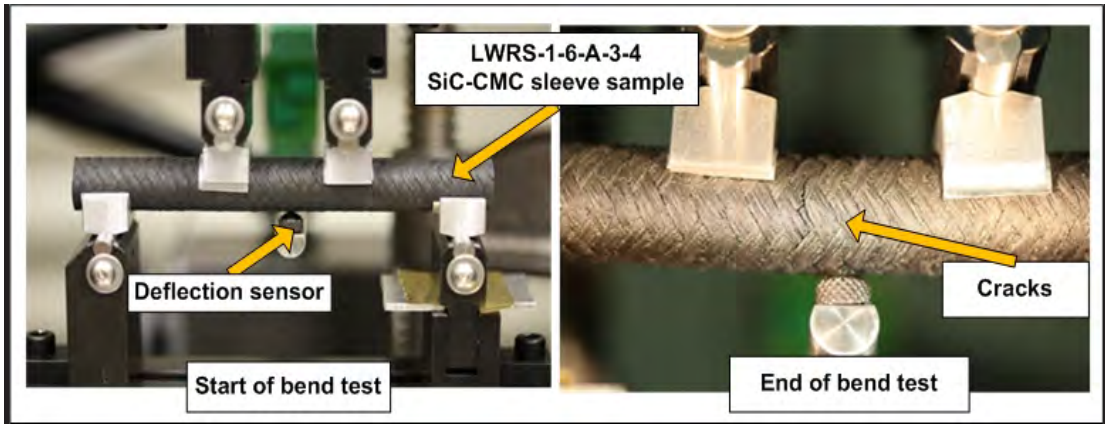

Figure 21. Bend test results of the 5 cycles, 1 ply LWRS-1-6-A-3-4 SiC-CMC sleeve sample at start and end of bend test, showing cracks.

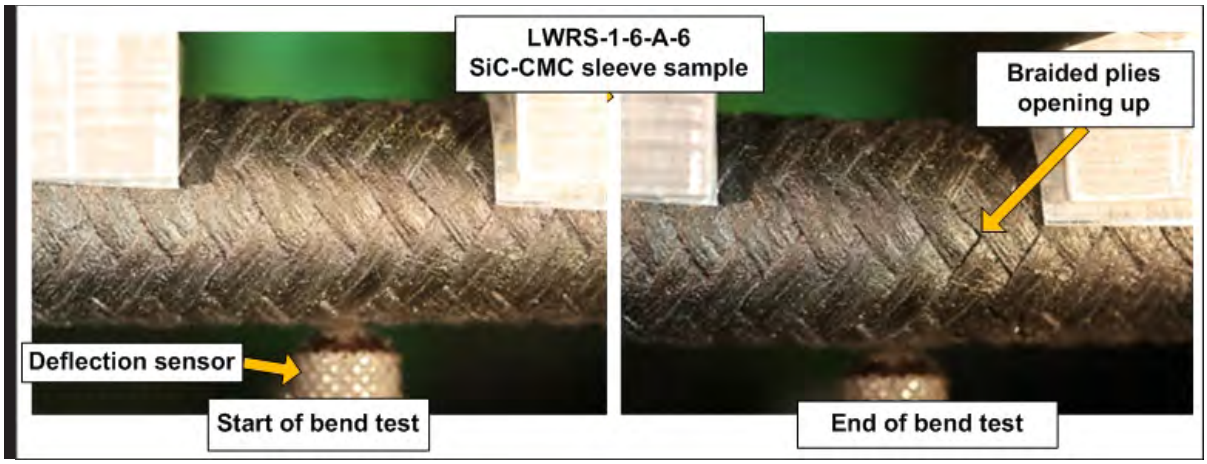

Figure 22. Bend test results of the 5 cycles, 1 ply LWRS-1-6-A-6 SiC-CMC sleeve sample at start and end of bend test, showing no fiber cracks but indication of "loosening" of weave pattern is noted and therefore the plies are opening up.

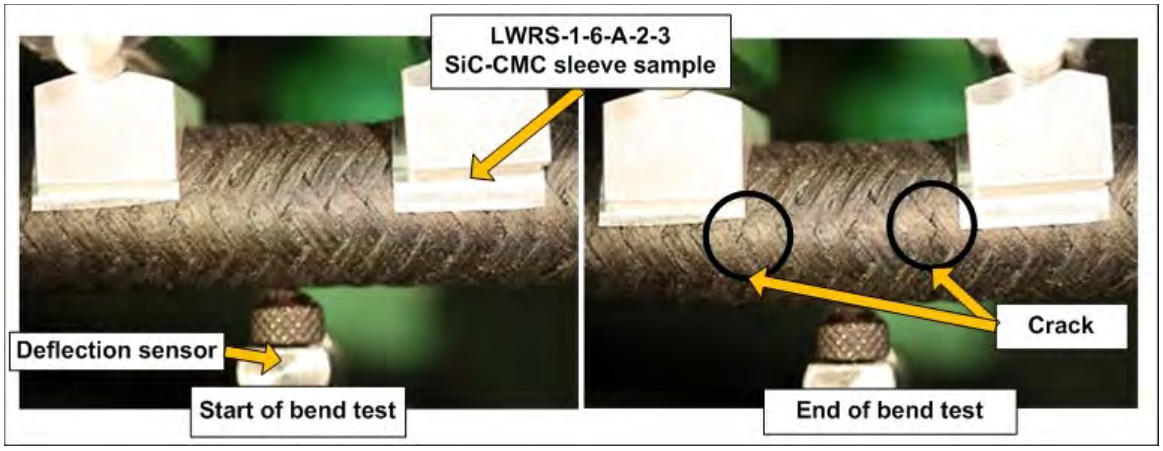

Figure 23. Bend test results of the 5 cycles, 2 ply (LWRS-1-6-A-2-3) SiC-CMC sleeve sample at start and end of bend test, showing cracks in the mid-span section.

3.3.3 Characterization of Bend Test Samples

3.3.3.1 Radiographic examination. Although 3D tomography was the recommended non-destructive inspection technique,[4] the equipment was out of commission at the time of the mock-up sample testing, therefore only 2D x-rays were taken prior to bend testing. The advantages of the 3 D tomography examination were again demonstrated with the inspection after bend testing. Fortunately at the time for method development for the SiC-CMC sleeves alone 3D tomography could be utilized prior to testing and therefore a direct comparison could be made.

Figure 24 shows a typical example of the deformation of the Zr-4 tube due to the bend test. It is observed that the inner Zr-4 tube of the SiC-1 sample showed more plastic deformation. Although not yet integrated, it is recommended that these results be integrated in future modeling of the hybrid tubes as this typically will show the actual constraints that the SiC-CMC sleeve placed on the inner Zr-4 tube. (Please take note that the two micrographs of SiC-6 and SiC-1 cannot be directly compared in this study, as both were not loaded to the same load due to the method alteration needed after testing SiC-6). For future tests this will be possible as the method can now be standardized.

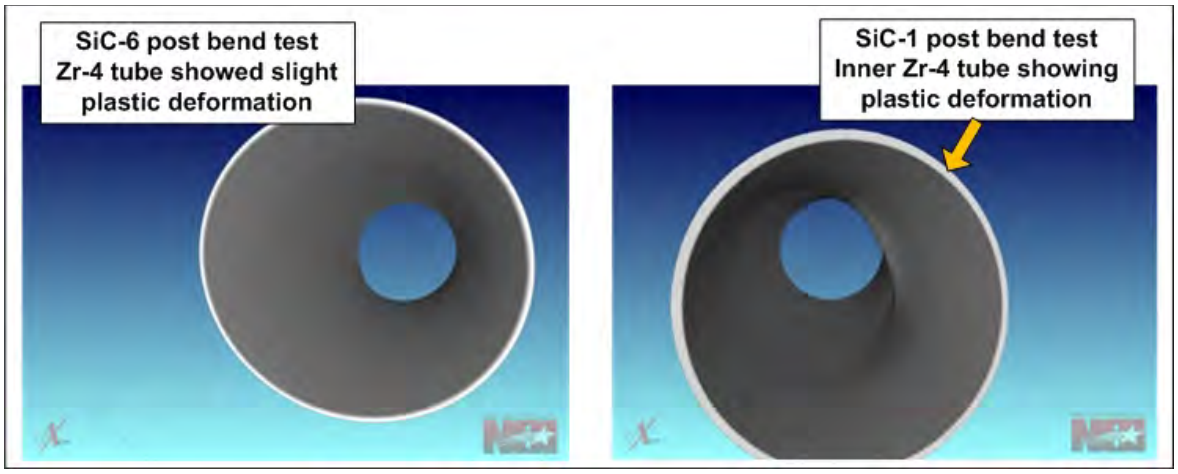

Figure 24. Tomography post bend test results showing amount of plastic deformation on the inner Zr-4 tube.

The 3D tomography images show in Figure 25 the effect that the distortions have on the SiC-CMC-Zr-4 gap at any position. This again may provide design inputs to the simulation codes for the cladding design and needs to be evaluated further in conjunction with the modeling experts.

Open porosity is detected in the 1 ply hybrid mock-up sample (SiC-2) even with the naked eye prior to the bend test (Figure 26). Additionally 3 D tomography examinations also detected open porosity in the two 1 ply SiC-CMC sleeve samples (LWRS-1-6-A-3-4and LWRS-1-6-A-6) prior to bend testing (Figure 27). No open porosity is observed for the 2 ply SiC-CMC sleeve sample (LWRS-1-6-A-2-3) during the radiographic and visual inspections.

The cracks due to the bend test on the three SiC-Sleeve samples are shown in Figures 28 to 30. It is interesting to note that the 2 ply sleeve showed two (almost) parallel cracks but the 1 ply samples showed one set of cracks branching.

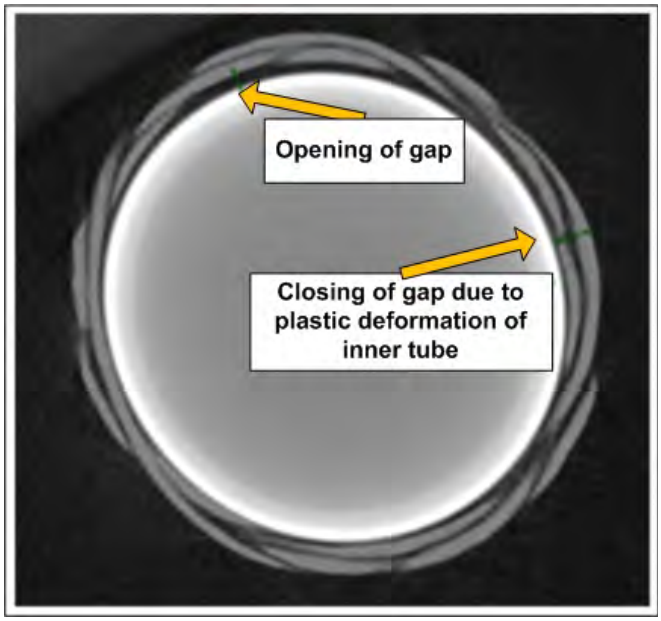

Figure 25. Tomography post bend test results of hybrid mock-up sample SiC-2 showing the bending of the inner Zr-4 tube and the subsequent closing of gap between the SiC-CMC sleeve and the Zr-4 tube.

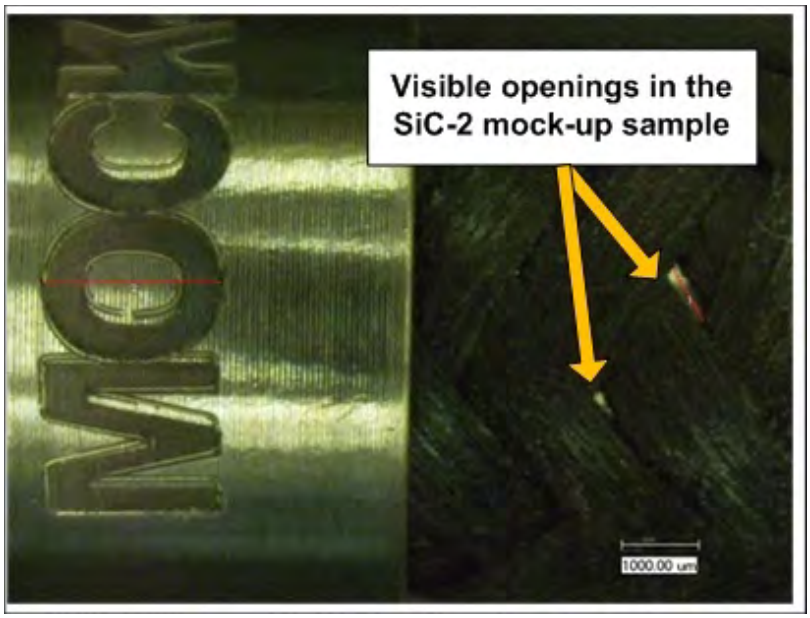

Figure 26. Open porosity is already visible prior to radiographic inspection with the naked eye on the SiC-2 mock-up sample.

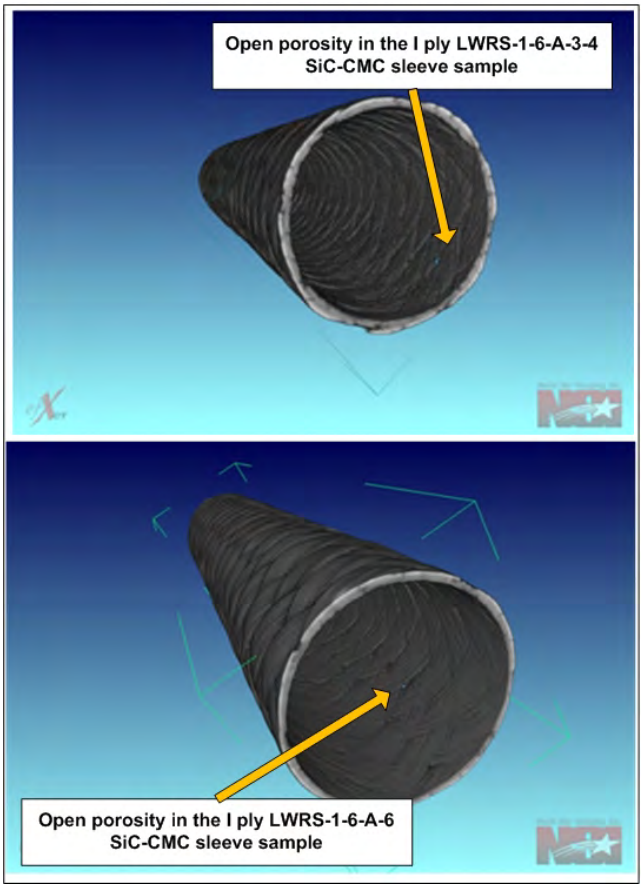

Figure 27. Open porosity is also detected in the two 1 ply sleeve samples (LWRS-1-6-A-3-4 and LWRS-1-6-A-6) during tomography examination.

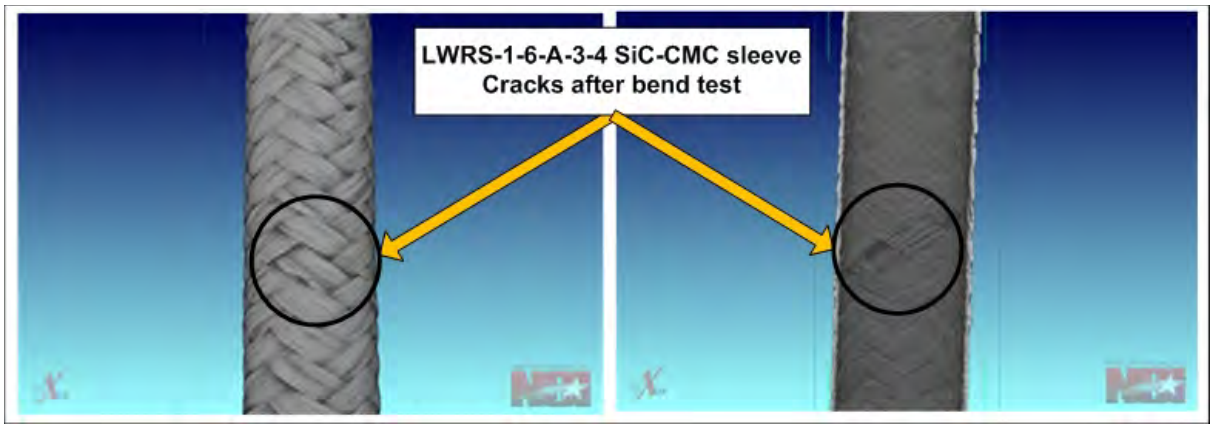

Figure 28. 3D Tomography results of the 5 cycles, 1 ply (LWRS-1-6-A-3-4) SiC-CMC sleeve sample post bend testing showing cracks.

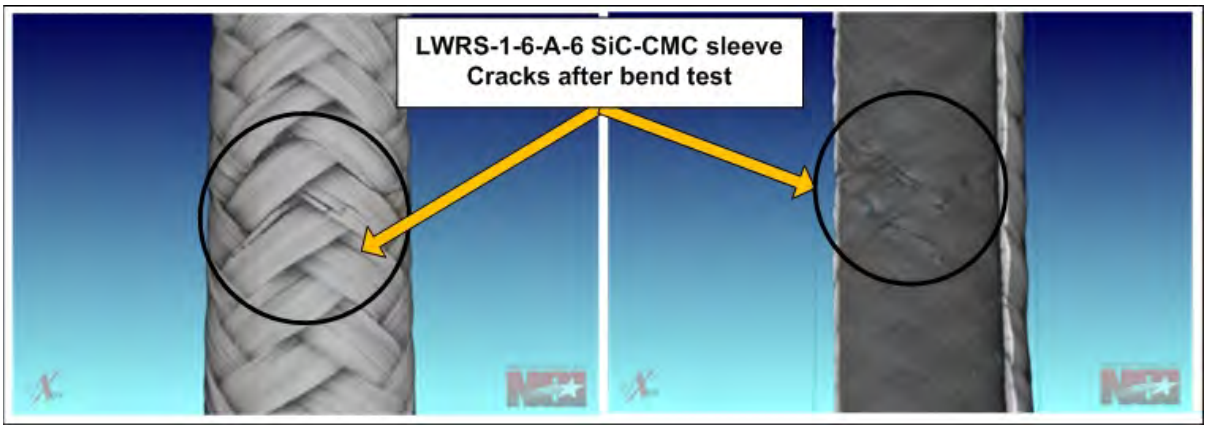

Figure 29. 3D Tomography results of the 5 cycles, 1 ply (LWRS-1-6-A-6) SiC-CMC sleeve sample post bend testing showing cracks.

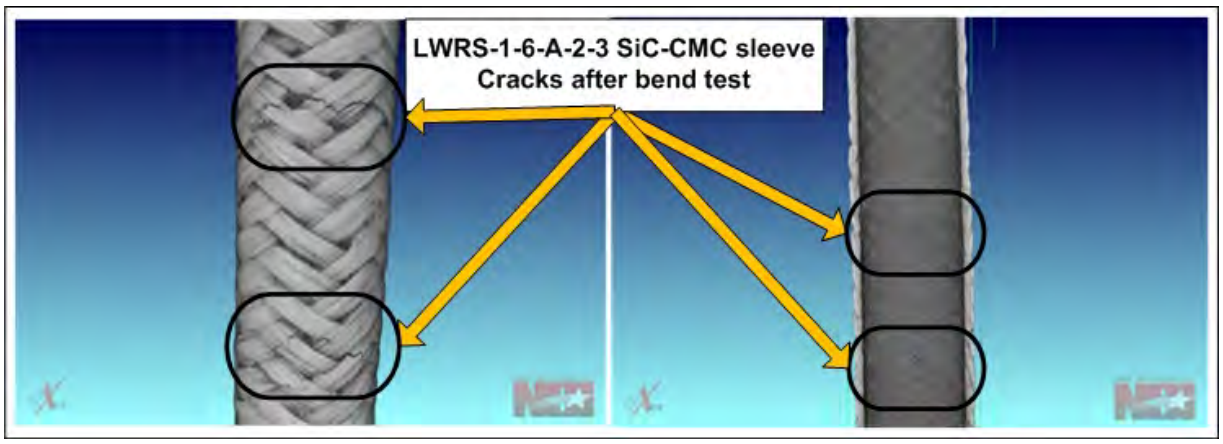

Figure 30. 3D Tomography results of the 5 cycles, 2 ply (LWRS-1-6-A-2-3) SiC-CMC sleeve sample post bend test showing two sets of cracks.

3.3.3.2 Metallurgical examination (SEM and SEM-EDS). A metallurgical examination was completed on the crack areas as well as at areas at the Zr-4 protection sleeve and SiC-CMC sleeve interface to establish any adverse effects due to the bend testing. A significant difference in microstructure is observed when comparing the 1 and 2 ply hybrid mock-up samples as shown in Figure 31. The 1 ply SiC-CMC sleeve matrix shows signs of distress and preliminary signs of defraying at these areas, especially at the braided seam. The microstructure of the 2 ply SiC-CMC sleeve seems still intact at the end of the protection Zr-4 and SiC-CMC sleeve interface. This tendency is also notable when examining the fracture areas itself. The SiC-CMC matrix material of the 1 ply sleeve, shows significant cracking and have a flaky appearance, while the 2 ply matrix material was still bonded together, except at the areas where the actual fracture took place. SEM-EDS analysis on the SiC-CMC sleeve show no difference between the 1 and 2 ply samples (Figure 33) and all three mock-up samples used for bend tests are identified as Zr-4, as no Nb or Hf were identified in the SEM-EDS analysis (Figure 34).

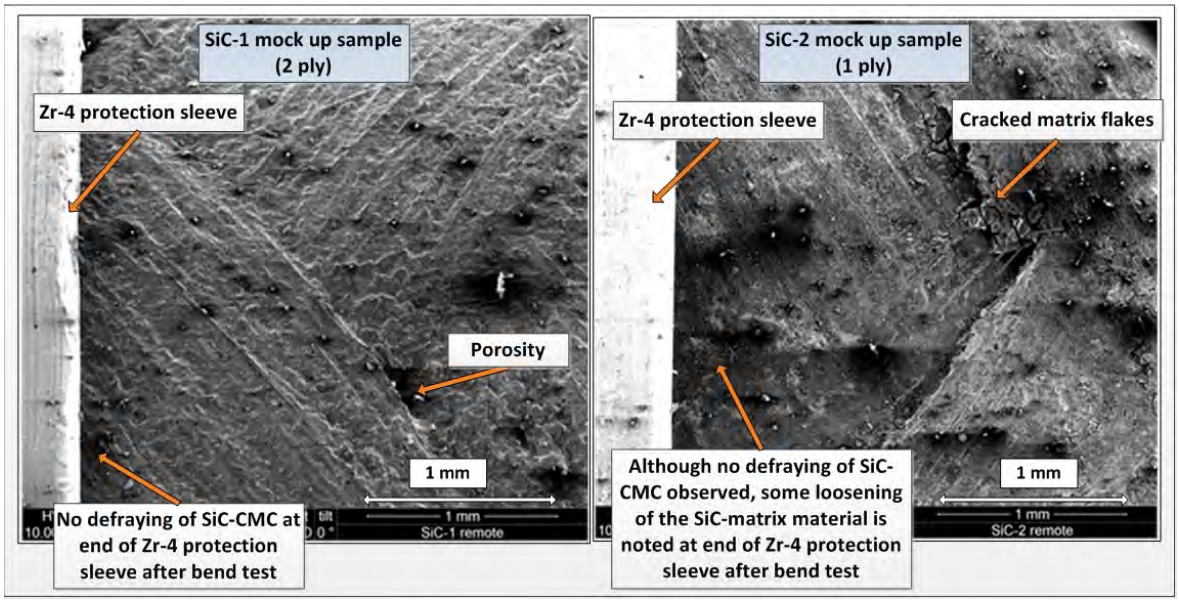

Figure 31. Difference between integrity of the sleeve at the end caps, 2 ply still intact, 1 ply shows signs of failure and modifications.

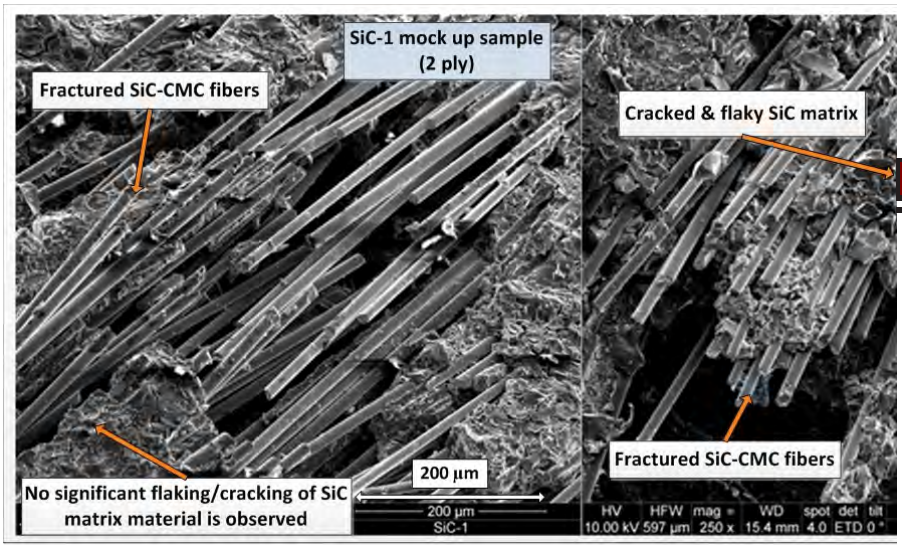

	Wt %	At %

Figure 32. The CMC fiber fracture morphology of the 1 and 2 ply SiC-CMC mock up samples appears to be similar. Differences are noted on the SiC matrix material as it appears to be more cracked and flaky in the 1 ply SiC-CMC sleeve compared to the more compact SiC-matrix material of the 2 ply SiC-CMC sleeve.

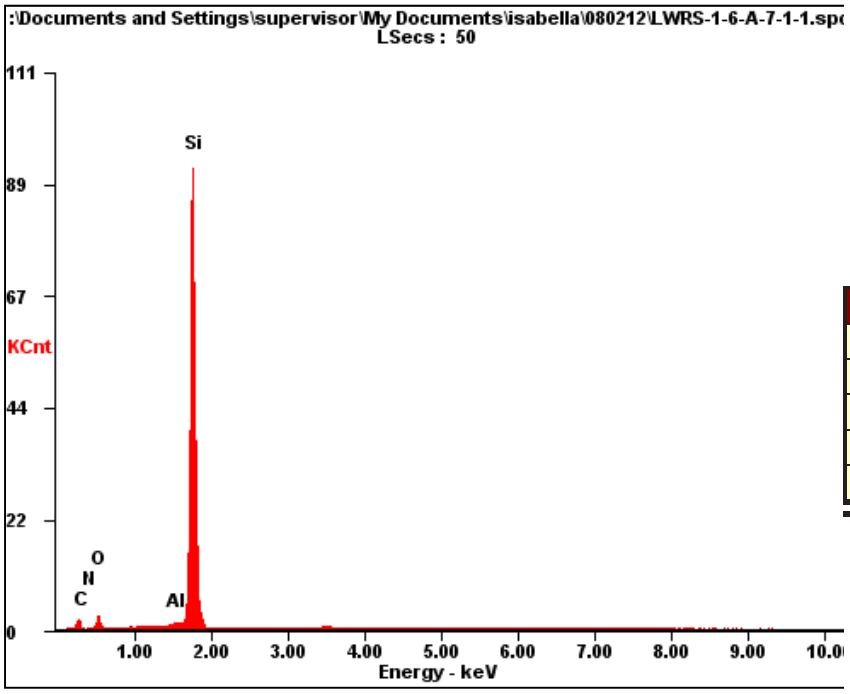

Element	Wt %	At %
C K	18.93	33.62
N K	00.12	00.19
O K	08.17	10.89
AlK	00.54	00.43
SiK	72.24	54.88

Figure 33. Typical SEM-EDS of the SiC-CMC sleeves showed no difference between all the samples tested.

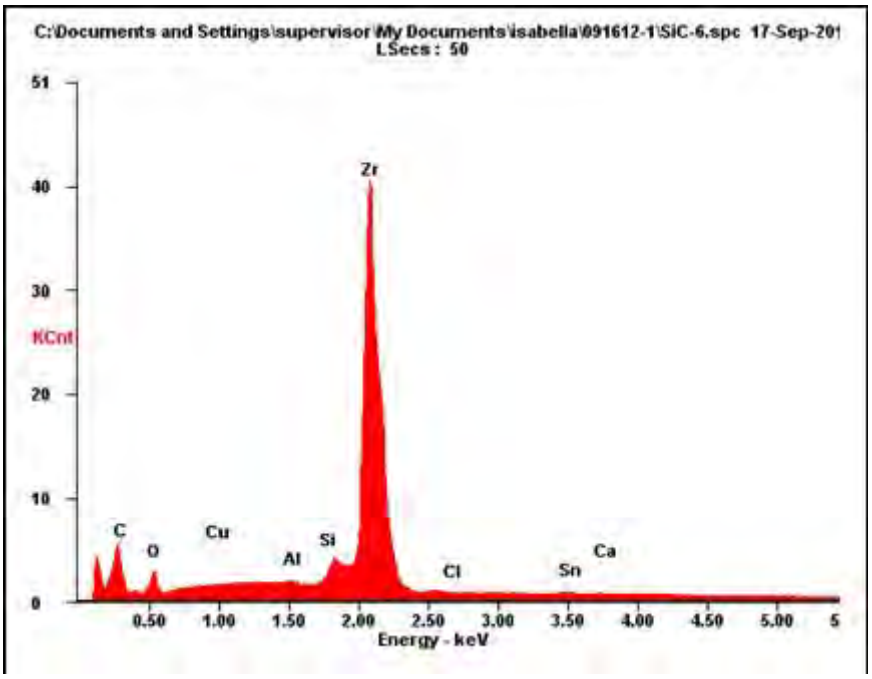

Element		
C K	11.39	45.85
O K	02.61	07.90
CuL	00.07	00.06
AlK	00.23	00.41
SiK	00.40	00.68
ZrL	83.39	44.21
ClK	00.00	00.00
SnL	01.77	00.72
CaK	00.14	00.17

Figure 34. Typical SEM-EDS of the Zr-4 tubes used for the bend mock-up samples (SiC-1, SiC-2, SiC-6). The chemical analysis showed no presence of Nb and Hf.

3.3.4 Conclusions on Bend Test

It is concluded that the method development for both hybrid SiC-CMC-Zr-4 mock-up and SiC-CMC sleeve samples were successful for a comparative method. The 2 ply sleeve samples show a higher bend momentum compared to those of the 1 ply sleeve samples. This is applicable for both the hybrid mock-up and SiC-CMC sleeve samples. Comparatively both the 1 and 2 ply hybrid mock-up samples showed a higher bend momentum if compared with the standard Zr-4 mock-up sample.

The characterization of the hybrid mock-up samples showed that the 1 ply SiC-CMC sleeve matrix shows signs of distress and preliminary signs of defraying at the protective Zr-4 sleeve areas. In addition, the microstructure of the SiC matrix at the cracks after bend test shows significant cracking and flaking. The 2 ply SiC-CMC sleeve samples showed however a more bonded cohesive SiC matrix structure. These cracking and fraying shows potentially concerns for increased fretting during the actual use fo the No difference in qualatiative SEM-EDS analsysis is noted and the Zr-4 tube is confirmed with no presence of Nb and Hf.

Tomography was proven as a successful tool to identify open porosity during pre-test characterization. Additionally the benefit of tomography as the indirect tool for establishing simulation parameters was identified and is recommended to be further explored.

3.4 Hot Water Corrosion Flow Test

3.4.1 Background

As mentioned in Subsection 2.2.3, method development and mock-up testing was conducted with constant conditions. As basic flow and heat-up profiles were performed to test the integrity of the piping system, components and safety features previously by Garnier *et al.*,[14] reporting in this section focuses on the initial 1 day dry-run analysis and the subsequent 3- and 10 day corrosion tests completed on the hybrid mock-up samples. Various operation runs without samples were completed to establish stable operation of the HWCF system and is discussed by Garnier *et al.*[14] As part of the handover to the

characterization team for method development, a dry-run was completed on stainless steel samples. During this test, copper contamination was detected on the stainless steel samples. Subsequently the chiller was identified as the main copper source (detail of the results are described in Reference 14). The chiller was removed and another dry-run was completed prior to insertion of the hybrid mock-up samples which is discussed in this report. In addition to the copper contamination, the copper plating pattern and other corrosion flow patterns indicated possible uneven water flow in the chamber. It was believed that this was caused by trapped air bubbles and therefore frequent purging was recommended for the subsequent runs to remove this trapped air bubbles. This second dry run was completed on a Zr-4-, Zircodyne - and stainless steel tube to establish the following baseline for hybrid mock-up sample insertion:

- Confirmation that the origin of the copper contamination was removed
- Testing the high temperature in-line measurement sensors prior testing the mock-up samples
- Confirmation that the uneven water flow in the chamber, which thought to be due to gas bubble stuck in the aluminum basket, was resolved.

Based on the visual inspection on the 3 dry run samples it was concluded that the “wetting/corrosion” of the samples were even and that no significant Cu contamination was present. Only traces of Cu plating on the bottom parts of the samples were visible as shown in Figure 35. The in-line measurement system was found to be in working order with specific reference to the pH stabilization over the one day period. The process parameters of the one day dry-run, shown in Figures 36 and 37, show that after the initial correction of the pH data logger scale, the pH stabilizes. Based on the 1 day dry run results, the tests on the mock-up samples continued. For all the process parameter plots, the following measurement errors are relevant; 1.0 % error for pH in the range of 2 – 12, +/- 2.0 % error for conductivity and a 0.2% error for dissolved oxygen. The drop in the conductivity value near the end of the 24 hours in Figure 37, is most probably due to a stop in the pump. The inlet pressure and outlet is logged also as zero, with the flow interlock went from 0 to 1 and the level interlock also went from 0 to 1 - indicating that the pump stopped. It is unclear why this happened prior to the end of the 24 hours completion. Although this stoppage occurred, it did not change the conclusions reached at the end of this dry run.

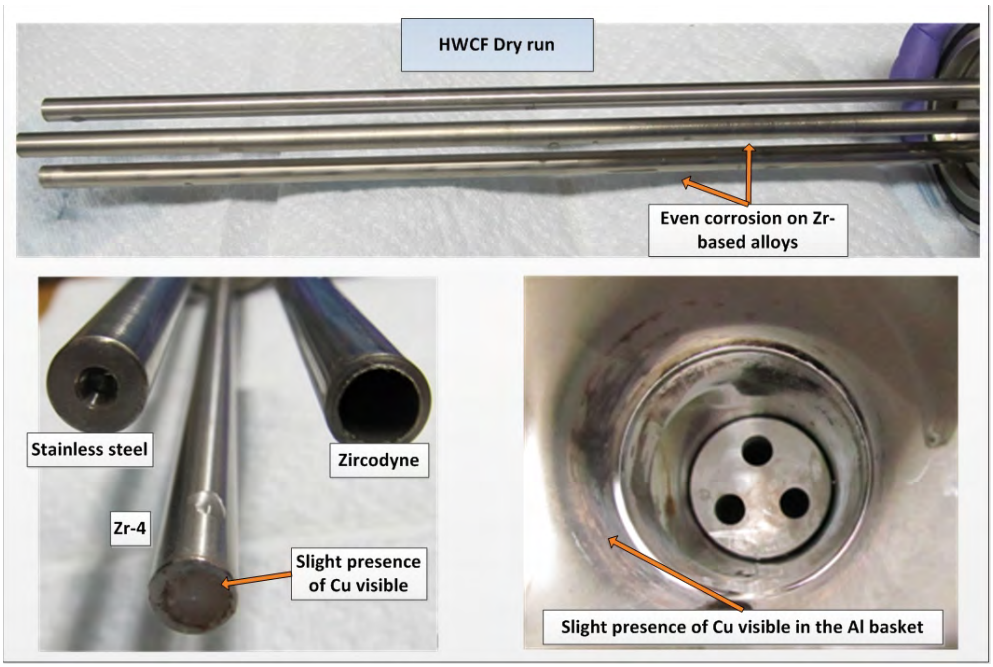

Figure 35. Visual examination of the dry run samples after the one day dry run showing no significant Cu contamination and even corrosive behavior.

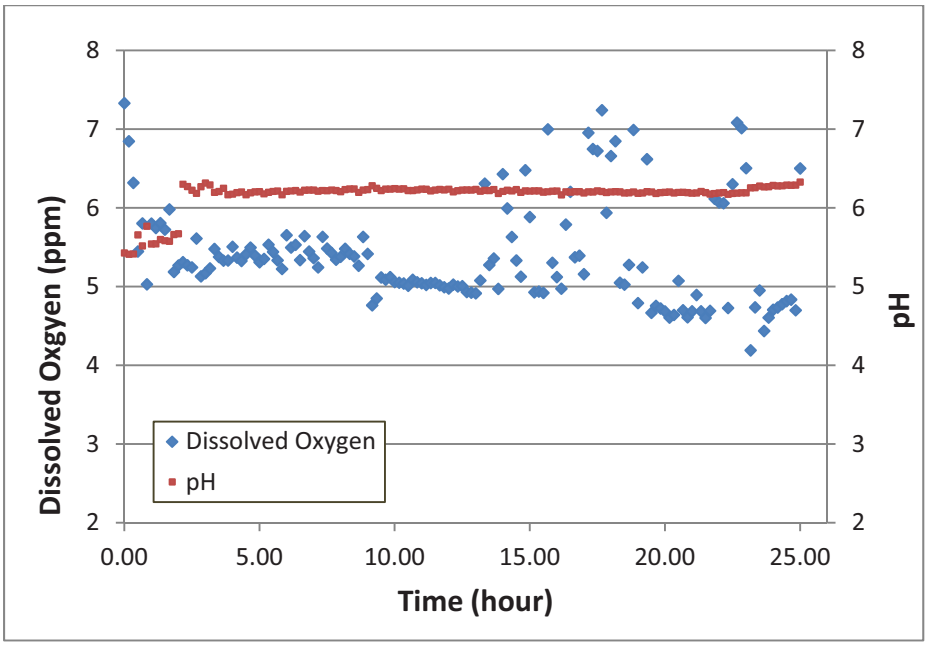

Figure 36. Graph representing the pH and dissolved oxygen of the one day dry run showing the initial correction of the in-line pH reading. The pH value increases from 5.4 to 6.1 where it stabilizes.

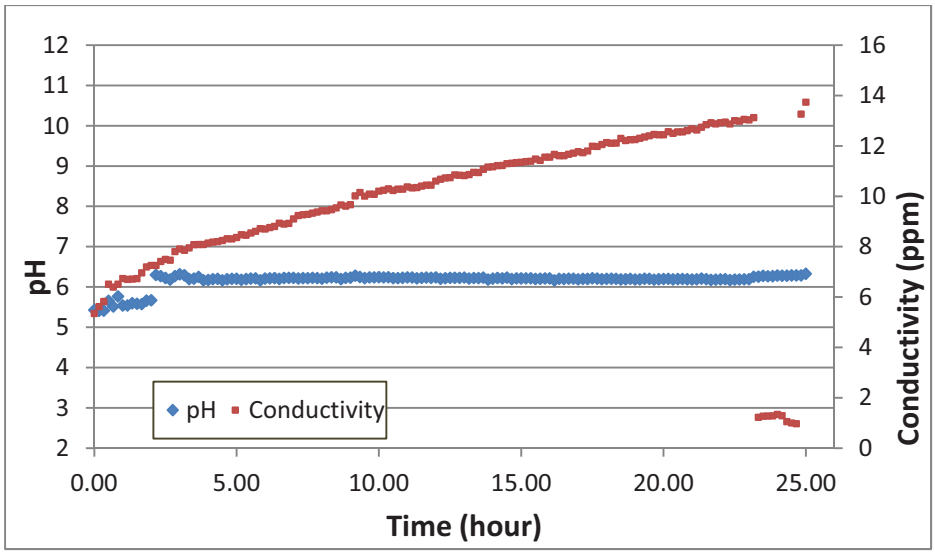

Figure 37. Graph representing the pH and conductivity of the one day dry run showing the initial correction of the in-line pH reading.

3.4.2 HWCF test conditions

Validation of the in-line process measurements was important as part of the test method development activities as the un-heated corrosion flow tests can be run without supervision and it is needed to validate these values as a characterization tool for future interpretation.

3.4.2.1 Validation of in-line process measurements. In-line pH measurements were taken with a Rosemont Analytical 3500VP sensor with temperature compensation at 25^0C. In-line pH measurements were verified with "tap" water samples taken directly into sterile sample containers and cooled to room temperature before measuring with a hand held pH meter (Accumet AP110 portable meter calibrated immediately before use with pH 4.0, 7.0 and 10.0 standards, Fisher Scientific, Pittsburgh, PA.) In some cases, due to scheduling limitations, "tap" measurements were taken after samples were stored in sealed sample containers held at room temperature.

"Tap" and in-line measurements were shown to be consistent during the first 3 data points in the 3-day run. During these first 3 days, the "tap" measurements were taken as soon as the sample cooled to room temperature. The in-line and "tap" measurements matched up very well, thereby verifying the accuracy of the in-line system (see Figure 38).

In cases where the "tap" pH was not measured immediately, the pH of the "tap" samples was found to be considerably lower as shown in Figure 39. The elapsed time ranged from 1 day to as long as 13 days. The pH was lower in all cases except one, and did not correlate with increased storage time (data not shown). The decrease observed in "tap" measurements stored before measurement was most probably due to the following factors:

1. CO_2 equilibrates in weakly-buffered aqueous solution according to the following reaction:

   $CO_2 + H_2O \leftrightarrow H_2CO_3$ (carbonic acid)

   $H_2CO_3 \leftrightarrow H^+ + HCO_3^-$ (hydrogen ions and bicarbonate ions)

   Carbonic acid dissociates releasing H^+ ions into solution, thereby lowering the pH. "Tap" measurements that were stored in sample containers with a headspace for several days before measuring had a lower pH than the in-line measurements.

2. Other corrosion elements in solution may have an effect on pH. In the closed flow corrosion system, the pH is raised and corrosion products are in equilibrium with system water. Upon removal of "tap" water samples, the samples come into equilibrium with atmospheric gases and the temperature drops. These effects can cause water chemistry to change and allow any corrosion products to further affect water pH.

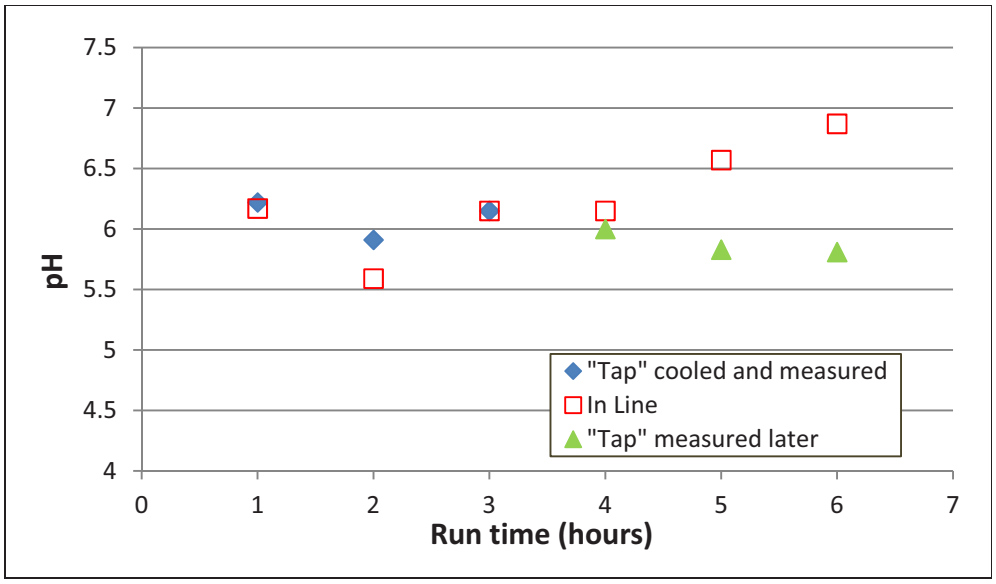

Figure 38. In-line and "tap" measurements taken during 3-day flow corrosion test.

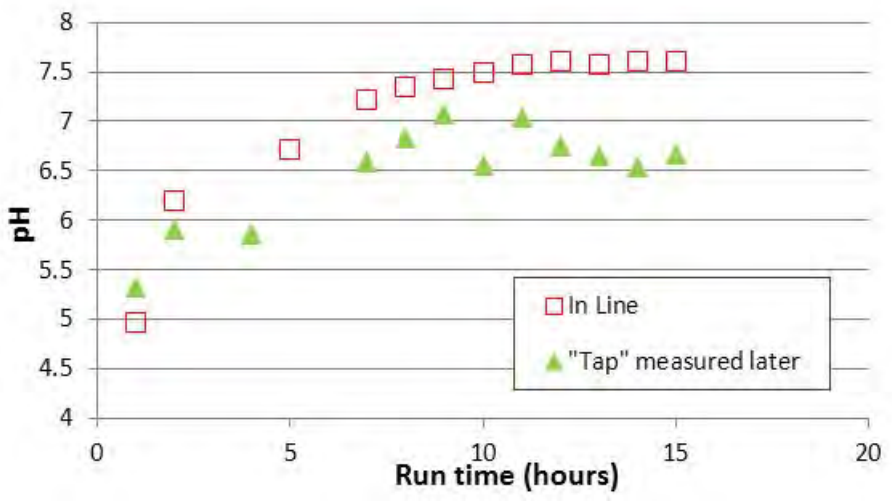

Figure 39. In-line and "tap" measurements taken during the 10 day test.

3.4.2.1 In-line process measurements of the 3 day corrosion test

The in-line measurements for the 3 day corrosion test are graphically displayed in Figures 40 to 42 to determine possible trends and interaction behaviors. These figures show that dissolved oxygen and pH measurements follow an opposite trend while pH and conductivity have the same trend. Possible explanations for these trends are provided by Garnier *et al.*[14]. Due to pressure build-up during the 3 day test, frequent releasing ("burping") of gasses was necessary and this is mirrored by the scattering of the dissolved oxygen levels in Figure 40. This burping of the system to maintain a safe working pressure, causing the oxygen levels to be much lower than the ATR control limits. Although the pH value started

within the ATR control limits, it is noted that the pH rose steadily over the 3 days to a maximum of approximately 8, which is above the control limits for the ATR (4.8 to 5.4). Manual alteration of the pH was undertaken at the end of the first day by adding twice 10 ml HNO_3 acid in the top of the water reservoir, but no changes of the pH were observed. Due to this higher than expected rise in pH, it was decided to start the 10 day test with a simulated water pH of 4.8, which is the minimum value of the ATR control limit.

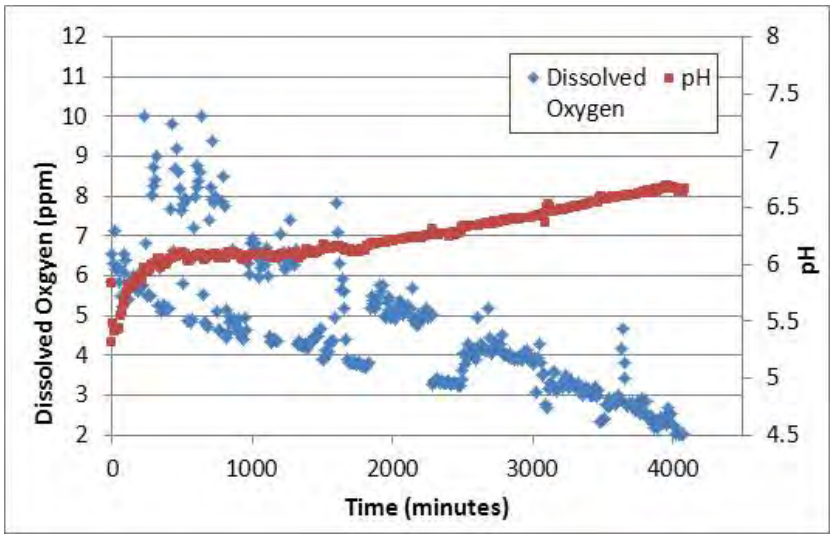

Figure 40. Graphical displays of dissolved oxygen and pH in-line measurements taken during the 3 day test.

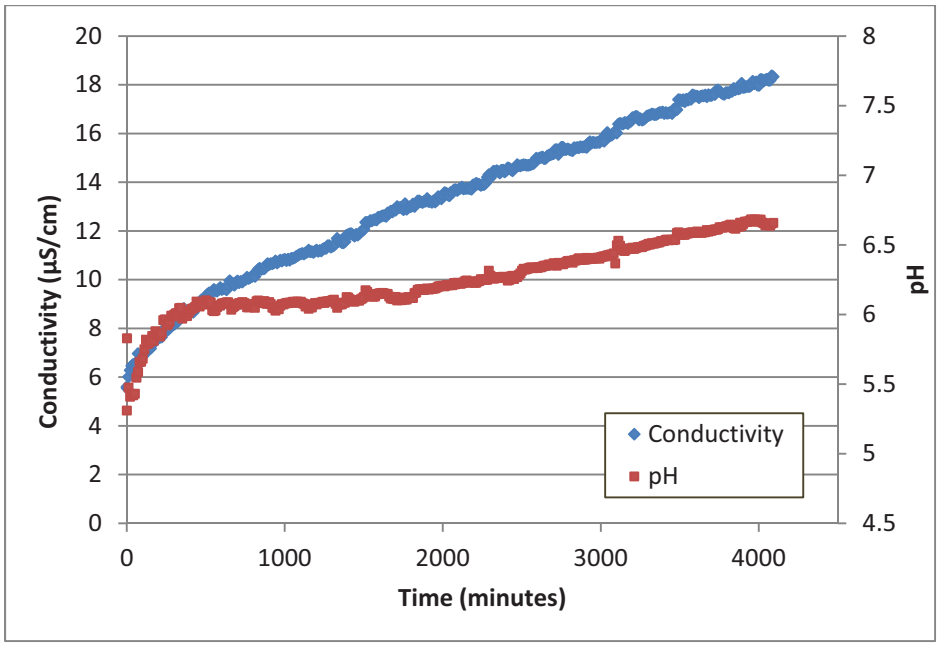

Figure 41. Graphical displays of conductivity and pH in-line measurements taken during the 3 day test.

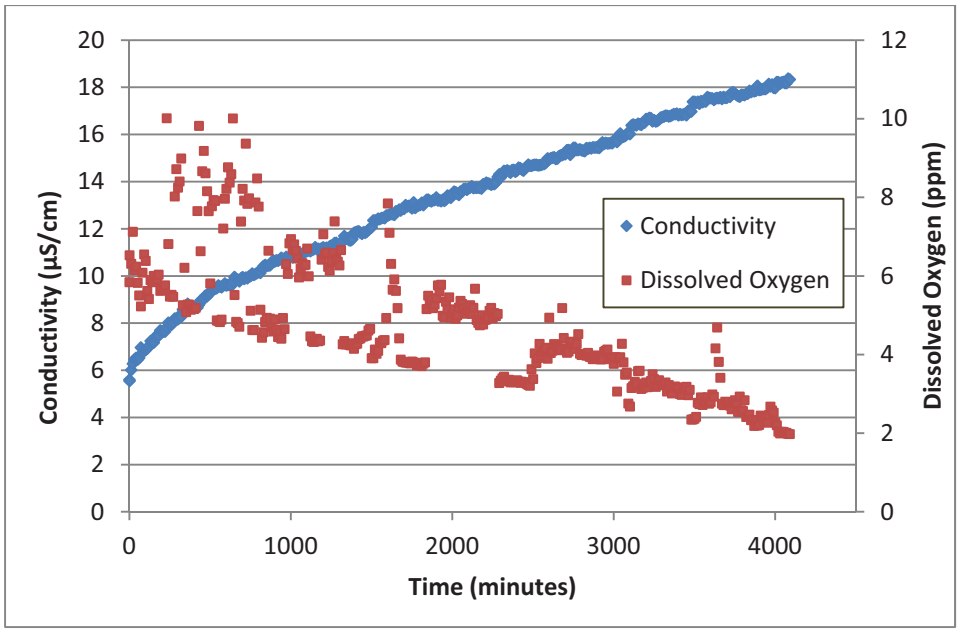

Figure 42. Graphical displays of conductivity and dissolved oxygen in-line measurements taken during the 3 day test.

3.4.2.2 In-line process measurements of the 10 day corrosion test

As mentioned previously, fresh water (4.8 pH) simulating ATR water chemistry was used for the start-up of the 10 day corrosion test. However, irrespective of the initial start up with lower pH water, the pH increased within the first hour to values above 6 as shown in Figure 43. Although this pH was already above the maximum control limit of the ATR (4.8 to 5.4) such that it was no longer representative of the ATR conditions, it was decided to allow the 10 day test continue to evaluate the trends and to observe if any stability is reached. No stabilization was reached by the end of the 10 day test. The graphical presentation of these process measurements (Figures 43 to 45) show that dissolved oxygen and pH measurements follow an opposite trend while pH and conductivity have the same trend. Possible explanations for these trends are provided by Garnier *et al.*[14]

It should be noted that there are two gaps in the data collected by the data logger during the 10 day test. The first gap is from 8/9/12 at 8:22 am until 8/9/12 at 2:27 pm, approximately 6 hours. This gap corresponds with the predetermined inspection time at the end of the first three days. At this stoppage point, a white colloidal suspension in the water was noted through the view port. No visible physical damage was noted during this predetermined inspection, but surface contamination was noted on both the SiC-CMC hybrid sleeves. These contaminations were removed for further SEM-EDS analysis (discussed in Subsection 3.4.3.3). No surface penetration/chemical reaction or damage was observed below these contaminations and therefore the samples were returned in the HWCF system and the test restarted. No water change was done during this stoppage; approximately 5 gallons of fresh water was used to top-up the water volume due to water lost during the removal of the samples. The second gap was from 8/12/12 at 12:58 pm until 8/13/12 at 7:15 am. This gap is approximately 19 hours. It was reported that this data gap occurred because of the memory of the data recording system reached full capacity. This was mainly due to the very small increments that data were taken for these tests to ensure that changes can be noted. Based on the preliminary trends observed, it was decided to increase the time between recordings of data to intervals of 10 minutes. This will need to be recorded in the work request and operating instructions for future long-term corrosion tests.

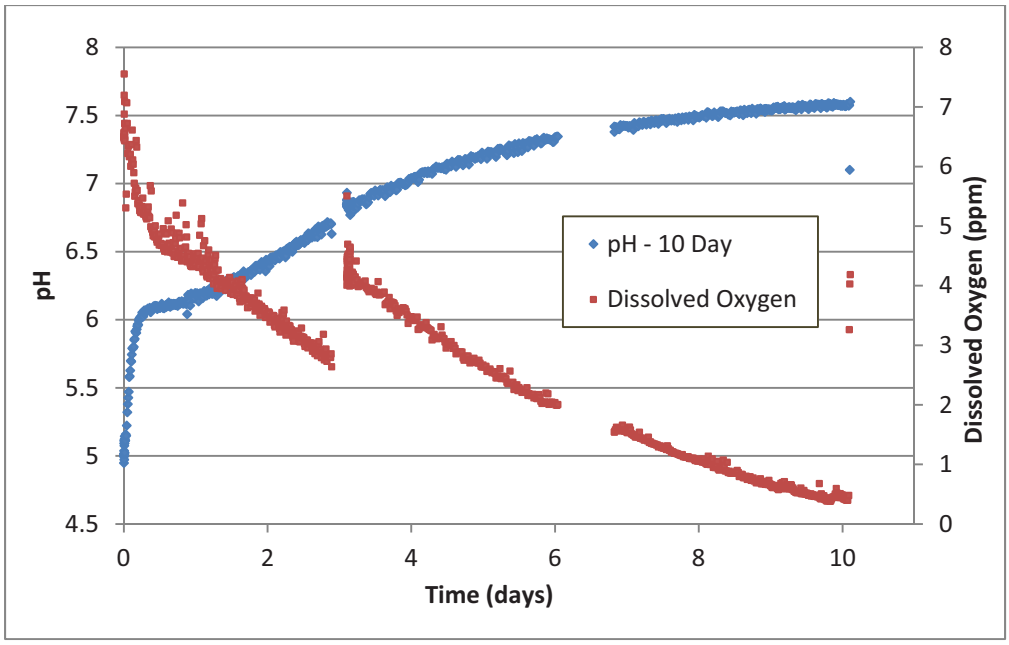

Figure 43. Graphical displays of dissolved oxygen and pH in-line measurements taken during the 10 day test.

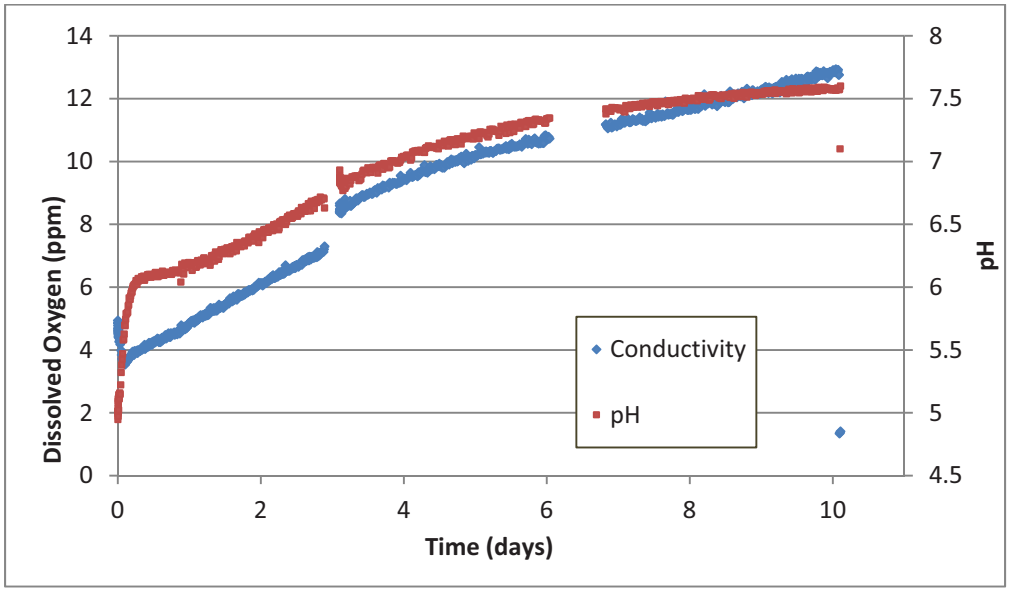

Figure 44. Graphical displays of conductivity and pH in-line measurements taken during the 10 day test.

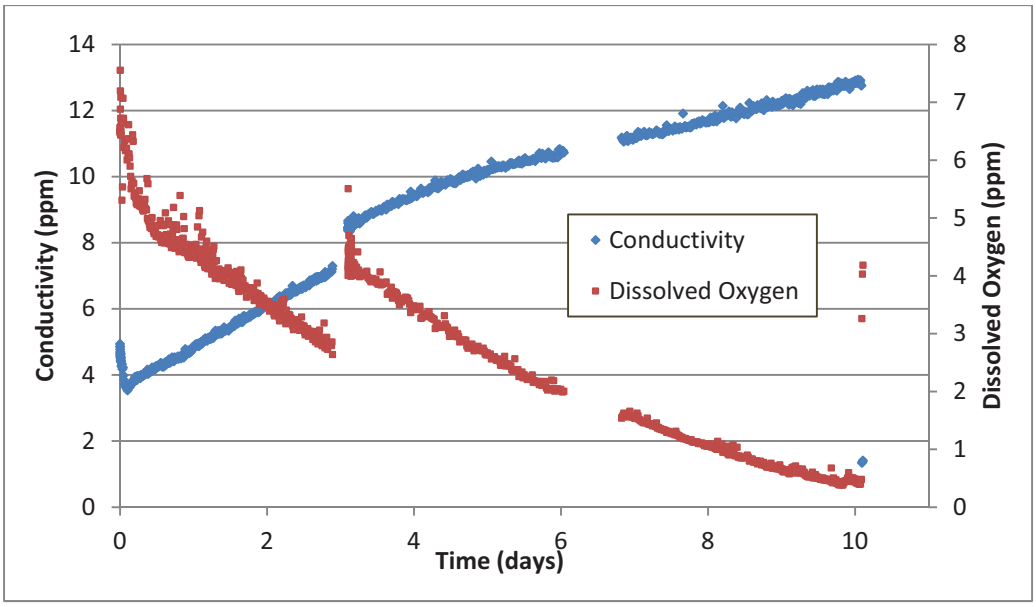

Figure 45. Graphical displays of conductivity and dissolved oxygen in-line measurements taken during the 10 day test.

3.4.2.1 Interpretation on the pH values. Regardless of the starting pH value of the flow corrosion run, the pH remains relatively constant during the first 24 hours. The starting pH values were 5.4, 5.3 and 4.9 for the dry run, 3-day, and 10-day tests, respectively. The slopes of the lines in the first 24 hours are flat and are very similar to each other (see Figure 46). The final pH values for all 3 tests at 24 hours were between 6.1 and 6.2. After 24 hours, the slope of the lines describing pH for the 3-day and 20-day tests continue to rise, as seen in the equations in Figure 46. The pH values for both the 3-day and 10-day tests are remarkably similar and continue to rise steadily for the duration of the test. After 3 days, the pH values were 6.83 and 6.63 for the 3-day and 10-day tests, respectively. For the 10-day test, the pH value continues to rise steadily and ends at a value of 7.6.

The similarity of the pH values regardless of the starting pH and the steady, consistent rise in pH after 24 hours appear to indicate that pH is governed by a physical parameter of the flow corrosion system itself. In fact, efforts to drop the pH during the first 24 hours of the 3-day run were unsuccessful – the pH remained elevated and steady despite the addition of small volumes of dilute nitric acid.

The short duration of the dry run did not show what would have happened to pH values after the 24 hour time point. At this time, it cannot be determined whether the rise in pH values was due to the presence of the SiC sleeves. A dry run of longer duration will need to be conducted to show what would happen to pH values as the run progresses without the SiC sleeves.

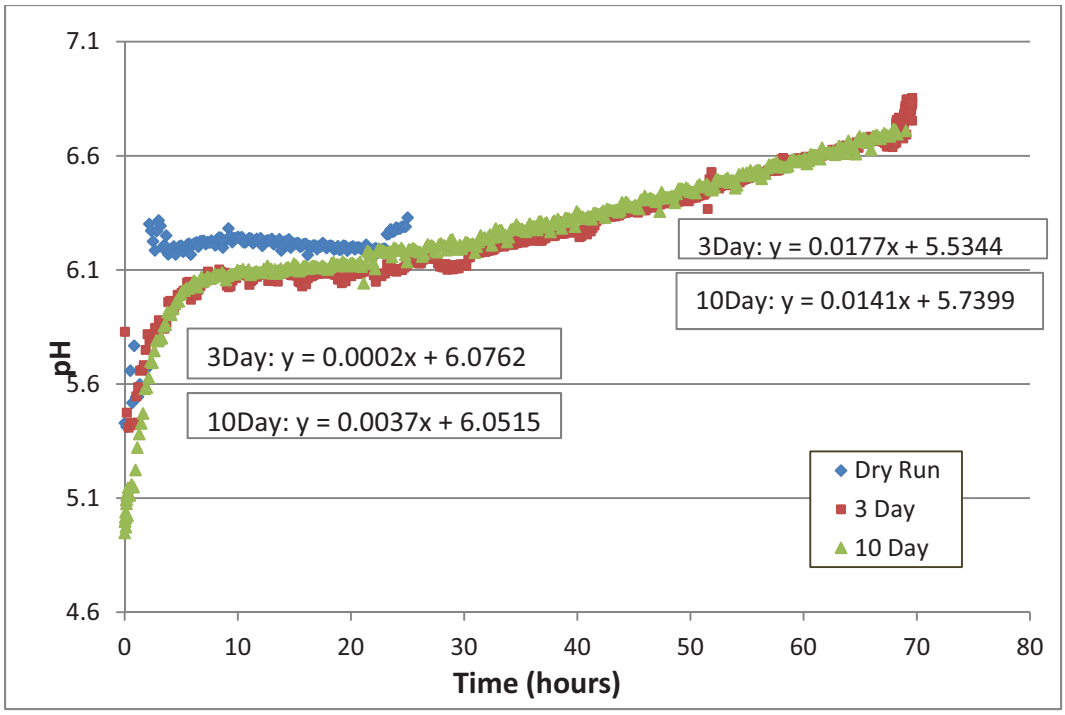

Figure 46. Graphical displays of the pH over time comparing the results of the 1 day dry run, 3 day and 10 day tests.

3.4.2.2 Water analysis after the HWCF tests. Various water samples were sent for F, Cl, Br, Al, Cu, Fe and Zr analysis but only some of the results were available at the time of report writing. The reader is therefore cautioned that this Section is not complete and fully integrated with the conclusions of this report. For this preliminary discussion on the water analysis, only the preliminary Cl results are graphically presented in Figure 47. Although duplicate measurements (for validation) are in process, preliminary observation is noted that the Cl content decreased as the 10 day corrosion test progressed. An explanation of this is still under investigation.

The possible cause(s) for the high Cl values initially measured are in under investigation, and a preliminary matrix for the investigation is shown in Table 8. It must be noted that this will be discussed and explained in detail in a follow-up report. Table 9 provides only a first indication of the results available at the moment and will be fully discussed in an updated version of this section and report. The choice of samples for analysis, were based on technical questions which needed to be resolved, therefore the indication of "Answer" number in Table 9.

Table 8. Preliminary investigation matrix for the higher Cl values.

Possible Cause of High Cl Concentration	Test By	Test case: sample name (Cl conc ppm)	Cross-reference Key	Results:	Conclusion:
High starting Cl in reservoir water	Test reservoir water straight from the reservoir	8/31/12 (0.897)	A3	Low Cl conc - <1.0 ppm	Water held in the reservoir does not contain elevated Cl concentrations.
Handling samples without gloves causes Cl from hands to contaminate water sample.	Finger wash and analyze	AM Finger Wash (0.702 ppm)	A6, A7, and A8	< 1.0 ppm	Sample handling without gloves does not cause Cl contamination.
Re-using sample holders results in cross-contamination	Questioning use of new or re-used sample holders	One holder only		All sample holders clean with exception of one	Sample holder re-use was not the cause of Cl contamination.
Some types of sample holders leach Cl into the water sample	Compare Cl concentration and sample holder type	Various	A4, A5	High Cl concentration not consistent with sample holder	High Cl not caused by leaching from the type of sample holder
Sample pH and conductivity measurement before IC analysis resulted in cross-contamination	Examine Cl concentration in all samples that were measured before IC analysis	Various		No correlation between pH and conductivity measurement and high Cl concentration	Sample pH and conductivity measurement did not contribute to Cl contamination
Cl is leaching from the SiC sleeve during the run	Examine Cl in water sample at later time points during the run	Various	A1 and A9	Cl concentration remains below 34 ppm during the latter time points in the 10-day run	Cl is not being released from the SiC sleeves during the run
Cl is released during the first few minutes of start up in the 3-day and 10-day test	Compare the results to the leach test where heating is applied		A8	Cl concentration low in the leach test sample (< 3.7 ppm)	SiC sleeves do not release Cl during heating
Cl is absorbed by the SiC sleeve during the run	SEM EDS		A4, A5 and A9		
Cl is absorbed by a corrosion product during the run	SEM EDS				
Cl becomes less soluble with pH and precipitates out, escaping IC analysis					

Table 9. Water analysis after HWCF tests comparing the results with the water at beginning of tests.

			F (ppm)	Cl (ppm)	Br (ppm)
ATR Normal range			ST	< 0.05	ST
ATR Control limit			ST	< 0.1	ST
3-Day Flow Corrosion Test					
Sample Date	Sample Run Time	1st Analysis or Answer Number	F (ppm)	Cl (ppm)	Br (ppm)
8/1/12	Before start – 3:50 pm	A8	NM	5.573	NM
8/2/12	Start of 3 day test	1st analysis, B6 (in progress)	<0.544	135.628	<0.116
8/3/12	24 hours	A7	NM	17.841	NM
8/4/12	48 hours	B1	NM	28.95	NM
8/5/12	72 hours	1st analysis, B7 (in progress)	<0.544	161.332	<0.116
ST: Specify total only NS: Not specified NM: Not measured ND: Not detected					
10-Day Flow Corrosion Test					
Sample Date	Sample Run Time (days:hours:mins)	Question/Answer Number	F (ppm)	Cl (ppm)	Br (ppm)
8/6/12	Start of 10 day test	1st analysis, B9 (in progress)	<0.544	129.033	<0.116
8/7/12	20:17	B2	NM	16.2727	NM
8/9/12	2:20:07	A6	NM	34.091	NM
8/9/12	Fresh water in reservoir	A2	NM	1.579	NM
8/9/12	Flow corrosion water cooled before sampling	1st analysis	<0.544	185.711	<0.116
8/11/12	4:17:32	B3	NM	22.2761	NM
8/12/12	5:19:50		NM	NM	NM
8/13/12	6:17:44		NM	NM	NM
8/14/12	7:17:38	B4	NM	8.2736	NM
8/15/12	9:00:31	A4	NM	4.998	NM
8/15/12	9:18:00	A5	NM	5.253	NM
8/15/12	9:23:27	B5	NM	2.2187	NM
8/16/12	10:00:01	1st analysis, B10 (in progress)	<0.544	2.157	<0.116
8/31/12	Flow corrosion water at end of test	A9		1.915	
8/31/12	Water in reservoir	A3	NM	1.1	NM
ST = Specify total only NS = Not specified NM = Not measured ND = Not detected					

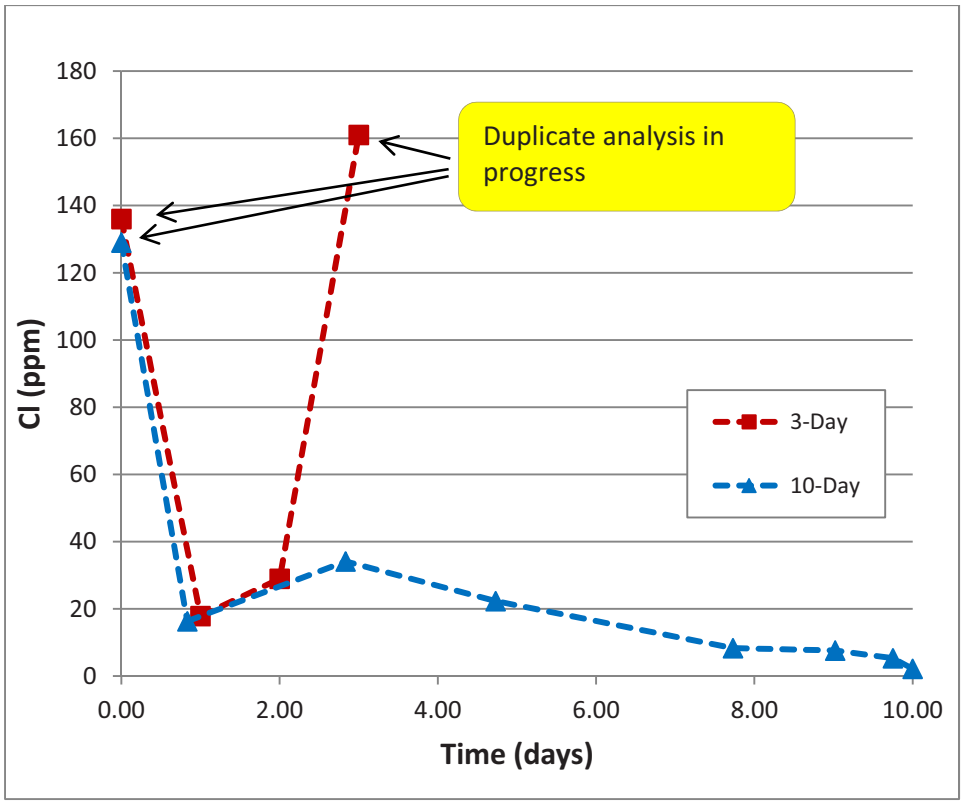

Figure 47. Figure showing the Cl content before and after the 3 and 10 day HWCF tests

3.4.3 Characterization of the HWCF mock-up samples

3.4.3.1 Dimensional inspection of the HWCF mock-up samples. Dimensional inspection is conducted on the mock-up samples to monitor possible outer diameter changes due to the HWCF tests. The null and alternate hypotheses were defined as follows:

- H_0= no difference in the outer diameter of the 2 SiC-CMC sleeves after the 10 day corrosion test
- H_a= there is a difference in the outer diameter of the 2 SiC-CMC sleeves after the 10 day corrosion test.

The difference could be that the outer diameter is greater due to swelling, or that it is smaller, due to mechanical shearing or other factors. Therefore, two-tailed tests of the non-paired measurements were performed on the 9 data points that were taken at each of the three points along the length of the SiC tube. The results below in Tables 10 and 11 describe the difference in outer dimension at each of the three locations along the SiC tube after 10-day flow corrosion. Since the calculated test statistic is smaller than the tabulated value in every case, we fail to reject the null hypothesis. Therefore, it is concluded that there is no difference in the outer diameter of either the SiC-3 or SiC-4 sleeves at any of the 3 points along the length.

Table 10. Analysis of the outer diameter of SiC-3 along its length.

Sample ID	Weave ply	Location along length of sleeve	Outer diameter BEFORE flow corrosion		Outer diameter AFTER flow corrosion		Test statistic	t-value (df = 8, α = 0.025)	Conclusion
			Average (mm)	stdev	Average (mm)	stdev			
SiC - 3	1-ply	"Zr tube" end	11.25	0.08	11.28	0.11	0.408033	2.36	Do not reject null hypothesis
		Middle	11.27	0.08	11.28	0.07	0.446674	2.36	Do not reject null hypothesis
		"SiC" end	11.33	0.08	11.37	0.13	0.223547	2.36	Do not reject null hypothesis

Table 11. Statistical analysis of the outer diameters of SiC-4 along its length.

Sample ID	Weave ply	Location along length of sleeve	Outer diameter BEFORE flow corrosion		Outer diameter AFTER flow corrosion		Test statistic	t-value (df = 8, α = 0.025)	Conclusion
			Average (mm)	stdev	Average (mm)	stdev			
SiC - 4	2-ply	"Zr tube" end	11.13	0.03	11.18	0.05	0.037760	2.36	Do not reject null hypothesis
		Middle	10.94	0.05	11.07	0.05	0.000038	2.36	Do not reject null hypothesis
		'SiC' end	11.37	0.05	11.42	0.08	0.205097	2.36	Do not reject null hypothesis

It was also determined whether there is a difference in the outer diameter (OD) of the 1-ply vs. 2-ply SiC sleeves. The null and alternate hypotheses were defined as follows:

- H_0= no difference in the outer diameter of the 1-ply and 2-ply SiC sleeves
- H_a= the outer diameter of the 2-ply weave is greater than the 1-ply weave.

The test statistic was calculated using all the outer diameter measurements that were taken along the length of each of the sleeves. There were 27 measurements for each sleeve, such that there are 26 degrees of freedom (Table 12). The test statistic is much less than the tabulated t-value therefore we do not reject the null hypothesis and conclude that there is no difference in the outer diameter of the 1-ply vs. the 2-ply weave.

Table 12. Overall comparison of the outer diameter of SiC-3 (1 ply) and SiC-4 (2 ply) using all measurements.

Sample ID	Weave ply	Outer diameter		Test statistic	t-value (df =26, α = 0.05)	Conclusion
		Average (mm)	stdev			
SiC-3	1-ply	11.28	0.08	0.037760	1.706	Do not reject null hypothesis
SiC-4	2-ply	11.15	0.19			

Finally, differences in the weave depth along the weave length were assessed for the 1 and 2 ply weaves. Measurements taken of the difference between the 'peaks' and 'valleys' at 2 points, the 'Zr tube' end and the middle, were used to determine whether the weave depth was different. The null and alternate hypotheses were defined as follows:

- H_0=there is no difference in the depth of the weaves of the 1-ply and 2-ply SiC sleeves
- H_a=there is a difference, and it could be greater or smaller.

The profile projector measurements (mm) were used to calculate the test statistic. There were 3 measurements taken at 3 rotations (0 degrees, 120 degrees, and 240 degrees) at both the 'Zr tube' end and the middle of the sleeve. Due to difficulty in correctly positioning the rodlet in the instrument, no measurements were taken at the SiC-marked end. The test statistic was calculated to see if there was a difference between the Zr end and the middle of SiC-3 and SiC-4 separately. These statistics in Table 14 show that there is no difference in the weave depth at the end and in the middle of either of the sleeves.

Table 13 Comparison of weave depth at two points along SiC-3 (1 ply)

Sample ID	Weave ply	Location along length of sleeve	Profile depth of weave BEFORE flow corrosion		Test statistic	t-value (df = 8, α = 0.025)	Conclusion
			Average (mm)	stdev			
SiC - 3	1-ply	'Zr end'	0.1298	0.01	0.667441	2.36	Do not reject null hypothesis
		Middle	0.1341	0.03			

Table 14. Analysis of weave depths at two points along SiC-4 (2 ply).

Sample ID	Weave ply	Location along length of sleeve	Profile depth of weave BEFORE flow corrosion		Test statistic	t-value (df = 8, α = 0.025)	Conclusion
			Average (mm)	stdev			
SiC - 4	2-ply	'Zr end	0.0944	0.02	0.250237	2.36	Do not reject null hypothesis
		Middle	0.1052	0.02			

All the weave depth measurements for SiC-3 and SiC-4 were used to compare the 1-ply sleeve and the 2-ply sleeve, respectively. The test statistic is much smaller than the tabulated t-value therefore we do not reject the null hypothesis and conclude that there is no difference in weave depth between the 1-ply and 2-ply weaves.

Table 15. Comparison of weave depth between SiC-3(1 ply) and SiC-4(2 ply).

Sample ID	Weave ply	Weave depth		Test statistic	t-value (df =17, α = 0.025)	Conclusion
		Average (mm)	stdev			
SiC-3	1-ply	0.134	0.07	0.000029	2.110	Do not reject null hypothesis
SiC-4	2-ply	0.100	0.02			

Although this detail measurement analysis were conducted and the null hypotheses was not rejected, meaning that no differences were not seen, final conclusions cannot be reached as the sample size is insufficient to do that. In addition, it may be that the measurement technique applied for these measurements are not sensitive enough to identify possible differences. It is therefore recommended that more investigation needs to be done on the measurement technique; however, the inclusion of surface roughness measurements, using atomic force microscope (AFM) analysis, is to be considered as it will provide information on the surface roughness, showing micron changes. This may be particular useful for further corrosion or chemical interaction studies.

3.4.4 Visual inspection of the HWCF mock-up samples

3.4.4.1 Sample loading detail

The three mock-up samples were loaded in fixed positions and orientations as shown in Figure 48. The 1 ply SiC-CMC hybrid mock-up sample, SiC-3, was loaded in the "1" position and the 2 ply SiC-CMC hybrid mock up sample, SiC-4, was loaded in position "2". The Zr-4 standard mock-up sample was placed in position '3'. These samples were specific orientated using the markings as a reference, to ensure that after the removal at predetermined inspection points, samples were inserted in the original orientation.

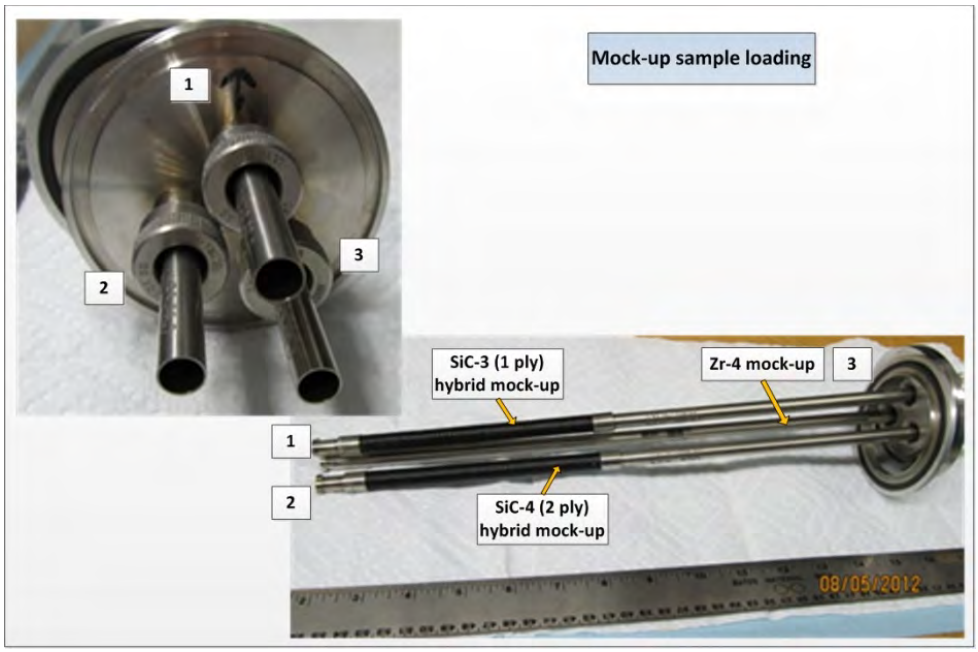

Figure 48. Figure showing the mock-up sample configuration and loading for the 3 and 10 day HWCF tests.

3.4.4.2 3 Day Corrosion Test. The samples were3 day test was completed on 08/05/2012 and no physical damage or fraying of the SiC-CMC sleeves was observed. There was some surface contamination observed on both the sleeves as shown in Figure 49. The surface contamination was removed for chemical analysis (SEM-EDS) and no chemical reaction or surface damage is observed in the areas where the contaminants were removed. The SEM-EDS analyses are typically containing Al, C, O, Si and Cu as shown in Figures 50 and 51. This is most probably due to the interaction of the aluminum basket, water and SiC-CMC sleeve in a lesser extent. Precipitates were also observed underneath the Zr-4 protective sleeve at the flow-end side of the mock-up samples. This is typically expected due to the flow direction of the water and this observation shows that this potentially can happen as well during ATR irradiation and future application of this design in the LWR. It is therefore recommended that the design of this protective sleeve needs to be modified.

Slight white discolorations are also observed at certain areas of the Zr-4 parts of all the mock-up samples as shown in Figure 52. Slight copper precipitation is also noted on the Zr-4 mock up sample at the end. The flow-in side of SiC-3 mock-up sample show more white discoloration on the Zr-4 parts of the assembly when compared to the other two mock-up samples. No precipitates or discoloration is noted at the far end of the mock-up samples. The visual inspection of the aluminum basket shows no significant detoriation at the end of the 3 day corrosion test (Figure 53).

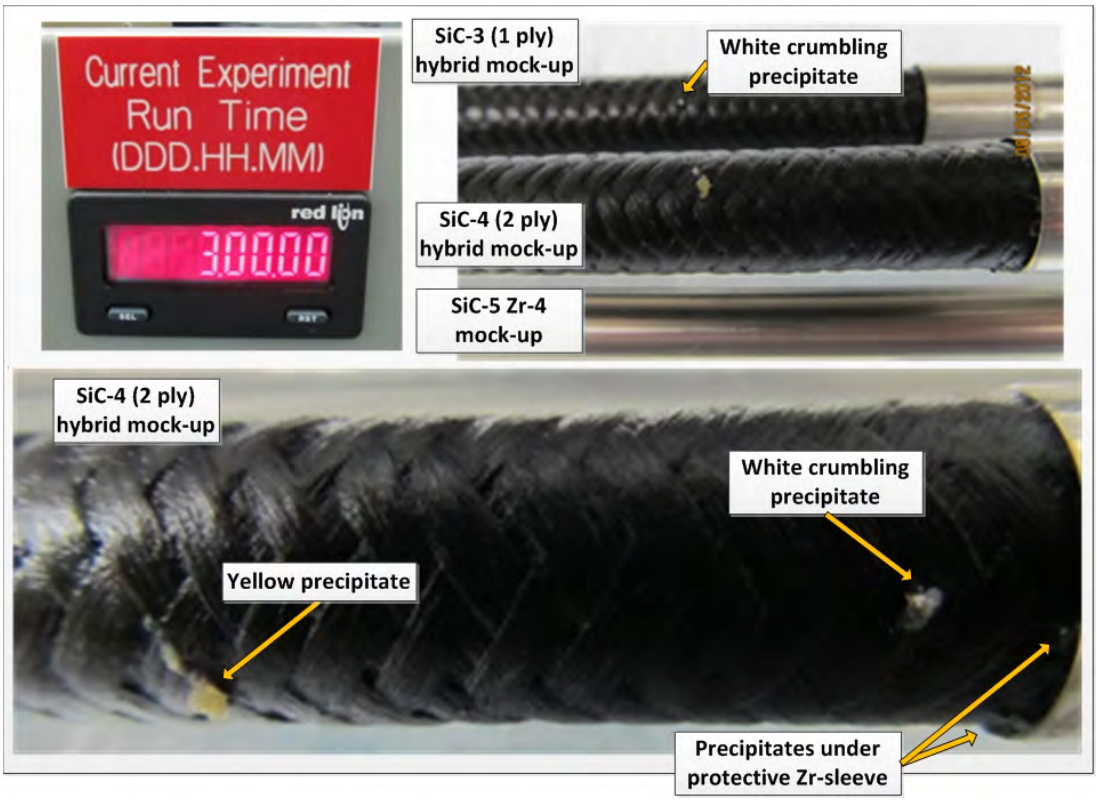

Figure 49. No fraying or surface damage is observed on both the SiC-CMC sleeves of the two hybrid mock-up samples, SiC-3 and SiC-4. Surface contamination on both SiC-CMC sleeves is observed.

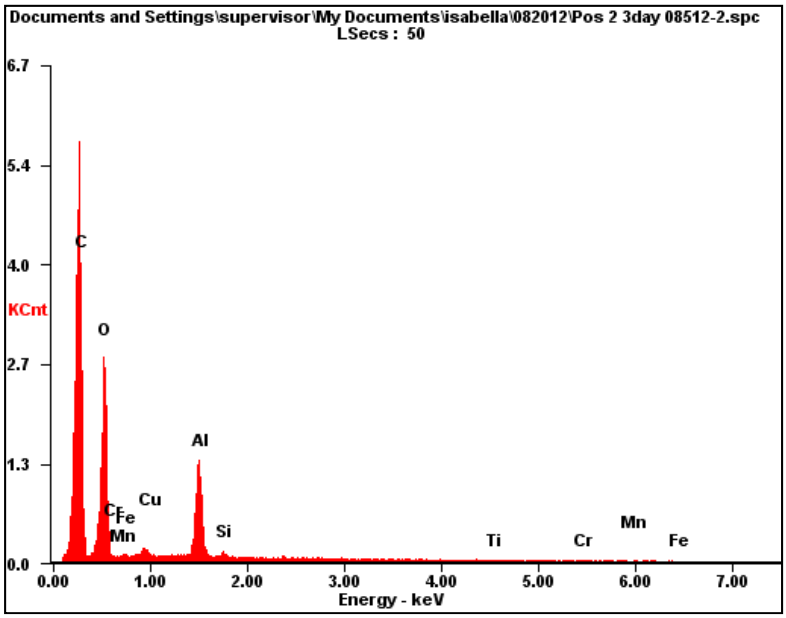

Element	*Wt %*	*At %*
C K	54.99	66.64
O K	28.04	25.51
FeL	01.30	00.34
CuL	01.67	00.38
AlK	11.74	06.33
SiK	00.68	00.35
TiK	00.41	00.12
CrK	00.49	00.14
MnK	00.68	00.18

Figure 50. The SEM-EDS analysis of the “white crumbling” precipitate found on the SiC-4 (2 ply SiC-CMC mock-up sample).

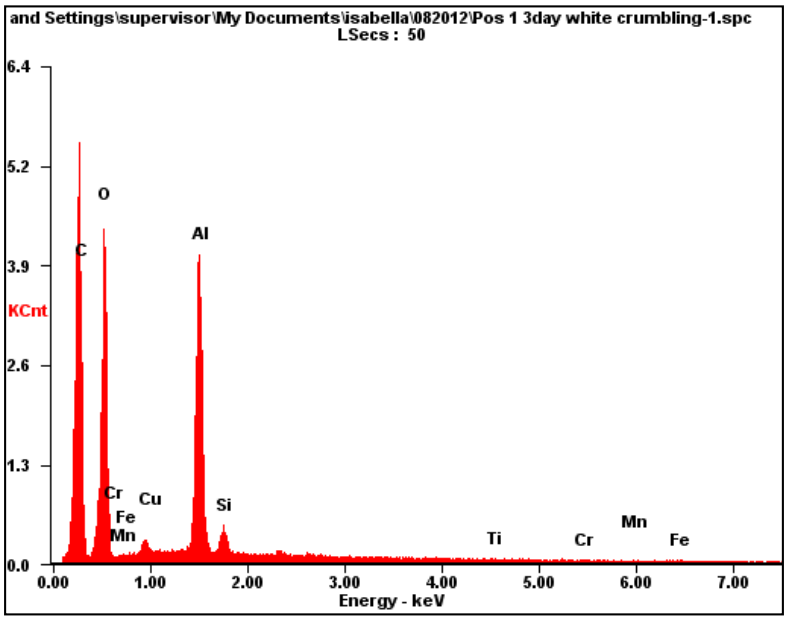

Element	*Wt %*	*At %*
C K	45.35	58.94
O K	26.61	25.96
FeL	00.23	00.06
CuL	01.76	00.43
AlK	22.18	12.83
SiK	02.38	01.32
TiK	00.37	00.12
CrK	00.69	00.21
MnK	00.43	00.12

Figure 51. The SEM-EDS analysis of the "yellow" precipitate found on the SiC-4 (2 ply SiC-CMC mock- up sample).

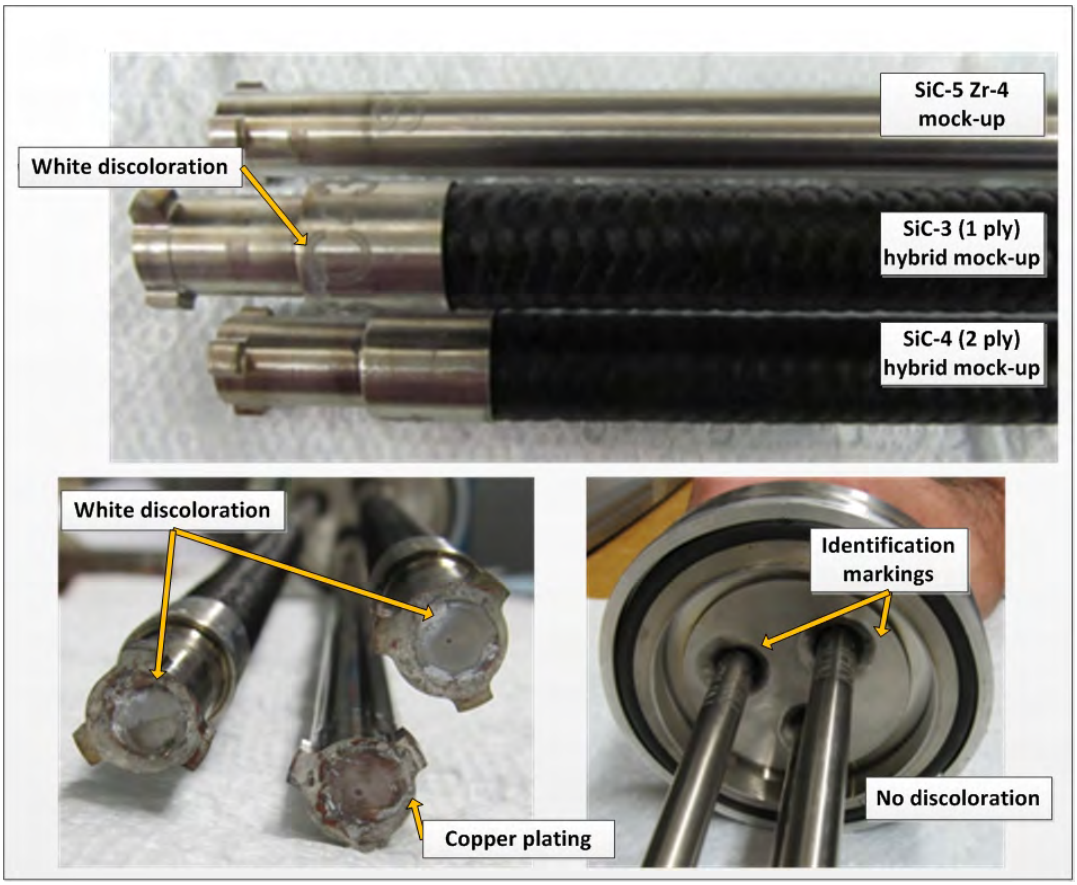

Figure 52. Slight white discolorations are also observed at certain areas of the Zr-4 parts of all the mock-up samples. Slight copper precipitation is also noted on the Zr-4 mock up sample at the end.

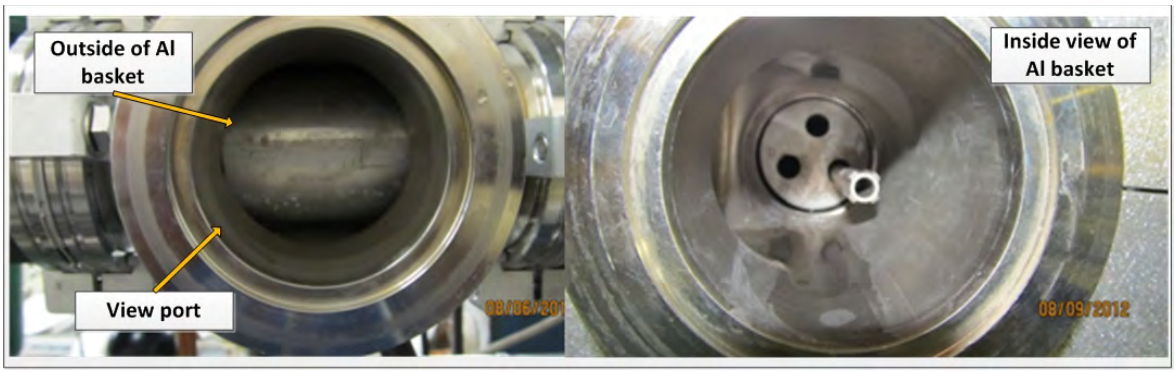

Figure 53. The visual examination of the aluminum basket at the end of the 3 day corrosion test shows no significant detoriation.

3.4.4.3 10 Day Corrosion Test. As mentioned in earlier, the 10 day test was started with fresh water (pH 4.8). A predetermined inspection was held after 3 days in the 10 day corrosion tests as a white suspension was noted in the water. After removal from the HWCF system, no fraying of the SiC-CMC hybrid mock-up samples was observed as shown in Figure 54. Again trapped precipitates were observed under the protective Zr-4 sleeve. The test continued and after the 10 day test, the visual inspection revealed that no significant corrosion or discoloration is noted on the Zr-4 mock up sample as shown in Figure 55. However, both hybrid mock-up samples were "covered" with a thin white layer as shown in Figure 56. A sample of the water with the white suspension after the 10 days HWCF test was taken for analysis and it showed mainly Al and O with small quantities of C, Si, Cl, Cu, Na and Ca (Figure 57). From this analysis it is expected that the alumina basket has corroded and that some Si and Cl were dissolute from the SiC-CMC sleeve.

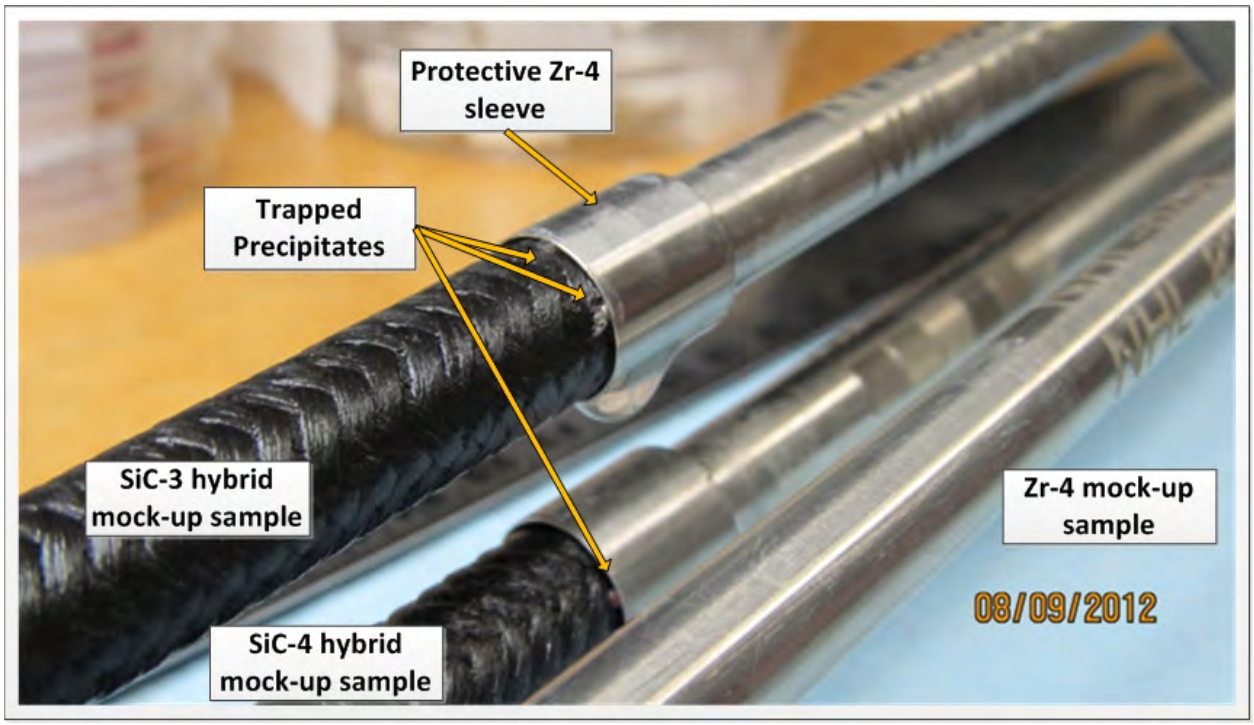

Figure 54. The visual examination of the mock-up samples after the 3 day inspection point of the 10 day test showing entrapped precipitates under the protective Zr-4 sleeve.

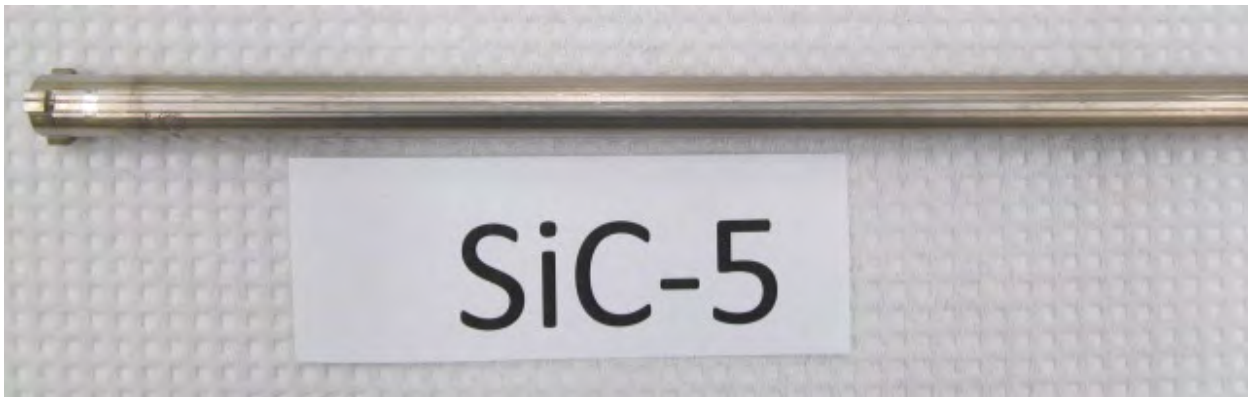

Figure 55. No significant corrosion or discoloration is noted on the Zr-4 mock up sample at the end of the 10 day HWFC test.

Figure 56. The visual examination of the mock-up samples at the end of the 10 day HWCF test showing white discoloration on most of the SiC-CMC sleeves of both hybrid mock-up samples.

Element	*Wt %*	*At %*
C K	13.63	23.00
N K	01.79	02.59
O K	30.61	38.78
NaK	02.28	02.01
MgK	00.50	00.41
AlK	31.14	23.40
SiK	02.82	02.03

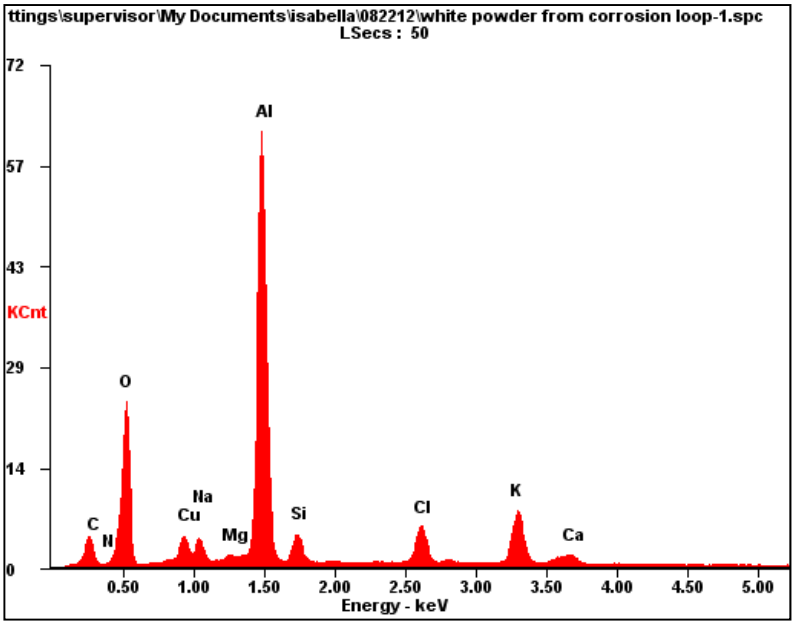

ClK	03.69	02.11
K K	05.67	02.94
CaK	01.12	00.56
FeK	00.30	00.11
CuK	06.47	02.06

Figure 57. A sample of the water with the white suspension after the 10 days HWCF test was taken for analysis and it showed mainly Al and O with small quantities of C, Si, Cl, Cu, Na and Ca.

3.4.4.4 Metallurgical analysis of the HWCF samples. The metallurgical examination of the microstructure after the 10 day HWCF test was completed on two areas namely at the centre of the SiC-CMC sleeve and at the end near the protective Zr04 sleeve at the end of the flow direction. Figures 58 and 50 shows the microstructures of the 1 ply SiC-CMC sleeve where white residue is noted at the end of the sleeve. At the end of the sleeve, signs of SiC-matrix removal are also noted. More residu (precipitates) are visible on the middle section, although this maybe misleading as it is not known what the effect of sample cutting was on these images. Material removal patterns are visible in Figure 59 which is most probably an indication of the water flow pattern at that specific area. Comparing the images taken from the SiC-4 (2 ply) mock-up sample shown in Figures 60 and 61, also white residu and SiC-matrix material removal is observed. The surface of the SiC-4 SIC-CMC after the 10 day corrosion test is however smoother. It may be argued that it is due to higher water flow compared to SiC-3, but this cannot be conclusively stated, due to the difference in microstructure noted during the metallurgical examination after bend testing which shows that the 1 ply material exhibits more grainy structures. Based on this microstructure examination, it seems possible that the Si, Cl and C observed in the corrosion products and in the water analyses, may be caused by SiC-matrix removal during the corrosion flow tests.

A preliminary SEM examination was completed on the Zr-4 tube of the respective mock-up samples. No significant differences are observed, but it is strongly recommended that further TEM and EBSD examinations be completed to determine differences. Figure 62 shows a typical microstructure with pitting and corrosive action noted.

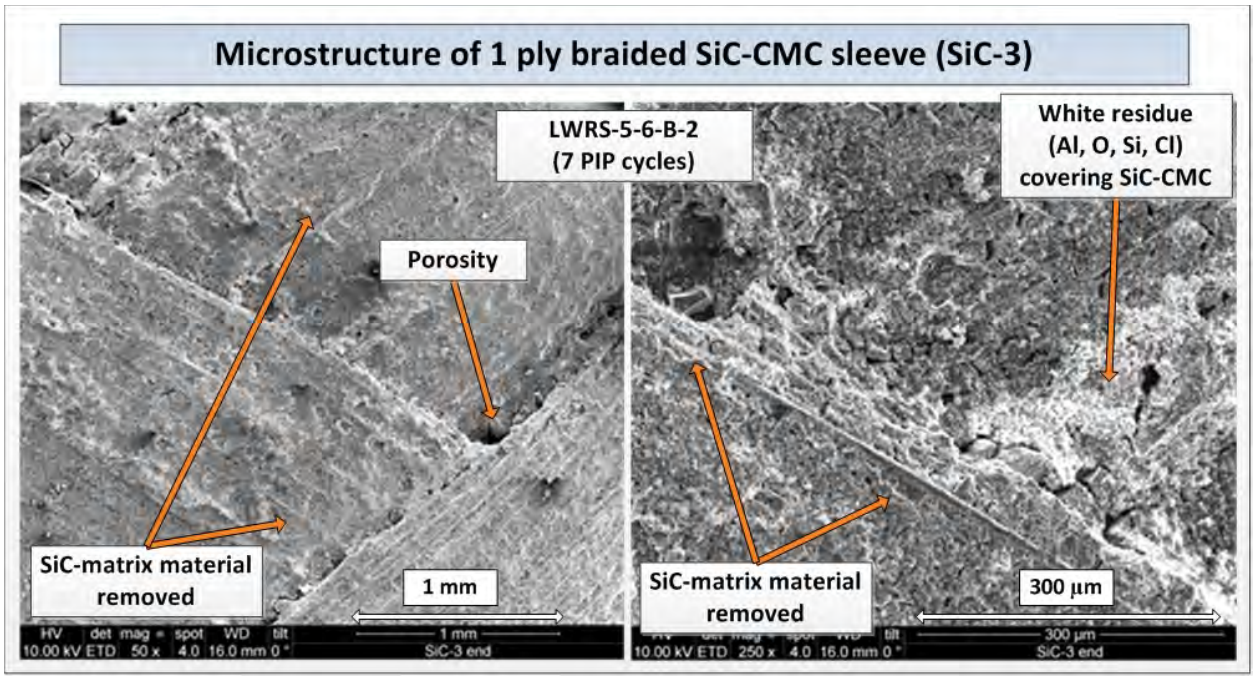

Figure 58. Figure showing the microstructures of the 1 ply SiC-CMC sleeve (SiC-3) where white residue is noted at the end of the sleeve. Areas is also noted where SiC-matrix material is removed.

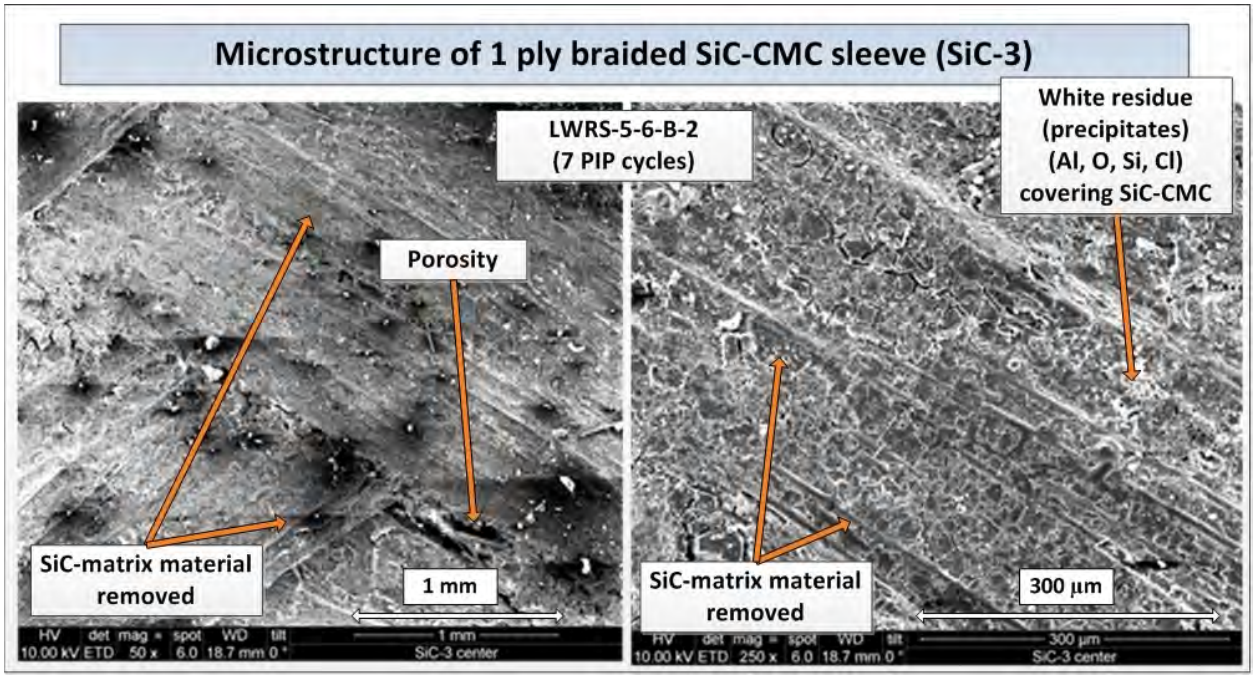

Figure 59. Figure showing the microstructures of the 1 ply SiC-CMC sleeve (SiC-3) where white residue is noted in the centre of the sleeve. More “chunky” residue are noted with areas where SiC-matrix material is removed.

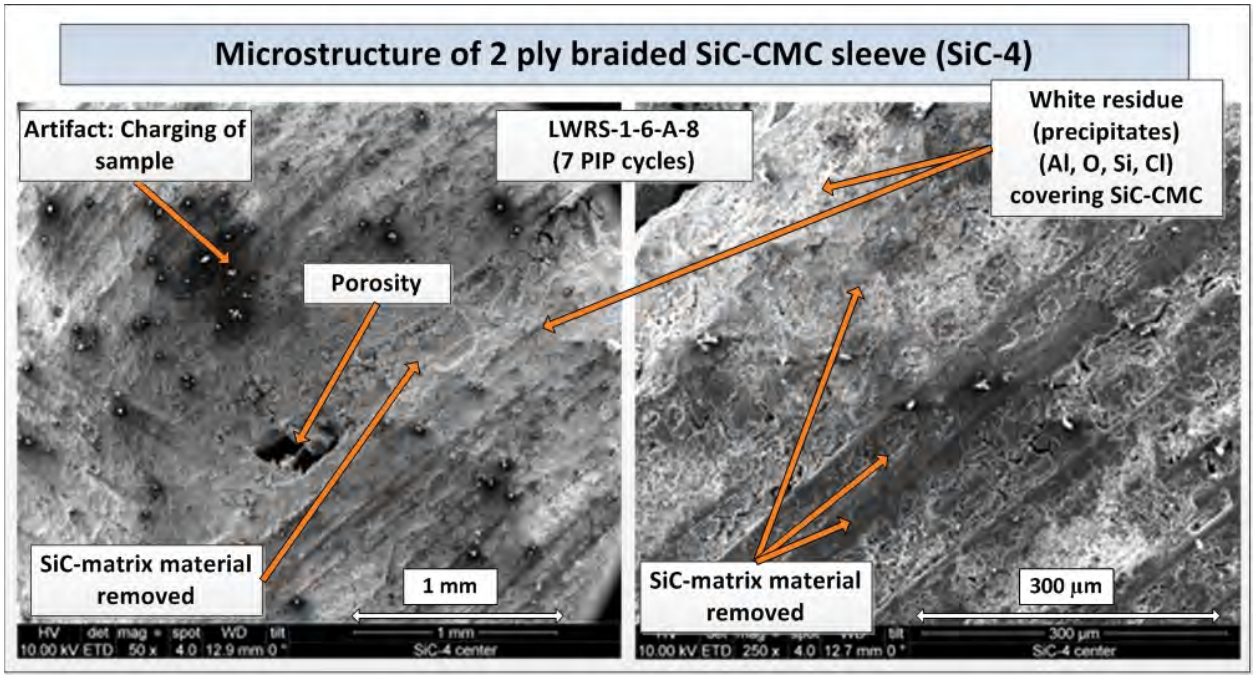

Figure 60. Figure showing the microstructures of the 2 ply SiC-CMC sleeve (SiC-4) where white residue is noted at the end of the sleeve. Areas is also noted where SiC-matrix material is removed.

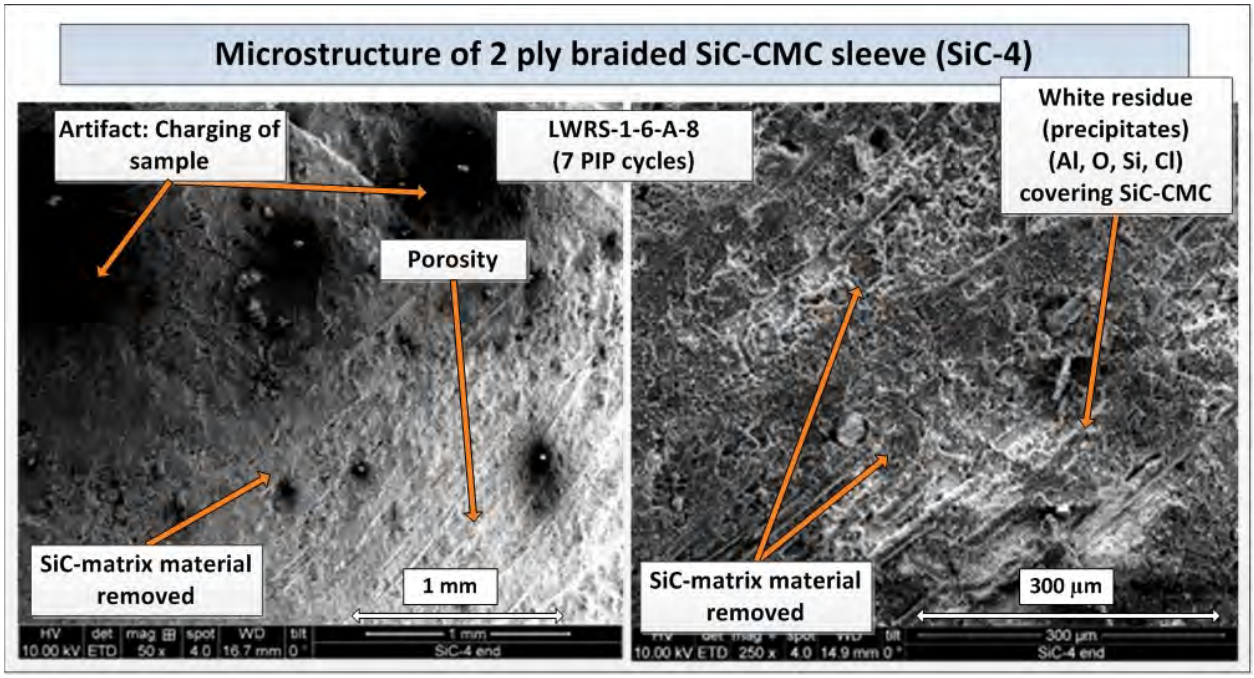

Figure 61. Figure showing the microstructures of the 2 ply SiC-CMC sleeve (SiC-4) where white residue is noted at the centre of the sleeve. Areas is also noted where SiC-matrix material is removed.

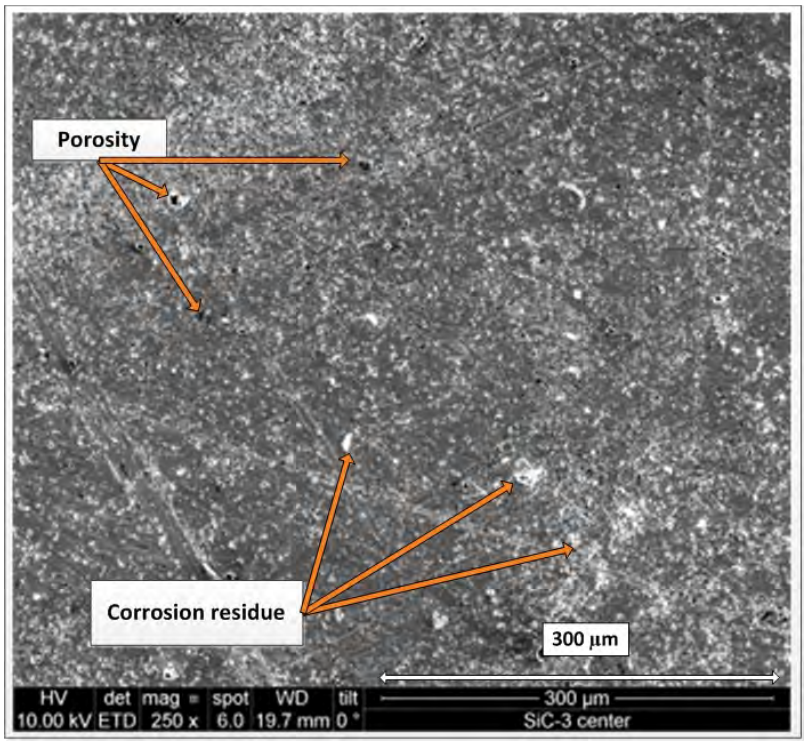

Figure 62. Representative SEM micrograph showing the microstructure of the Zr-4 tube of SiC-3 (1 ply). Porosity and corrosion product residue are noted.

3.4.4.5 Raman examination of the HWCF samples. Preliminary work is completed using Raman spectrometry to identify changes in the oxidation behavior of SiC due to the HWCF test. The Raman spectra of the two mock-up samples SiC-3 and SiC-4 after HWFC testing as well as a fresh (un-exposed) representative LWRS-1-6-A-7 sample were measured and shown in Figure 63. Peaks at ~790, 965, and 1120 cm^{-1} indicate presence of SiC while peaks at ~1355 and 1600 cm^{-1} indicate present of C. A small shift from ~1120 to ~1140 cm^{-1} in the third SiC peak is noticed in the SiC-3 and SiC-4 samples and needs further investigation for final conclusion.

According to Lazzeri and Mauri [25], SiO_2 forms (Cristobalite, in particular) produce several Raman peaks in the 100 to 500 cm^{-1} range. According to Revesz and Walrafen [26], vitreous SiO_2 produces peaks at 440, 490, and 604 cm^{-1}. As can be seen in Figure 64, no such peaks are evident in the scans of the SiC-CMC sleeves when comparing the Raman spectra of SiC-3 after exposure to the HWCF test to the fresh (un-exposed) representative LWRS-1-6-A-7 sample. No discernible differences between the samples are observed.

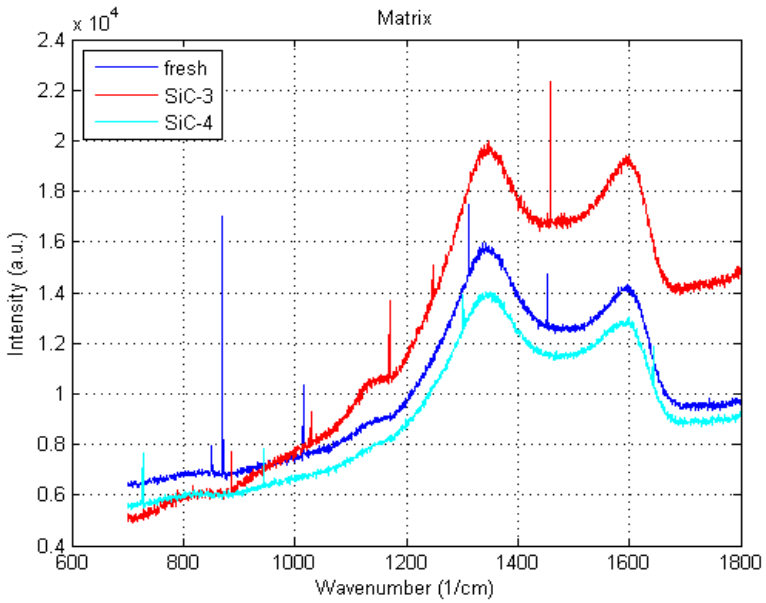

Figure 63. Figure showing comparative Raman spectra of SiC-3(HWCF tested), SiC-4(HWCF tested) and LWRS-1-6-A-7(fresh). Peaks at ~790, 965, and 1120 cm-1 indicate presence of SiC while peaks at ~1355 and 1600 cm-1 indicate present of C. A small shift from ~1120 to ~1140 cm-1 in the third SiC peak is noticed in the SiC-3 and SiC-4 samples.

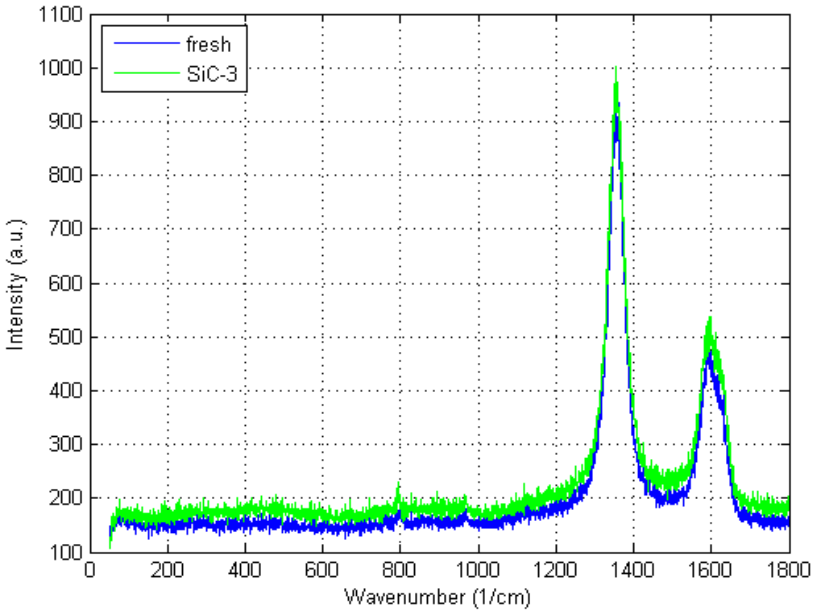

Figure 64. No SiO_2 Raman peaks are evident in the scans of the SiC-CMC sleeves when comparing the Raman spectra of SiC-3 after exposed to the HWCF test to the fresh (untested) representative LWRS-1-6-A-7 sample.

3.4.4.6 XRD examination on the HWCF samples. Preliminary XRD analysis showed no significant differences between the XRD graphs of the 1 ply SiC-CMC sleeves due to the 10 day corrosion test (Figure 65). Also no phase changes are detected for the 2 ply SiC-CMC sleeves after the corrosion testing, but the intensity (counts) is lower for the sleeve exposed to corrosion test (Figure 66). This needs to be further investigating in conjunction with surface roughness measurements, to determine if it is due to the removal of material or a possible surface chemical change.

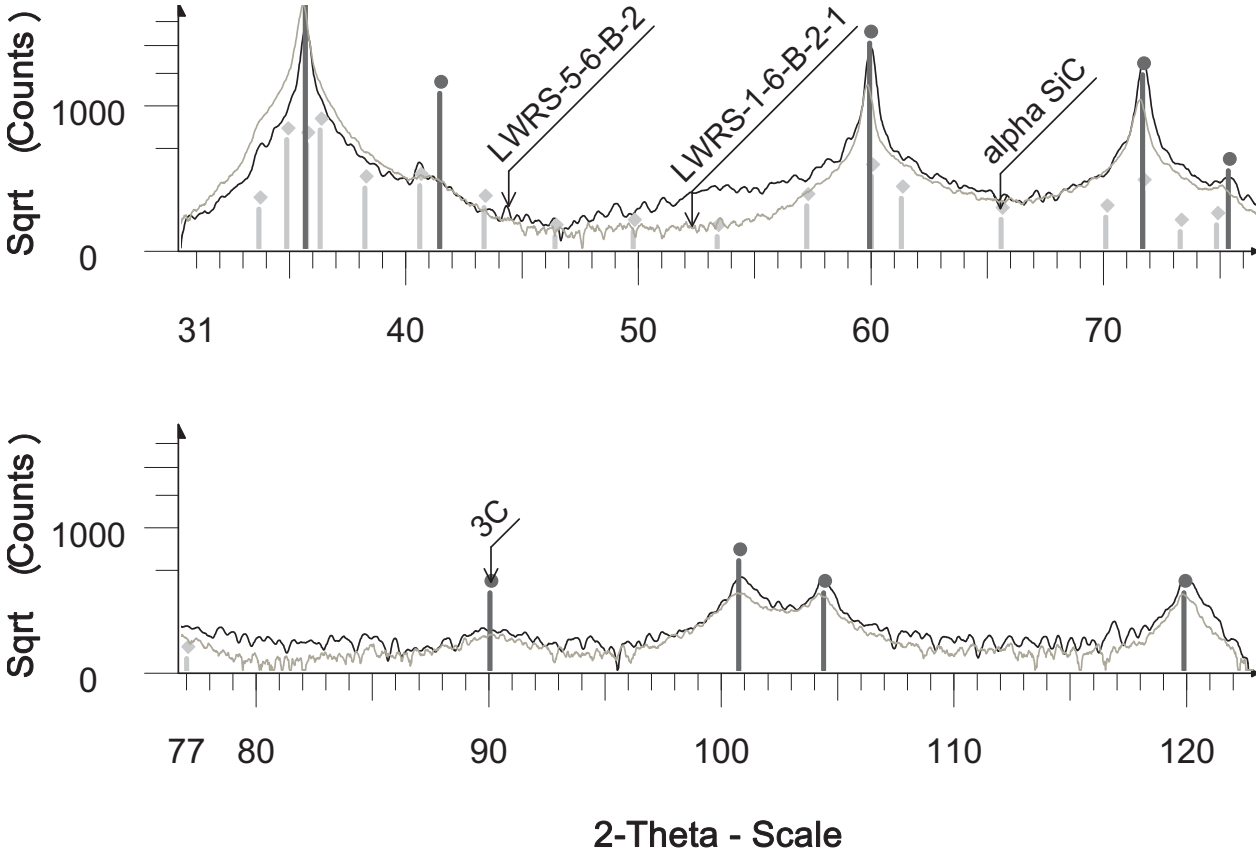

Figure 65. XRD spectra of 1 ply braided SiC-CMC sleeves when comparing the Raman spectra of SiC-3 (LWRS-5-6-B-2) after exposed to the HWCF test to the fresh (un-tested) representative LWRS-5-6-B-2-1-2 sample.

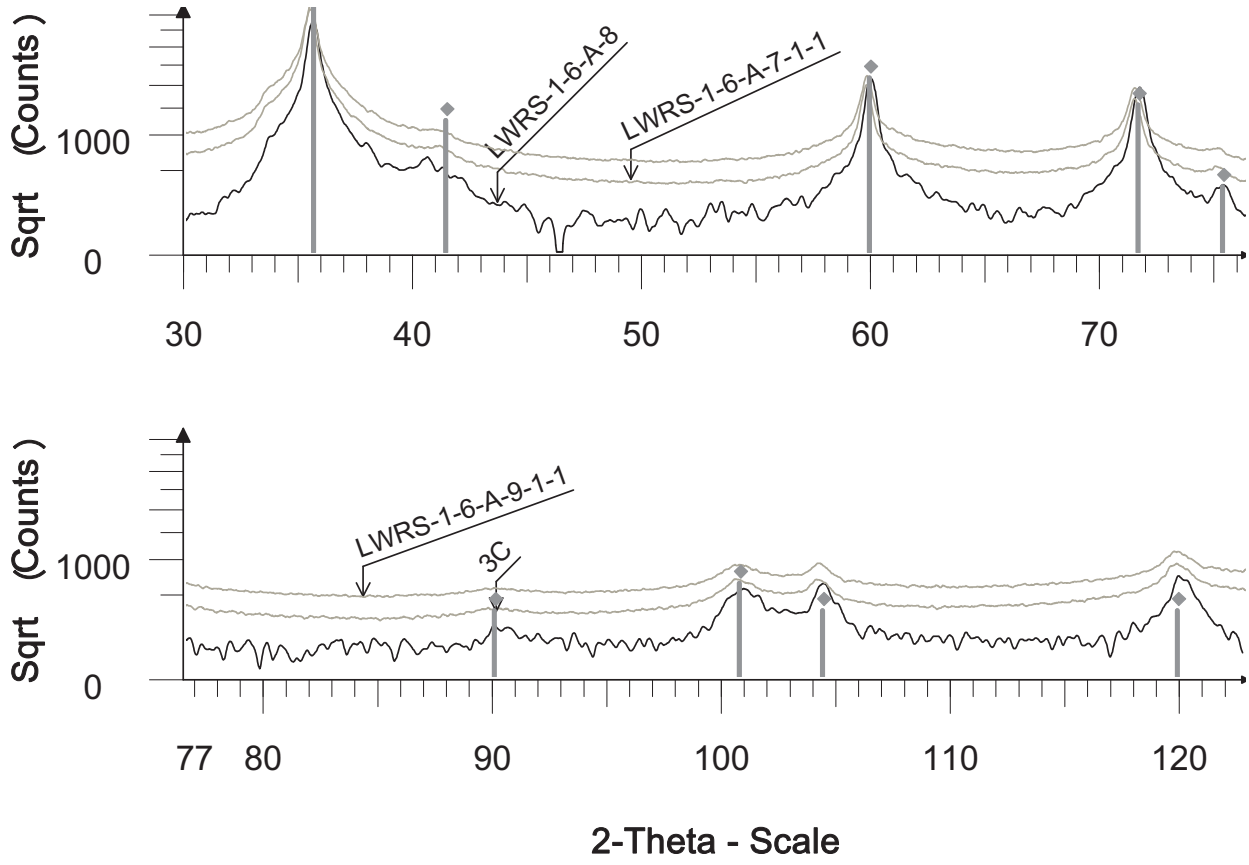

Figure 66. XRD spectra of 2 ply braided SiC-CMC sleeves when comparing the Raman spectra of SiC-4 (LWRS1-6-A-8) after exposed to the HWCF test to the fresh (un-exposed) representative LWRS-1-6-A-7-1-2 and LWRS-1-6-A-9-1-2 samples

3.4.5 Failure Analysis of SiC-CMC Sleeve During Mock-up Sample Fabrication at INL

3.4.5.1 Background. The design engineer provided a fractured SiC-CMC sleeve (LWRS-1-6-A-7) for metallurgical analysis. This SiC-CMC sleeve cracked during assembly of a mock-up sample for the HWCF method development. Reportedly the welder had welded the first of the Zr-4 protective sleeves (item 1 in Figure 67) in place and placed the SiC-CMC (item 2 in Figure 67) into place on the tube. The second Zr-4 protected sleeve (item 3 in Figure 67) is pressed or tapped into place over the tube by the distance of the spacer (item 4 in Figure 67) which is 0.250". The SiC-CMC sleeve (item 3) is easily installed to 0.221" and therefore the additional 0.030" of press caused a fracture indicating that the SiC-CMC sleeve was longer with approximately 0.030". The length specification of the SiC-CMC (item 2) sleeve is 6.000" ± 0.100", but the assembling technician assumed that it would at most be 6.000". The welder was therefore under the impression that the second protective sleeve must be 0.250 inches from the end of the tube, and due to the SiC-CMC tube being a bit longer than expected, he attempted to force the protective sleeve into place. While tapping on the sleeve using a hammer, the SiC-CMC cracked in several places.

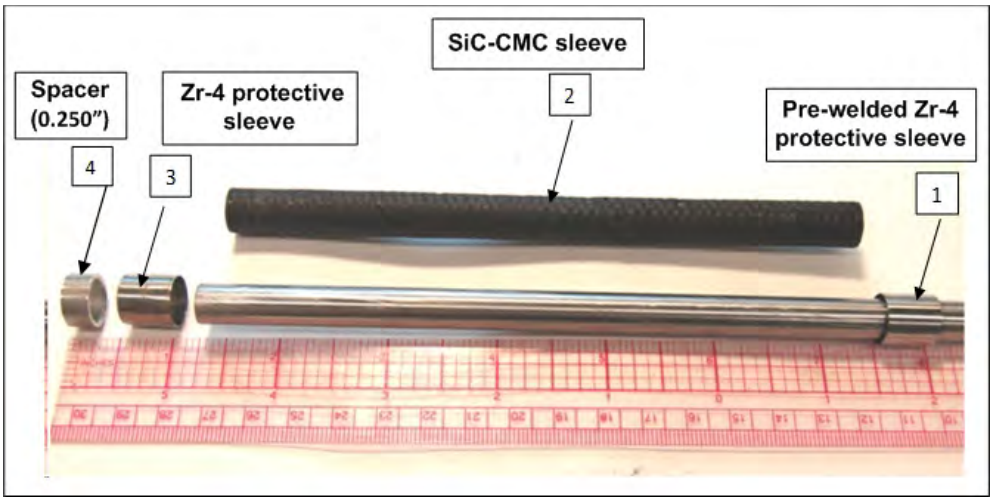

Figure 67. Figure showing all the parts used for the assembly of the HWCF mock-up samples.

3.4.5.2 Visual examination. The fracture is visible at a distance of approximately one third of the total SiC-CMC sleeve length at an approximate 45°angle. As the crack spirals around the circumference at approximately 45°angle but the sleeve is not broken in two and still in one piece as shown in Figure 68. At least three sections are visible where the material separated and is shown as crack areas in Figure 68. No visual damage was observed at or near the crack area(s) to show impact markings, nor was any discoloration identified. The visual examination also revealed that the crack did not only follow the CMC weaving pattern, as some cross-cutting of the fibers are observed.

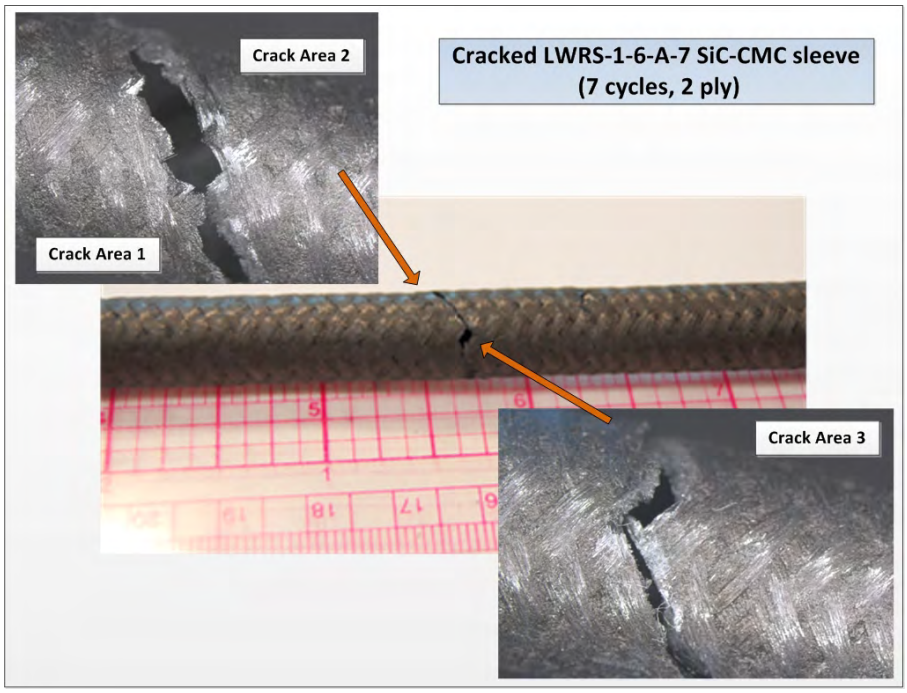

Figure 68. Figure showing the fractured LWRS-1-6-A-7 SiC-CMC sleeve. This sleeve cracked during the INL fabrication of the HWCF mock-up sample.

3.4.5.3 SEM fracture examination. The fractured surfaces were examined using SEM and SEM-EDS. No evidence of macro inclusions or defects were found at the origin of the cracks. Figure 69 shows a representative SEM micrograph of crack area 1. The higher magnification images shown in Figure 70, show typical CMC-fiber brittle fracture morphology. The images also show that final rupture occurred as the ultimate strength of the fibers was exceeded. No defects were identified at the area of failure initiation shown in Figure 69.

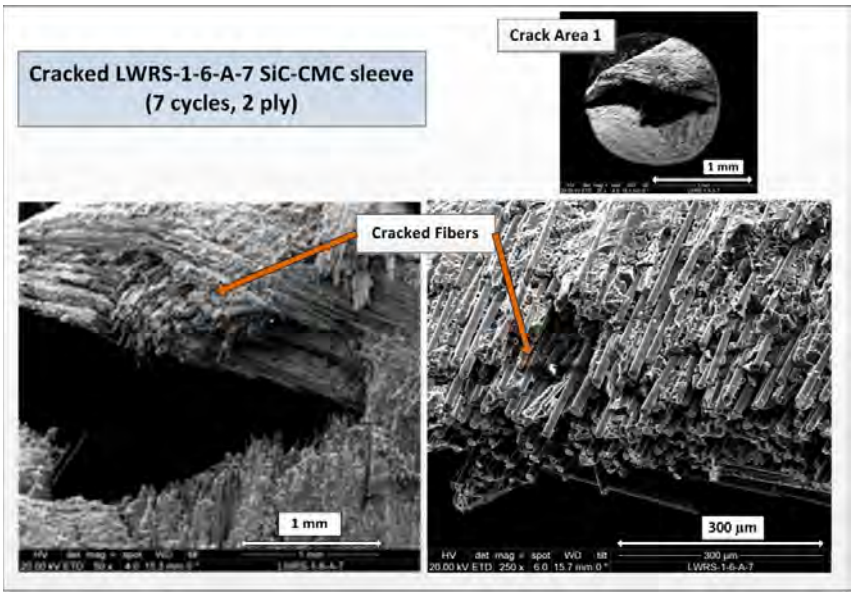

Figure 69. Figure showing SEM images of the fractured LWRS-1-6-A-7 SiC-CMC sleeve at crack area 1. No evidence of macro inclusions or defects is noted in the fracture.

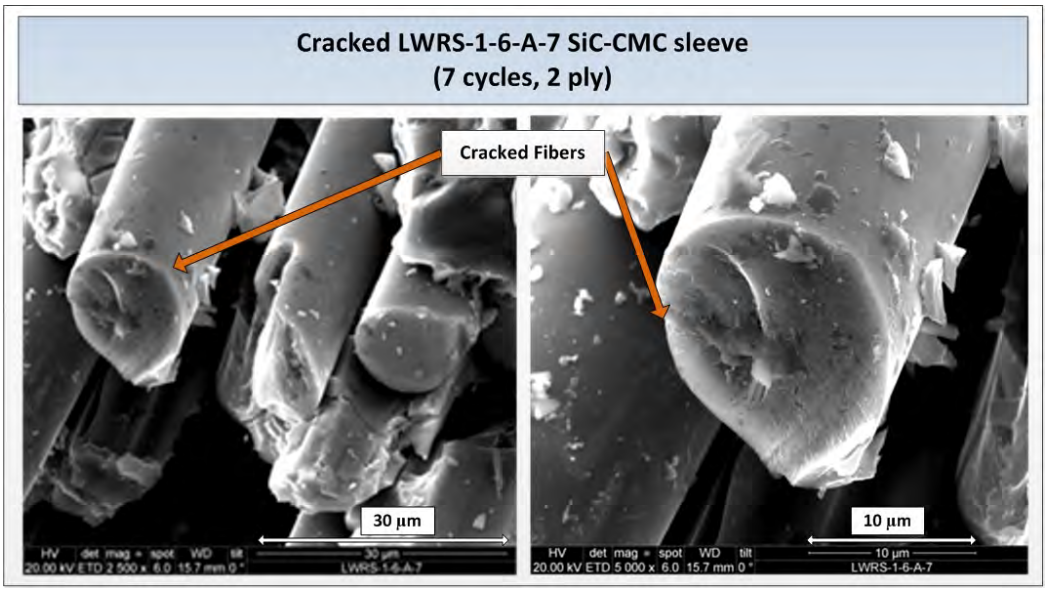

Figure 70. Figure showing SEM images of the fractured fibers of the LWRS-1-6-A-7 SiC-CMC sleeve at crack area 1.

3.4.5.4 SEM-EDS analysis. A qualitative SEM-EDS analysis (Figure 71) was also conducted on the fracture surface in comparison with the surface analysis at an area remote from the cracked area. No significant differences in chemical elements were observed. The elements ~ 20% C, ~10% O, trace amounts of Cl and Na, with Si as the main element, was identified in the SiC-CMC spectra.

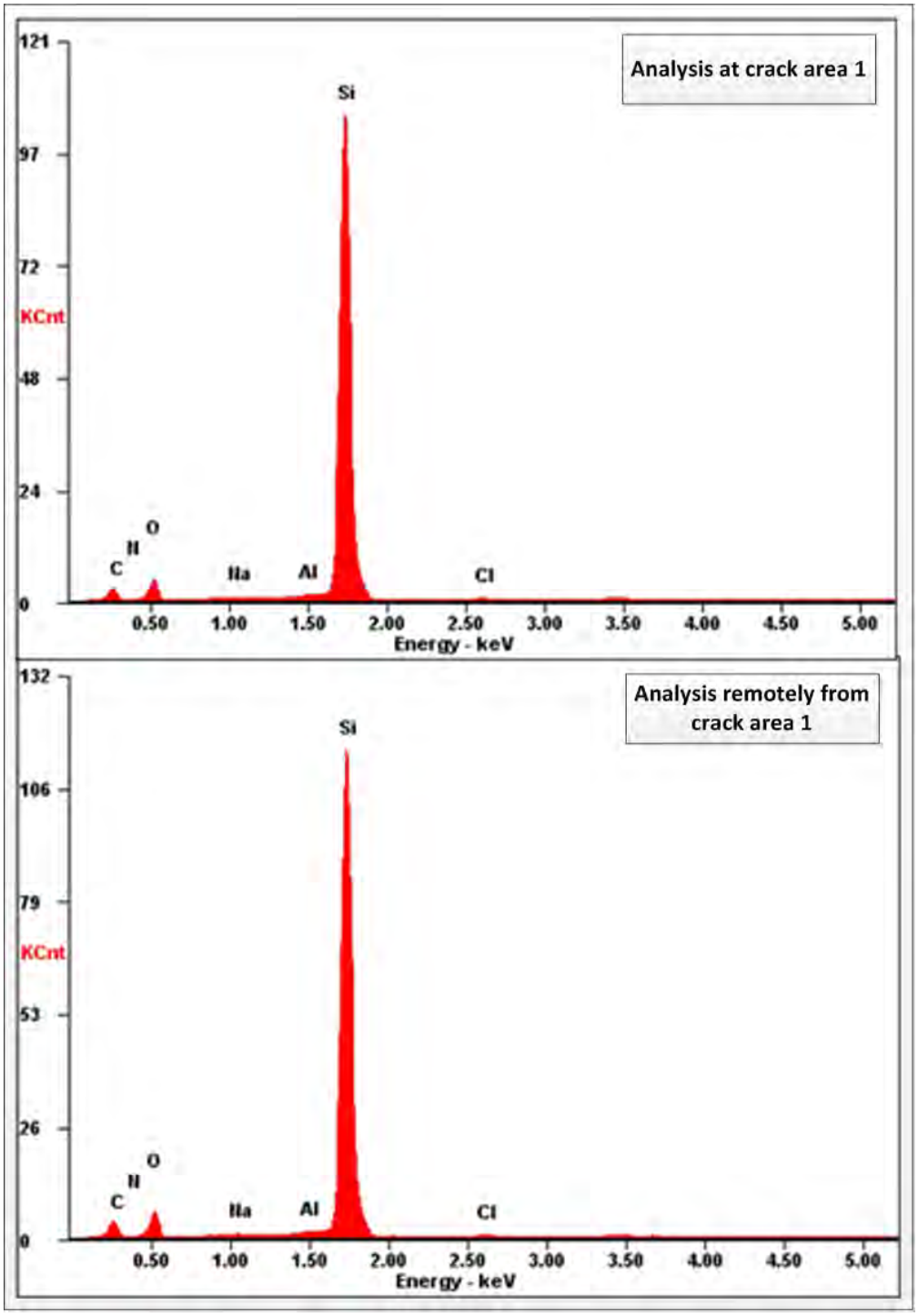

Figure 71. SEM-EDS of the LWRS-1-6-A-7 SiC-CMC sleeve at crack area 1 and at a distance away from the cracks show no differences in chemical composition.

3.4.5.1 Raman analysis. Raman analysis is completed and show no discernible differences in the fresh sample between locations near and away from the crack as shown in Figure 72.

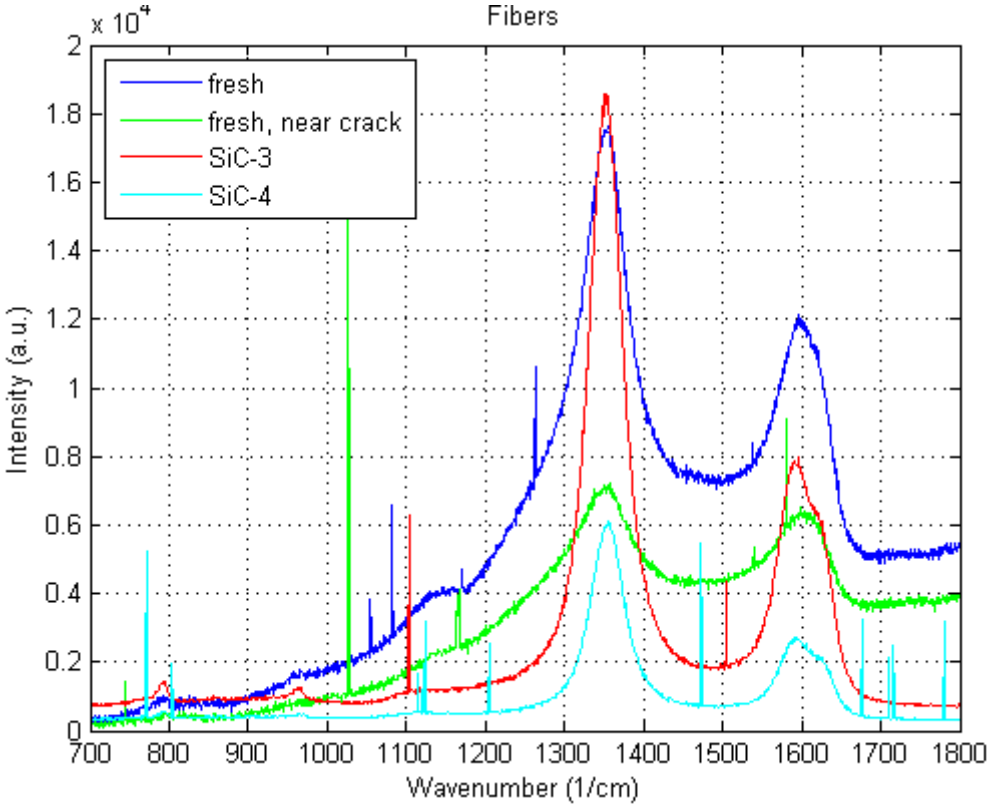

Figure 72. Raman spectra showing no difference between the material of the cracked 2 ply SiC-CMC (called fresh on graph) sleeve remote from the crack if compared to material at the crack. (SiC-3 and SiC-4 is tested after exposure to a 10 day corrosion test).

3.4.5.2 Conclusion. It is concluded that the SiC-CMC sleeve cracked due to an overload (applied load exceeded the local yield strength) that resulted from the "hammering" and forcing of the sleeve during fabrication which caused excessive strain on the material. This incident shows the importance of detailed fabrication instructions with corresponding pre-job briefings. Additionally, this lesson learned should be specifically added to the work sheets for future fabrication of the mock-up samples.

3.5 Summary of Gamma Irradiation Tests

The purpose of the gamma irradiation tests conducted at the Idaho National Laboratory (INL) was to obtain a better understanding of chemical interactions and potential changes in microstructural properties of a mock-up hybrid nuclear fuel cladding rodlet design (unfueled) in a simulated PWR water environment under irradiation conditions. Full documentation of the tests and analysis of test results are provided in [4]. The gamma irradiation tests were performed in preparation for neutron irradiation tests planned for a silicon carbide (SiC) ceramic matrix composite (CMC) zircaloy-4 (Zr-4) hybrid fuel rodlet that may be tested in the INL Advanced Test Reactor (ATR) if the design is selected for further development and testing. Although the effects of gamma irradiation on the hybrid design was expected to be different than effects from neutron irradiation, no data were currently available on the effects of any type of irradiation (gamma or neutron) on the SiC-CMC matrix processed via polymer impregnation pyrolosis (PIP). There was concern that degradation of the PIP processed SiC-CMC matrix may be enhanced due to irradiation effects. In addition, the gamma irradiation tests would provide information on the chemical stability of a proposed bonding agent to bond the SiC-CMC tube to the inner Zr-4 tube.

Preliminary testing in a gamma irradiator was easy, quick, safe (fully contained samples) and inexpensive, therefore the tests were conducted to support a better understanding of the behavior of the SiC-CMC material.

Two gamma irradiation experiments, denoted gamma irradiation test 1 and test 2, were conducted using a Nordion gamma cell 220E gamma irradiator with cobalt-60 source at a dose rate of 7.2 kGy/hr for 96 hours for test 1 and 167 hours for test 2. Selected specimens were contained in synthetic ATR primary coolant system water to test the potential effect of constituent chemicals in the water affecting the experiment samples. The pH of this synthetic water was 5.07 and 5.03 respectively for the two tests. The total irradiation dose was 60 mRad and 104.6 mRad respectively for the two experiments and the irradiation temperature was 50°C.

A set of initially fabricated SiC-CMC-Zr-4 hybrid cladding tubes were chemically bonded together during the PIP process to cure the SIC-CMC tubes. The the high temperature bonding processing caused the inner Zircodyne 702 to embrittle and therefore this set of hybrid tubes were not representative of the final design preventing the rodlets from being used for further testing in the ATR. Due to the failure of this bonding technique, a decision was made by the program to continue with the development and testing of a non-bonded hybrid design until an improved bonding technique could be developed and tested. An attempt was made to salvage the SiC-CMC braided tubes chemically bonded to the Zr-702 embrittled tubes by acid leaching the Zr-702 out of the assembly so the SiC-CMC tubes could be used for prototype characterization testing. At the time, it was assumed that the SiC CMC braided tubes would not be damaged or chemically altered due to the acid leaching, however this assumption was not validated (major lesson learned). The salvaged SiC-CMC tubes were used in the gamma irradiation test 1. As part of this lesson learned, the gamma irradiation test 2 used SiC CMC tubes that had not been acid leached and were representative of the hybrid final design.

Two samples sets were fabricated namely bonded and non-bonded sleeve samples. Characterization focus was placed on the non-bonded samples as this was the design to be initially irradiated in the ATR until an improved bonding technique could be developed and tested. The main findings of the first experiment is that the reclaimed sleeves were not very representative of the prototypes as most of the SiC matrix material was removed during the acid leaching process. However, irrespective of this fact, valuable information was gained on the bonded samples where the instability and lack of bonding agent integrity under these experiment conditions were highlighted. The various bonding agents used for gamma irradiation test 1 resulted in an increased Cl-, F- and Si concentrations soluble in the water during irradiation with the Cl content exceeding the ATR control limit. The metallurgical examination of the bonded samples further also shows that cracking and degrading of the bonded layer and SiC matrix material occurred which may be the reason for the increased Cl-, F- and Si concentrations found. The XRD analysis after gamma irradiation shows predominantly β-SiC with a trace of α-SiC. It was found that the 2 D x-ray radiographic inspection provided no significant information as comparative purposes to evaluate the effect of gamma irradiation.

Many of the lessons learned from the first gamma test were corrected during the second gamma irradiation test. One of the biggest lessons learned was the loss of data because of the unknown conditions of the samples prior to gamma cell insertion and the speed in which the samples were prepared and not integrated with the rest of the program to ensure specific characterization was done prior to gamma irradiation. The main reason for the speed of gamma irradiation insertion was due to the push to irradiate quickly in the ATR. The advantages of pre-gamma irradiation characterization are fully demonstrated by the battery of characterization test results in the second gamma irradiation experiment.

Both a 1-ply and a 2-ply set of SiC-CMC tube samples were prepared for the second gamma irradiation test to support the final design selection. Various subsamples from the two sample sets were prepared which included a mock-up mini tube (2 ply SiC-CMC tube) and one pre-cleaned SiC-CMC sleeve sub-sample. One sample was cleaned with ethanol prior to irradiation as it was found that no

cleaning was done prior to the first gamma irradiation test. It was decided to pre-clean one sample for comparative reasons to determine the effect of cleaning on the water chemistry. Program management advised that the 2 ply sample was technically representative of the prototypes although dimensionally non-compliant. The 1 ply sample was included to provide comparative data for development purposes.

Density measurements of the gamma irradiation 2 tests showed no large differences in the density values between the 1- and 2 ply SiC-CMC tubes and that no change in density could be conclusively determined due to gamma irradiation in either the 1 or 2 ply samples. However, this finding needs to be validated with a larger sample set to determine statistical variations and significance. . The XRD patterns showed that no α-SiC was present in either prior or after the irradiation. Leach test analysis on representative sub-samples prior to gamma irradiation revealed that more Cl (20 times) and Si (3 times) are released for the 2 ply braided SiC-CMC tube compared to the 1-ply tube. Similar results were observed in the water analysis after gamma irradiation for the Cl content of the 1ply tube water generally lower than for the 2-ply tube water samples with exception of the pre-cleaned 2-ply SiC-CMC tube water which had the overall lowest Cl dissolution during gamma irradiation. Significant higher Cl, F and Si dissolution from the mini tube (2-ply) suggest possible contamination during the fabrication/sample preparation process. The SEM microstructural examination of the 2-ply samples shows that visibly more cracks and flakes are visible in the SiC matrix material after the gamma irradiation treatment.

The application and advantages of 3D Tomography as a characterization technique were demonstrated during this experiment by showing gaps between the SiC-CMC sleeve and Zr-4 tube at any distance alongside the tube, the inner and outer surface morphology, and identification of open porosity can be evaluated and the braided weave patterns were observed.

These two preliminary gamma irradiation tests provided relevant technical information for the improvement of the SiC-CMC sleeve design of the prototypes. Specifically, the post gamma irradiation characterization revealed a chemical and mechanical breakdown of the bonding processes used and assist the program managements to make a decision not to continue with a non-bonded hybrid cladding design for the initial neutron irradiation due to the immaturity of the bonding technique. It is recommended that the gamma irradiation experiment results be used as an input for design selections and neutron reactor insertion. It is further recommended that the future gamma irradiation experiments include EBSD, FTIR and TEM examinations to provide insight in possible changes on nano level which typically will provide more detail on the actual irradiation effects. Updates and modifications to the various test plans are needed based on the lessons learned during the execution of the tests/characterization techniques. These modifications must be in place prior to the gamma irradiation experiment of the actual prototypes. As these samples were processed using 5 PIP cycles which is different than the anticipated 7 PIP cycles of the prototypes, it is recommended that the gamma irradiation test prior to reactor insertion be executed on samples of fully representative processing cycles and therefore be fully be classified as “prototype” samples.

4. LESSONS LEARNED

The lessons learned by doing these characterization tests are not only applicable to technical knowledge, but also to the methods and process controls. Main lessons learned are summarized below:

- Control of the samples was difficult as no designated laboratory was available for the full duration of the first gamma irradiation experiment and only during the very last of the post irradiation characterization, a laboratory was made available.
- Method development:
  - Although the bend test method development was successful, the full documentation of the process was not immediately captured and needed some back tracking for the update of the test plans.

- The design and fabrication of the HWCF equipment was not fully integrated in the project plan, resulting that design requirements were not fully incorporated. Many ad hoc changes caused that the impact of these changes to the full system was not taken into account, resulting in secondary effects. It is recommended that a systems approach is followed for future designs or for the gap analysis for ATR representativeness.
- Memory limitations of the data recorder of the HWFC tests need to be address in pre-job briefings, test plans as well as operating instructions.
- The actual execution of the leach test needs more attention as the repeatability of the volume and the addition of water needs to be updated in the procedure as current process can be interpreted differently.

- Quality:
  - Chemical composition sample labeling and follow-up caused initially delays and re-testing with Gamma irradiation tests (possibly symptom of lack of control and methods). This was improved during the characterization of the bend test and HWCF test.
  - The cleaning and handling precautions are not standardize and needs more attention during the actual fabrication of samples and execution of experiments. All work requests, test plans, instruction documents needed to be reviewed and updated to include this. This needs to receive attention in pre-job briefings as well.
  - Fabrication controls and requirements needs to be recorded to ensure that full traceability exist in raw material etc.
  - Zr-4 raw material storage and traceability need attention and detail descriptions and record keeping of the samples provided for characterization needs to be provided to the characterization PI for review and inclusion in future characterization reports.
- Importance of pre-experiment characterization is demonstrated by the first gamma irradiation test. As an example the density values that could not be compared and fully used. Additionally the microstructural examination prior to experiment would have shown that the SiC matrix material is basically fully removed and then the experiment could have been re-evaluated.
- Control sample tests were not performed for comparison to the gamma irradiation results. Without this information, definitive conclusions about the effect of gamma irradiation on the material properties cannot be determined. Additional tests should be performed with a control sample set to validate the results.
- Lessons learned from the cracked mock-up sample during fabrication is that detail instructions and pre-job briefings needs to be held with the fabrication welder.

5. CONCLUSIONS

5.1 Baseline characterization

No significant density differences are observed between the 5 and 7 PIP processed cycles or the 1 and 2 ply braided SiC-CMC sleeves. These characterization revealed a specific subsample, LWRS-1-6-A-1-5, to have the highest density which could not be attributed to the number of PIP cycles. Thus another SiC-CMC sleeve fabrication parameter plays a role in the higher density value and it is recommended that this trend be further investigated. The PIP polymer properties, such as the polymer composition, temperature of pyrolysis heat treatment or the time of pyrolysis, should be investigated for this higher value.

Metallurgical examination showed that the SiC-CMC sleeves fabricated with only 5 PIP cycles exhibit open fibers and larger cracked flakes (approximately 30 μm) of SiC matrix material to the more compact and smaller flakes (approximately 5 μm) SiC matrix material of the 7 PIP cycle sleeves. It was

further found that the 1 ply SiC-CMC sleeves revealed a higher amount of open and broken CMC fibers. The effect of the difference in microstructure becomes very apparent during the bend test results and subsequent crack evaluations.

It was further found that the SiC-CMC sleeves exist from mainly 3 C SiC (cubic or beta) with very small indications of 6H SiC (hexagonal or apha) also present.

5.2 Conclusions on Bend Test

It is concluded that the method development for both hybrid SiC-CMC-Zr-4 mock-up and SiC-CMC sleeve samples were successful for a comparative method. The 2 ply sleeve samples show a higher bend momentum compared to those of the 1 ply sleeve samples. This is applicable for both the hybrid mock-up and SiC-CMC sleeve samples. Comparatively both the 1 and 2 ply hybrid mock-up samples showed a higher bend momentum if compared with the standard Zr-4 mock-up sample.

The characterization of the hybrid mock-up samples showed that the 1 ply SiC-CMC sleeve matrix shows signs of distress and preliminary signs of defraying at the protective Zr-4 sleeve areas. In addition, the microstructure of the SiC matrix at the cracks after bend test shows significant cracking and flaking. The 2 ply SiC-CMC sleeve samples showed a more bonded cohesive SiC matrix structure. The cracking and fraying in the 1 ply sleeve shows potential concerns for increased fretting during the actual use of the material in cladding. No difference in qualitative SEM-EDS analyses is noted and the Zr-4 tube is confirmed with no presence of Nb and Hf.

Tomography was proven to be a successful tool to identify open porosity during pre-test characterization. Additionally the benefit of tomography as an indirect tool for establishing simulation parameters was identified and is recommended for further investigation.

5.2.1 Preliminary conclusions on HWCF Test

It should be noted that at this stage only preliminary conclusions can be given on the samples exposed to HWCF tests due to test and analysis delays. Preliminary results can be summarized as follows:

- The in-line measurements were validated by “tap” measurements taken periodically though the HWCF tests. It is, however, found that the time delay between verification measurements caused difference in readings and is currently under investigation. Possible causes are the precipitation of certain chemical/substances, and the change in oxygen potential due to the pressure differences.
- The current HWCF system could not provide stable conditions to conduct the tests under ATR representative conditions.
- Cl content was determined for water taken periodically from the HWFC tests. Although duplicate measurements (for validation) are in process, preliminary observation is noted that the Cl content decreased as the 10 day corrosion test progressed. An explanation of this is still under investigation.
- No dimensional differences due to the HWCF tests were observed. Although detailed measurement analyses were conducted and the null hypotheses was not rejected, meaning that no differences were seen, final conclusions cannot be reached as the sample size is insufficient. In addition, it may be that the measurement technique applied for these measurements are not sensitive enough to identify possible differences. It is therefore recommended that more investigation needs to be done on the measurement technique; however, the inclusion of surface roughness measurements, using atomic force microscope (AFM) analysis, is to be considered as it will provide information on the surface roughness, showing micron changes. This may be particular useful for further corrosion or chemical interaction studies.
- Precipitates were observed underneath the Zr-4 protective sleeve at the flow-end side of the mock-up samples. This is typically expected due to the flow direction of the water and this observation shows

that this potentially can happen as well during ATR irradiation and future application of this design in the LWR. It is therefore recommended that the design of this protective sleeve needs to be modified.

- Material removal patterns (or flow patterns) were observed in the SiC-CMC microstructures of both the two hybrid mock sample. This is most probably an indication of the water flow pattern at that specific area. Images from the SiC-4 (2 ply) mock-up sample surfaces after the 10 day corrosion test is however smoother when compared to the SiC3 sample. It may be argued that it is due to higher water flow compared to SiC-3, but this cannot be conclusively stated.
- A white layer covered most of the SiC-CMC surface of both the SiC-3 and SiC-4 samples at the end of the 10 day test. Based on the SEM-EDS results, Al, O, Cu, Si, Cl were the main elements of this layer.
- Evidence is provided during the metallurgical examination that SiC-CMC sleeve material was removed during the tests. The presence of Cl and Si in the corrosion products filtered from the system water, also suggest this observation.
- Preliminary test using Raman as a characterization technique to determine corrosion properties, showed no significant differences. A small shift from ~1120 to ~1140 cm^{-1} in the third SiC peak is noticed in the SiC-3 and SiC-4 samples and needs further investigation for final conclusion.
- A preliminary SEM examination was completed on the Zr-4 tube of the respective mock-up samples. No significant differences are observed, but it is strongly recommended that further TEM and EBSD examinations be completed to determine differences. Pitting and corrosive action are noted on these samples.
- Preliminary XRD analysis showed no significant differences between the XRD graphs of the 1 ply SiC-CMC sleeves due to the 10 day corrosion test. Also no phase changes are detected for the 2 ply SiC-CMC sleeves after the corrosion testing, but the intensity (counts) is lower for the sleeve exposed to corrosion test. This needs to be further investigating in conjunction with surface roughness measurements (AFM), to determine if it is due to the removal of material or a possible surface chemical change.

5.2.2 Conclusions on fractured SiC-CMC sleeved during fabrication

The SiC-CMC sleeve cracked due to an overload (applied load exceeded the local yield strength) resulted from the “hammering” and forcing of the sleeve during fabrication which caused excessive strain on the material. This incident shows the importance of detail fabrication instructions with corresponding pre-job briefings. Additionally, this lesson learned should be specifically added to the work sheets for future fabrication of the mock-up samples.

5.2.3 Final Conclusion: Meeting the objectives of this study

The value of this report is measured and summarized against the objectives of these mock-up sample tests as follows:

- Method development or method/test confirmation, as many of these methods are first of a kind and uniquely designed for this type of cladding design.
    a. Bend test method development was successful and test plans can be updated for standard prototype tests.
    b. HWCF test method development is not yet in the final stages as many unknown operational issues were identified during the test method development.

- Comparative results on two different preliminary SiC-CMC sleeve designs based on PIP processing techniques.
    a. Supportive evidence is provided in this study that the 1 ply braided material exhibits reduced performance.
    b. Data indicate that density cannot be used as the only acceptance criteria for the fabricated SiC-CMC material.
    c. Results further showed that 5 PIP cycled material has more grainy and loose structure, but due to the small quantities of samples investigated, it is recommended that the development work on all the effects of other fabrication process parameters be identified.
- Analytical results from these tests as an *early* indication of ATR insertion readiness.
    a. The entrapment of the precipitates during the HWCF test showed on a possible design change for the protective Zr-4 sleeve. This was an early indication that this typically will enhance fretting and degradation of the SiC-CMC sleeve in that area.
    b. The gamma irradiation test, although not conclusively, showed that the specific bonding technique will not withstand neutron irradiation. Alternate bonding techniques should be investigated.
    c. The bend test, although not a direct measurement of irradiation behavior, provide information that the 2 ply SiC-CMC sleeves are more stable at the protective Zr-4 sleeve ends compared to the 1 ply. This may be an early indication that 2 ply SIC-CMC sleeves will withstand more vibration (decreased fretting) in the reactor appreciation. This needs to be confirmed with actual vibration studies to be fully conclusive.

6. RECOMMENDATIONS

It is recommended that the full interpretation and reporting of the HWFC test be completed to enhance the current data provided. A full gap analysis of the actual system capabilities needs to be conducted. This will enable the development team to set the parameter limits for representative comparison of any reactor conditions. Additionally, the actual flow characteristics of the HWCF system need to be finalized and understood.

It is further recommended that the bend test tomography analysis be expanded for incorporation of this information in the development of cladding model. This will benefit decisions on process design changes as well as fuel performance modeling.

The finalization of the electron back scatter diffraction (EBSD) technique for hydrogen embrittlement identification is also strongly recommended. This necessitates the controlled hydrogen gas embrittlement studies with EBSD analyses to set a standard.

It is also recommended that prototype test (quality level 2) to be completed after all the actions are finalized.

7. REFERENCES

1. INL/MIS-12-25696, “LWRS Fuel Development Plan”
2. PLN-3927, “Cold Characterization Plan for LWRS-1 hybrid SiC-CMC/Zircalloy-4 fuel experiment”
3. PLN-3971, “Project Execution Plan for the Light Water Reactor Sustainability (LWRS) Advanced LWR Nuclear Fuel Development Pathway experiments in the ATR”
4. INL/EXT-12-27188, “Characterization of LWRS Hybrid SiC-CMC-Zircaloy-4 Fuel Cladding after Gamma Irradiation”
5. INL/MIS-10-19844, “Light Water Reactor Sustainability Program Quality Assurance Program Description Document”
6. LWP-9201, “Briefings”
7. MCP-2875, “Proper service and Maintenance of Laboratory Notebooks”
8. LWP-1201, “Document Change Configuration Management”
9. INL/EXT-12-27089, “LWRS ATR Irradiation Testing Readiness Status”
10. ASTM standard C1161-02C
11. PLN-3959, “Bend test”
12. ASTM E4-10
13. PLN-3951, “Flow/Corrosion”
14. INL/EXT-12-27172, “Initial Testing of the Hot Water Corrosion System”
15. ASTM Standard G 2/G 2M, “Standard Test Method for Corrosion Testing of Products of Zirconium, Hafnium, and Their Alloys in Water at 680°F [360°C] or in Steam at 750°F [400°C]”
16. PLN-3960, “Leach test plan”
17. SAR-153, Chapter 10, Section 10.1.7.3.3, “Containment of Materials”
18. SP-10.3.1.13 (referencing SAR-153) “Material Practices and Restrictions for ATR PCS and Experiment Loops”
19. PLN-3950, “X-Ray Tomography”

20. PLN-3957, “Density Test Plan”

21. ASTM B 311-08, “Standard Test Method for: “Density of Powder Metallurgy (PM) Materials Containing Less than Two Percent Porosity”

22. PLN-3961, “Visual and Dimensional inspection test plan”

23. R. L. Williamson, J.D. Hales, S.R. Novascone, M.R. Tonks, D.R. Gaston, C.J. Permann, D. Andrs, R.C. Martineau, “Multidimensional Multiphysics Simulation of Nuclear Fuel Behavior,” Journal of Nuclear Materials, Vol. 423, pp. 149-163, 2012

24. D. Gaston, C. Newman, G. Hansen, and D. Lebrun-Grandie, “MOOSE: A Parallel Computational Framework for Coupled Systems of Nonlinear Equations,” Nuclear Engineering and Design, Vol. 239, p. 1768, 2009

25. Michele Lazzeri and Francesco Mauri, First-Principles Calculation of Vibrational Raman Spectra in Large Systems: Signature of Small Rings in Crystalline SiO_2, Physical Review Letters, Volume 90, Number 3, 24 January 2003

26. A.G. REVESZ, Structural Interpretations for some Raman lines from vitreous silica, *COMSAT Laboratories, Clarksburg, MD 20871, USA* G.E. WALRAFEN, Journal of Non-Crystalline Solids 54 (1983) 323-333 North-Holland Publishing Company

Appendix A
An Example of the Characterization Routing Card Used for the Execution of Characterization of the Mock-up Samples on the Actual LWRS Generic Activity Sheet

Routing Floor
7/30/2012
Isabella VanRooyen.

LWRS Generic Activity Sheet

Requested By: Amber Miller
Completed By: Susan Case
Project: LWRS
Date: 6/27/2012

Material ID#: LWRS-1-6-A-2 **Material Description:** SiC/CMC tube

Process Description:

LWRS-1-6-A-2 SiC tube was picked up from 3EL502 (Susan's office) by Amber Miller for delivery to IRC 603, Lab C-17.

A copy of the "conditional use only" tag (NCR Tag No 46343 Tag 1) was included in the bag along with tube.

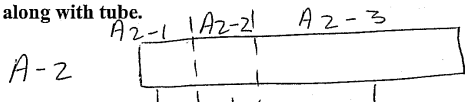

Notes:

SEM → XRD → Leach → chemical analysis
Density
Dimensional → 3D Tomography → Bend test → 3D tomography → SEM

- **Properly bag, label, and stow material as applicable**

Original is signed and dated.

Technician Signature and Date:

Appendix B
List of Relevant Laboratory Notebooks Used for Recording of the Characterization Data

Laboratory note book number	Owner	Purpose of laboratory notebook	Relevant page numbers if applicable
LAB-E-101	Isabella van Rooyen	Relevant to all characterization and initially technology development notes	Total book
Lab note book 1834	Tammy Trowbridge	Bend test specifically and other characterization notes as needed	Total book
LAB-2000	Amber Miller	Corrosion flow specifically and other characterization notes as needed	Total book
Log book #6	Arnold Erikson	Density and XRD	p79-77, 79
	Byron White	Chemical analysis	
Mechanical testing journals	Randy Lloyd	Bend test	Jan 2012: p18, 20, 22 April 2012: p22-26, 30

Note: relevant data are summarized electronically and added in the LWRS characterization drive with Isabella van Rooyen, Tammy Trowbridge and Amber Miller having “read and write” access.

Appendix C

3D Computed Tomography X-ray imaging system

Idaho National Laboratory

NSI-CT X-Ray Imaging System

- System Components
  - Hamamatsu 130kV Microfocus X-Ray Source
  - PaxScan 2520V Flat Panel Digital X-Ray Detector
  - Rotate Stage
  - Digital Imaging Work Station
  - Computed Tomography Work Station
- System Capabilities
  - 2D Film Radiography
  - 2D Digital Radiography (DR)
  - 2D DR with Magnification
  - 3D Computed Tomography (CT)
- Future Upgrades
  - 7-Axis Manipulator
  - 225kV X-Ray Generator

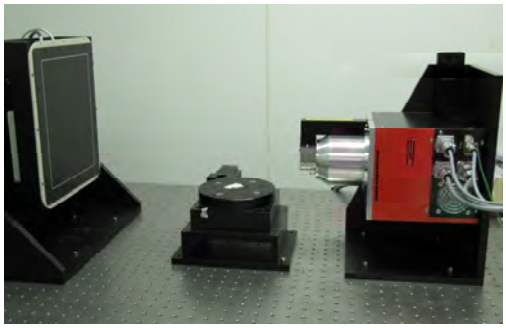

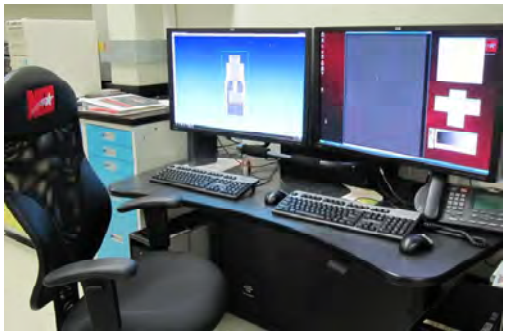

The 3D Computed Tomography X-ray imaging system at the INL Research Center was designed by North Star Imaging of Rogers, MN. Possibly the most important components of the system are the extremely powerful graphical processing unit housed in the image reconstruction computer and the proprietary image processing software.

Additional system components consist of a Hamamatsu 130kVp microfocus x-ray unit capable of producing approximately 10µm resolution images, a Varian PaxScan flat panel digital x-ray detector, and a rotational stage.

Appendix D

Detail of Density Measurement of Baseline Representative Sub-Samples

Density Measurements of SiC Fiber

Theo-dens means the accepted density of SiC and (Sample Densisty/ Theo-dens) x 100 is **%**

Rep 1	8/1/2012 #	Mass Dry	Mass Immersed	Water Density			Sample Density	Theo-dens	%		Water°C
	A-2-2	1.1745	0.7175	0.9978	0.4570	1.1719	2.56	3.9976	64.15	A-2	22.5
	A-7-1-2	1.6925	1.0358	0.9978	0.6567	1.6887	2.57	3.9976	64.33	A-7	22.5
	A-9-1-2	1.6711	1.0218	0.9978	0.6493	1.6674	2.57	3.9976	64.24	A-9	22.5
	B-2-1-2	1.1476	0.7094	0.9978	0.4382	1.1451	2.61	3.9976	65.37	B-2	22.5

Rep 2	8/1/2012 #	Mass Dry	Mass Immersed	Water Density			Sample Density	Theo-dens	%		
	A-2-2	1.1745	0.7220	0.9978	0.4525	1.1719	2.59	3.9976	64.79	A-2	22.5
	A-7-1-2	1.6925	1.0372	0.9978	0.6553	1.6887	2.58	3.9976	64.47	A-7	22.5
	A-9-1-2	1.6711	1.0170	0.9978	0.6541	1.6674	2.55	3.9976	63.77	A-9	22.5
	B-2-1-2	1.1476	0.7080	0.9978	0.4396	1.1451	2.60	3.9976	65.16	B-2	22.5

Rep 3	8/1/2012 #	Mass Dry	Mass Immersed	Water Density			Sample Density	Theo-dens	%		
	A-2-2	1.1745	0.7200	0.9978	0.4545	1.1719	2.58	3.9976	64.50	A-2	22.5
	A-7-1-2	1.6925	1.0368	0.9978	0.6557	1.6887	2.58	3.9976	64.43	A-7	22.5
	A-9-1-2	1.6711	1.0164	0.9978	0.6547	1.6674	2.55	3.9976	63.71	A-9	22.5

	B-2-1-2	1.1476	0.7082	0.9978	0.4394	1.1451	2.61	3.9976	65.19	B-2	22.5

Rep 4	8/1/2012 #	Mass Dry	Mass Immersed	Water Density			Sample Density	Theo-dens	%		
	A-2-2	1.1745	0.7191	0.9978	0.4554	1.1719	2.57	3.9976	64.37	A-2	22.5
	A-7-1-2	1.6925	1.0368	0.9978	0.6557	1.6887	2.58	3.9976	64.43	A-7	22.5
	A-9-1-2	1.6711	1.0160	0.9978	0.6551	1.6674	2.55	3.9976	63.67	A-9	22.5
	B-2-1-2	1.1476	0.7092	0.9978	0.4384	1.1451	2.61	3.9976	65.34	B-2	22.5

Rep-Sample	A-2-2	A-7-1-2	A-9-1-2	B-2-1-2
1	2.5645	2.5717	2.5682	2.6131
2	2.5900	2.5772	2.5493	2.6048
3	2.5786	2.5757	2.5470	2.5470
4	2.5734	2.5757	2.5453	2.6119
Average	2.5767	2.5751	2.5524	2.5942
STDEV	0.0106586	0.0023436	0.01061	0.03171
Max	2.5900	2.5772	2.5682	2.6131
Min	2.5645	2.5717	2.5453	2.5470
Dif	0.0255	0.0055	0.0229	0.0662

Work Compleeted 8-1-2012

Data recorded in Log Book "Operation Log for Graphite Pole Figures" pp. 76-79

These measurement follow ASTM B 311-08, "Stanadard Test Method for: "Density of Powder Metallurgy (PM) Materials Containing Less Than Two Percent Porisity"